Measurements of Thermal Properties and Blood Perfusion Using the Heat Flux Microsensor

by

Michael Douglas Michener

Thesis submitted to the Faculty of the

Virginia Polytechnic Institute and State University

in partial fulfillment of the requirements for the degree of

Master of Science

in

Mechanical Engineering

APPROVED

T. E. Diller, Chairman

Brian Vick

W. C. Thomas

January, 1991

Blacksburg, Virginia

Measurements of Thermal Properties and Blood Perfusion Using the Heat Flux Microsensor

by

Michael Douglas Michener

T. E. Diller, Chairman

Mechanical Engineering

(ABSTRACT)

A thin-film heat flux sensor was used in two transient conduction applications. First it was used in a device for simultaneously determining the thermal conductivity, k, and the thermal diffusivity, α, of solid materials. The device was heated and then touched to metal samples at room temperature. The thermal properties were characterized based on the heat flux response of the gage, and the change in temperature of the metal surface at a specified distance away from the gage. A finite difference program was developed and used to model the system response. The effect of α was most evident by the time delay in the temperature response on the metal surface. The effect of k was most evident in the heat flux response after the first few seconds of contact.

In the second application, the gage was used in a probe that was cooled and then touched to biological materials. A numerical model was used to demonstrate the effect of tissue blood perfusion on the surface heat flux. Experimental tests were performed on live dogs. Both the numerical model and the experiments showed that increases in blood perfusion could be

detected from the transient heat flux measurements. In both applications, this research forms the basis for instrumentation which will be able to measure k, α, and blood perfusion.

Acknowledgements

I would like to thank Dr. Tom Diller for his guidance and support with this research. His encouragement has made this work very enjoyable.

I would next like to thank the Vatell Corporation for supporting much of this research. Thanks also to Jon Hager and Jim Terrel for helping with the experimental work covered in this thesis.

I would also like to thank Dr. Brian Vick and Dr. W. C. Thomas for serving on my committee.

I would like to thank my parents for putting me through college. Thanks to my whole family for your support, advice and encouragement.

Finally, I would like to thank my girlfriend and all my other friends who have made my time at Va Tech great.

TABLE OF CONTENTS

LIST OF FIGURES

LIST OF TABLES

NOMENCLATURE

c	specific heat (J/kg·K)
Emf	gage output (μv)
h	convection coefficient ($W/m^2 \cdot K$)
k	thermal conductivity (W/m·K)
l	change in length in axial or radial direction
M	nondimensional blood perfusion
q	internal heat generation (W)
q"	heat flux (W/cm^2)
r	radial coordinate
R	radius of probe head
S	gage sensitivity ($\mu v/W/cm^2$)
t	time (sec)
t'	nondimensional time
T	temperature in degrees Celsius
w	blood perfusion (ml/ml·s)
y	axial dimension

Subscripts

0	imaginary node
1	edge node
a	artery
b	blood or boundary node

p	probe
T	tissue
v	vein

Greek

α	thermal diffusivity (m^2/s)
Δ	change in the following quantity
η	nondimensional radial coordinate
θ	nondimensional temperature
ξ	nondimensional axial coordinate
ρ	density
τ	period (sec)
∂	partial derivative
∇	gradient

1. INTRODUCTION

Heat transfer is a phenomenon that occurs any time a temperature difference exists. It plays an important role in the operation of mechanical devices and in medicine. The Diller and Onishi Heat Flux Microsensor enables a large range of heat fluxes to be measured with excellent accuracy. Because of its fast response time, the gage can measure heat flux transients never before measured. This transient capability is being exploited in the current work.

The purpose of this research is to test the validity of two applications for the Heat Flux Microsensor that were previously in the conceptual stage. One application is to use the gage to measure the thermal conductivity and thermal diffusivity of solid materials. The second application is to use the gage to measure blood perfusion in biological tissue. For both projects a specialized device was constructed to make the measurements, and a finite difference program was used to model the problem.

The relevant characteristics of the Heat Flux Microsensor are demonstrated in some recently published tests. A Heat Flux Microsensor was tested in the supersonic wind tunnel at VPI which produces an 8-10 second blast of air at Mach 2.35 [1]. Since the gage is so thin and since the sputtering process makes the gage almost an inherent part of the ceramic

disk, no air gets under the gage to rip it off. A larger gage that required attachments to hold it in place might not survive such a high speed airflow. The recorded output in Fig. 1 shows that the initial heat transfer is out of the gage into the air stream. This is due to the higher temperature of the initial compression wave coming down the tunnel. After the initial tunnel start-up transients, the signal drops negative indicating heat flowing out of the gage into the colder expanded flow.

The gage has also been placed in a propane flame which has a flame temperature of 2000 °C [1]. The heat flux is shown in Fig. 2 for a five second exposure to the flame. The signal produced is indicative of a very turbulent and unpredictable environment. This particular gage was tested like this many times before being destroyed.

The object of the research covered in this paper is to develop methods for obtaining accurate values for material properties using the Heat Flux Microsensor. Quantities of interest include the thermal diffusivity and thermal conductivity of a solid homogeneous material. The material could be a new alloy or composite material for which the thermal properties are not yet known, or a standard material that needs a quality check. The microsensor could be used to test biological tissue quantities as well. Most important is the blood perfusion, which is a measure of the volume of blood

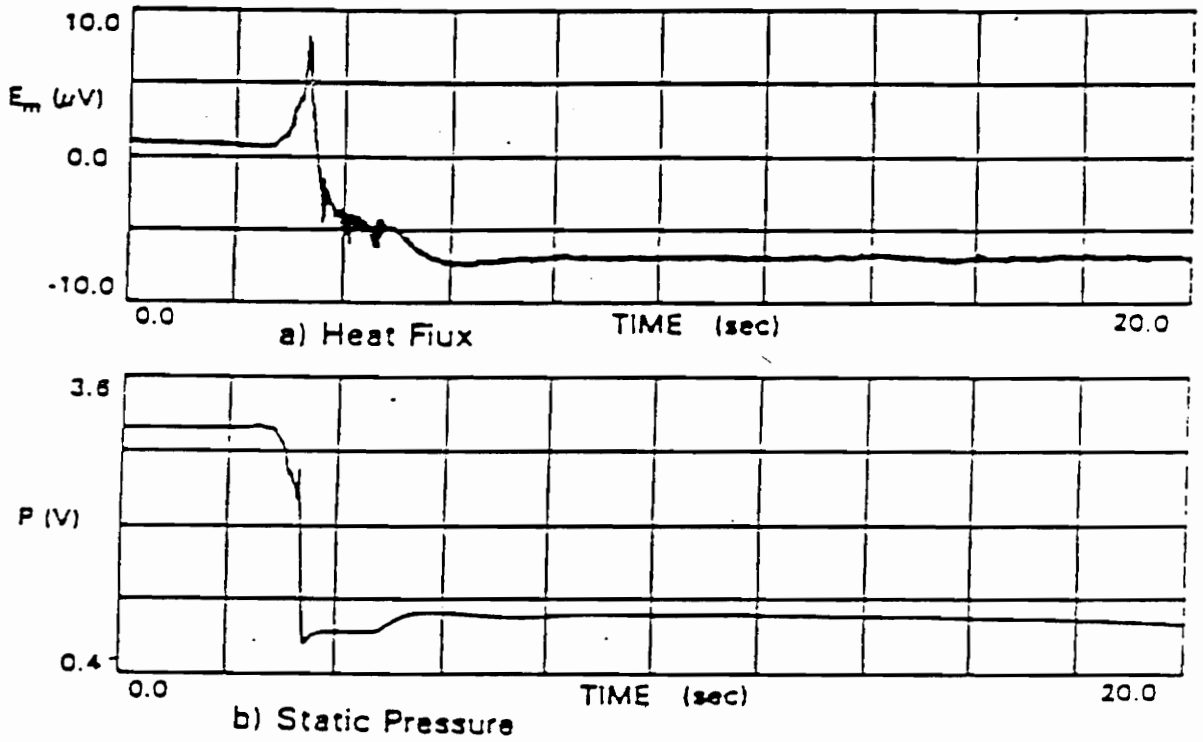

Fig. 1 Supersonic Wind Tunnel Test

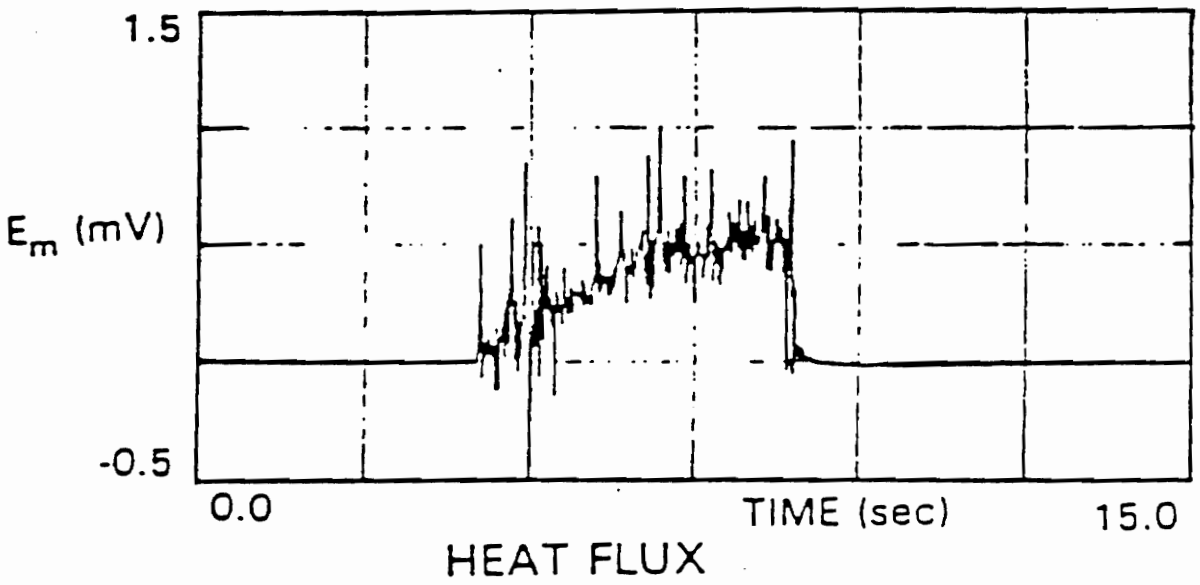

Fig. 2. Propane Flame Test

flowing through a volume of tissue per a unit of time.

Simultaneous measurements of transient temperature and heat flux provides the information required to find thermal conductivity and thermal diffusivity. The improvement to be made with this new probe is that the measurements can all be made on one surface rather than the front and back of an object. Additionally, the time required for each test is much shorter than that of most other methods. The heat flux will be produced by heating a probe holding the gage, and touching the gage surface to the material of interest. The device developed to make these measurements is the thermal conductivity and diffusivity probe.

Similarly, cooling a probe containing the gage and touching it to warm tissue can provide data used to find the blood perfusion. Knowing this quantity is important for understanding the healing process, athlete conditioning, detecting tumors, and mapping out circulation patterns. Blood perfusion is also a reliable indicator of a patient's status during surgical procedures. Blood perfusion in a transplanted organ is a good indicator of how well the organ is adjusting to the new environment. Several other diseases result in abnormal blood perfusion to the affected areas. Currently there is no good method for obtaining blood perfusion noninvasively. The bioprobe was the device developed to measure blood perfusion in this research.

Chapter two of this paper provides a literature review of thermal properties measurements and biological heat transfer measurement methods. Analytical and numerical models for predicting heat transfer are discussed in chapter three. Chapter four will cover the heat flux microsensor design and calibration tests. Chapter five examines the experimental and analytical results of the thermal conductivity and diffusivity probe. Chapter six examines the experimental and analytical results of the bioprobe.

2. LITERATURE REVIEW

In this chapter two topics will be covered. The first section reviews the various methods for determining the thermal properties of homogeneous materials such as metals. The principle properties of interest are the thermal conductivity, k, and the thermal diffusivity, α. The second section will cover the different ways of measuring blood perfusion. The techniques used in the research done for this thesis will be briefly compared to the other methods.

2.1 Thermal Properties Measurements

Thermal conductivity is a transport property that indicates how much heat will flow across a medium for a given temperature gradient. Heat transfer by conduction increases with increasing thermal conductivity over the same temperature gradient. Solids, especially pure metals, have high thermal conductivities, while gases and liquids usually have much lower thermal conductivities. Thermal conductivity is often measured by steady-state tests.

Thermal diffusivity is defined as the conductivity of a material divided by its density and specific heat. It is the thermal transport property associated with transient conduction, and is therefore measured with unsteady tests.

Leidenfrost [2] discusses several methods for determining k, including the ones currently used by the NIST. For low conductivity solids a steam calorimeter apparatus is used. Heating elements on one side of the sample create a steady, controlled heat flux through the sample. Thermocouples on the opposite side of the sample allow an accurate determination of k. For metals and other highly conductive materials a special apparatus based on the steam calorimeter is used. A long thin sample of the metal is required. The sample is heated on one end and actively cooled on the other. Thermocouples are distributed along the sample surface, and k is determined from this data and the known heat flux.

Hoch [3] discusses a method to determine k at temperatures between 1000 °C and 3000 °C. A sample of the metal is machined in a cylindrical shape so that L/D = 0.18 (L is the 1/2 height of the cylinder). The sample is heated by high frequency induction. The system is brought to equilibrium so that conduction through the solid to a point on the solid surface equals the radiation from that point. Thermal conductivity can be solved by:

$$k=\frac{\epsilon\sigma T^4}{4\left(\frac{\partial T}{\partial r}\right)L} \tag{2.1}$$

Takegoshi [4] used a transient hot-wire method to measure

conductivity in metals and other high conductivity materials. The hot-wire is placed between infinite specimens of the unknown thermal conductivity material and a known thermal conductivity material. The technique appears to only work for materials up to 100 W/m·K.

Some unsteady methods have been used to characterize k, but in general k is best isolated by controlling the heat flux and measuring the steady-state temperature distribution.

Thermal diffusivity is a measurement of how quickly heat transfers through a material. Thermal diffusivity is usually measured by monitoring the time for heat to move a certain distance, and is therefore measured using unsteady methods.

One technique is to subject a long, thin cylindrical rod to a sinusoidal heat flux at one end (Danielson [5]) and to measure the rate that heat is propagated down the rod. A simple one dimensional partial differential equation describes this problem. Thermal diffusivity can be solved for explicitly as:

$$\alpha = \frac{lv}{2\ln(q)} \tag{2.2}$$

v = velocity of propagation

l = length between two thermocouples

q = amplitude decrement in temperature

Using a flat plate, semi-infinite solid or thick cylinder to

do this analysis is also discussed by Danielson, but the solutions are considerably more complex.

For some ceramics α has been approximated by heating a sample very rapidly (NASA brief [6]). The heater subjects the sample to a temperature of 2000 °F. The rate in temperature rise is recorded for the sample. By comparing each test relative values for α are determined. Each test takes approximately ten minutes.

The laser pulse method is probably the most common way of determining α. Kobayasi [7] used a rectangular heat pulse to heat a small cylindrical specimen and monitored the temperature on the opposite side to determine α. The apparatus was interfaced with a computer to analyze the data. In this method specific heat can simultaneously be extracted from the data.

Several other periodic and pulse heating methods are discussed in the review by Kobayasi [7]. These methods appear satisfactory for finding α.

There is also some research being done to find values for k and α simultaneously. Takahashi [8] discusses a measurement system which ideally will provide values for k, α, specific heat, and coefficient of thermal expansion. This system is only in the conceptual stage, but the method for finding α is presented. Rods of silver and stainless steel are heated in a vacuum and then the radiative cooling rate is measured after

the heater is turned off. Thermal diffusivity is determined from the cooling rate.

Fukai [9] has developed a technique to simultaneously measure k and α. It uses a hollow cylinder with an unsteady periodic heat source produced from the inside. The values for k and α are found by measuring the amplitude and phase lag of the temperature response in the cylinder. In their experiments they have accounted for finite specimen size and thermocouple location errors. The results correlate well with hot-wire techniques for aluminum oxide and potassium perchlorate samples between 300 and 600 °K. The samples are not actual solids, but rather packed beds of fine particles.

The Heat Flux Microsensor is currently being used as an integral part of a device that also will be able to measure k and α simultaneously. This heat flux gage provides accurate data, and the measurement process is much faster than the others discussed. The probe makes its measurement on any flat surface which makes it more applicable on a commercial scale. The apparatus and results from its use are presented in chapter 5.

2.2 Blood Perfusion Measurements

As discussed in the introduction, accurate knowledge of the local blood perfusion in tissue can be very valuable. It

is, however, a quantity that is hard to measure and is often confused with blood flow rate. Patel et al. [10] state that blood flow and perfusion are related, but a tissue volume can have normal blood flow but significant perfusion abnormalities. Therefore, a method to accurately and reliably measure blood perfusion must be developed.

Chato [11], in a review article on biological properties measurements, includes much information on thermal techniques used to measure local blood perfusion. These techniques are all invasive in nature which is a very undesirable characteristic and should be avoided if possible.

The invasive technique that has been most successful is the category of thermistor probes. Valvano et al. [12] tested steady-state heated thermistors on the canine kidney cortex. The procedure involves supplying continuous power to the thermistor, and measuring the steady-state temperature rise of the thermistor. Heat is conducted away from the thermistor head, but heat is also removed by perfusion. Knowing the thermal conductivity of the tissue and the thermistor temperature allows the perfusion to be determined. In Valvano's research, the Weinbaum-Jiji model for bioheat transfer was used to predict results.

A similar technique was used by Bowman [13]. He used a thermal diffusion probe in which electrical energy is supplied to the thermistor bead. The temperature of the bead is held

constant by a feedback control system. Therefore, the energy supplied to the bead is equal to the energy diffused from the bead in the tissue. The amount of electrical power required to hold the temperature constant is a function of blood perfusion.

Thermistor beads have several problems. If they are too large then the invasiveness of the instrument can damage or traumatize the organism. If they are small, they will not cover an effective area of tissue.

Several noninvasive techniques have been developed to avoid this problem. Anderson [14] uses an ultrasound heating source at the tissue surface and monitors the resulting temperature at the surface. The ultrasound is focused on a specific volume of tissue. The phase difference between the sinusoidal ultrasound power supply and the sinusoidal surface temperature curve is sensitive to perfusion. The longer the heating period, tested up to 40 seconds, the more sensitive the data was to perfusion. The resolution of the perfusion measurement is anticipated to be approximately 0.005 ml/ml/s. However, no exact numbers have yet been extracted from the raw data with this technique.

Walsh and Bowman [15] employed another noninvasive technique which uses a thermal probe constructed of two flake thermistors. The probe was heated and touched to an isolated rat liver. The probe is sensitive to the perfusion of the

tissue, but can only quantify it to within a 15% error.

Patel et al. [10] used self-heated spherical thermistors partially embedded in an insulator. The spherical bead simultaneously heats tissue and measures the resulting temperature rise. The rate and amount of power dissipated to the tissue is a function of tissue conductivity and perfusion. This probe was also tested on a rat liver. The conclusion of this research was that the probe was sensitive to perfusion, but actual values could not be determined.

Castellana [16] used an electrically isolated thin film thermal sensor to noninvasively estimate perfusion. These tests were performed on the surface of dog hearts, and showed sensitivity to perfusion changes. The probe is heated to 3.6 and 5.72°C above the tissue temperature, and the power required to maintain this temperature difference is measured and related to tissue perfusion. The experimenters were able to relate heat fluxes to specific perfusion rates and show that heat flux increases with increasing perfusion.

Obviously, there is plenty of space for improvement in measuring blood perfusion. At this stage the noninvasive techniques do not have enough sensitivity to perfusion to produce accurate results. The spherical thermistors create three-dimensional temperature fields which are not as sensitive to perfusion changes as a one-dimensional field. The invasive techniques are dangerous to the patient.

The Heat Flux Microsensor has great potential for this application. The resulting bioprobe has several advantages over other perfusion probes. The design creates a nearly one-dimensional thermal field as described by Diller [17]. This results in greater sensitivity than the three-dimensional temperature fields created by the spherical thermistors. The probe is designed to work by cooling the gage to temperatures lower than tissue rather than heating the probe as all of the other researchers did to create the heat transfer. This allows a greater temperature difference to be produced and therefore larger heat fluxes. The vast majority of the other researchers tested their noninvasive instruments on animal kidneys, livers, or hearts which are the most highly perfused organs. The method used in this research has been successfully tested on the skin surface of live animals and humans without any harm to the subject, and is therefore a truly noninvasive blood perfusion instrument.

3. THEORETICAL MODELING OF HEAT TRANSFER SYSTEMS

In the study of any field of engineering, a reliable theoretical model is usually a good place to begin the actual design of any apparatus. Theoretical models for heat flux problems assist in determining the required size and other characteristics of the device. Models also predict the necessary temperature difference or heat flux that must be induced in the problem to produce measurable results. Perhaps most importantly, experimental results can be compared to those obtained theoretically, proving ideally that the actual apparatus is working correctly, or at least providing clues as to why a discrepancy is occurring.

The Heat Flux Microsensor is being used for several unique applications, thus there is a need to demonstrate the validity of the gage's output. Several of these applications involve touching the gage to a surface of different temperature, and monitoring the heat flux and temperature time-history response. An analytical solution and a finite difference solution were used to model these experimental tests.

The gage was fabricated on a circular substrate. Therefore, the analytical and numerical solutions were performed in cylindrical coordinates. For the applications of the gage covered in this thesis, the disk is touched to a

metal or biological tissue surface (assumed semi-infinite) of a different temperature to produce the heat flux by conduction (see Fig. 3). The heat transfer effects in the semi-infinite solid were modelled and studied. The disk was only included in the analysis as a boundary condition for the semi-infinite solid. Contact resistance between the disk and semi-infinite solid was not modelled.

3.1 Constant Heat Flux Analytical Solutions

The analytical solutions which most closely approached the physical problems of interest were found in a paper published by Jaeger [18]. Three solutions were provided for constant heat flux supplied over different geometries: an infinite strip, a square, and a circle (see Appendix A). Graphs were provided which gave some limited number of solutions to these equations (see Appendix A).

Two short Fortran programs were written to evaluate the infinite strip and circular solutions. Since both equations involve the evaluation of integrals, approximation methods were used to calculate the integrals. In the infinite strip program, the exponential integral was evaluated using its series expansion. In the circular program the integral was approximated using the trapezoidal rule of integration. Care was taken to ensure that the integral had converged for each

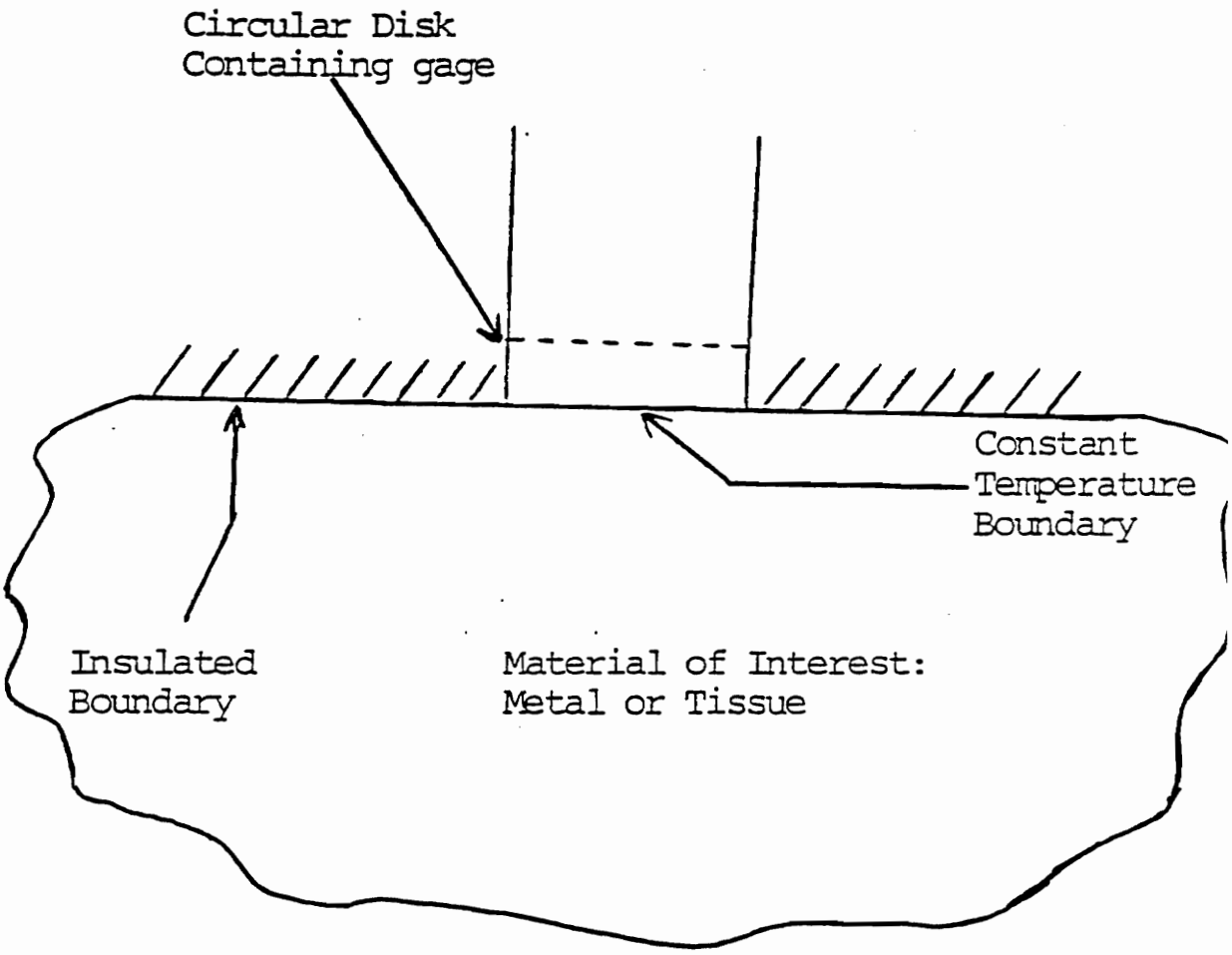

Fig. 3. General Test Configuration

set of thermal properties tested. Listings of these programs are given in Appendix B.

The circular program closely models the experimental configuration of most of our tests. The infinite strip solution is only of interest to check that the programs are written correctly, and to provide a comparison to the circular solution.

3.2 Numerical Solutions

Numerical solutions can be used to solve more complicated problems with additional terms for which no exact solution exists. The additional term of interest is the blood perfusion term that must be accounted for in solving heat transfer problems in biological tissue. Also numerical solutions allow the boundary conditions to be changed to model slightly different problems or to check the validity of the solution. If used correctly these types of solutions can provide data as accurate as if obtained analytically. A numerical program tends to be much longer in length than an analytical program, however, and requires a great deal of formulation.

3.2.1 Pennes Bioheat Equation

A numerical solution was required to solve the Pennes Bioheat Equation [19]. This equation is an accurate representation of an energy balance for a section of biological tissue

$$(\rho c)_T \frac{\partial T}{\partial t} = k_T \nabla^2 T + (\rho c w)_b (T_a - T_v) + q \tag{3.1}$$

This equation does not account for nonhomogeneities in the tissue, heat transfer between adjacent arteries and veins, and the physiological effects of the blood vessels. Still, this equation has been widely accepted since 1948 when it was first published. Attempts have been made to improve this equation, notably the Bioheat equation of Weinbaum and Jiji [20]. However, all such improvements require detailed information on the structure of the microvasculature.

The Pennes equation is based on an energy balance on a section of biological tissue. A control volume showing the different terms is shown in Fig. 4. The numerical analysis started with the Pennes equation. Standard assumptions were made to simplify the equation. Using radial coordinates, it is possible to model the tissue in two dimensions by assuming symmetry about the probe axis. Radial coordinates are valid because of the circular shape of the probe head. The

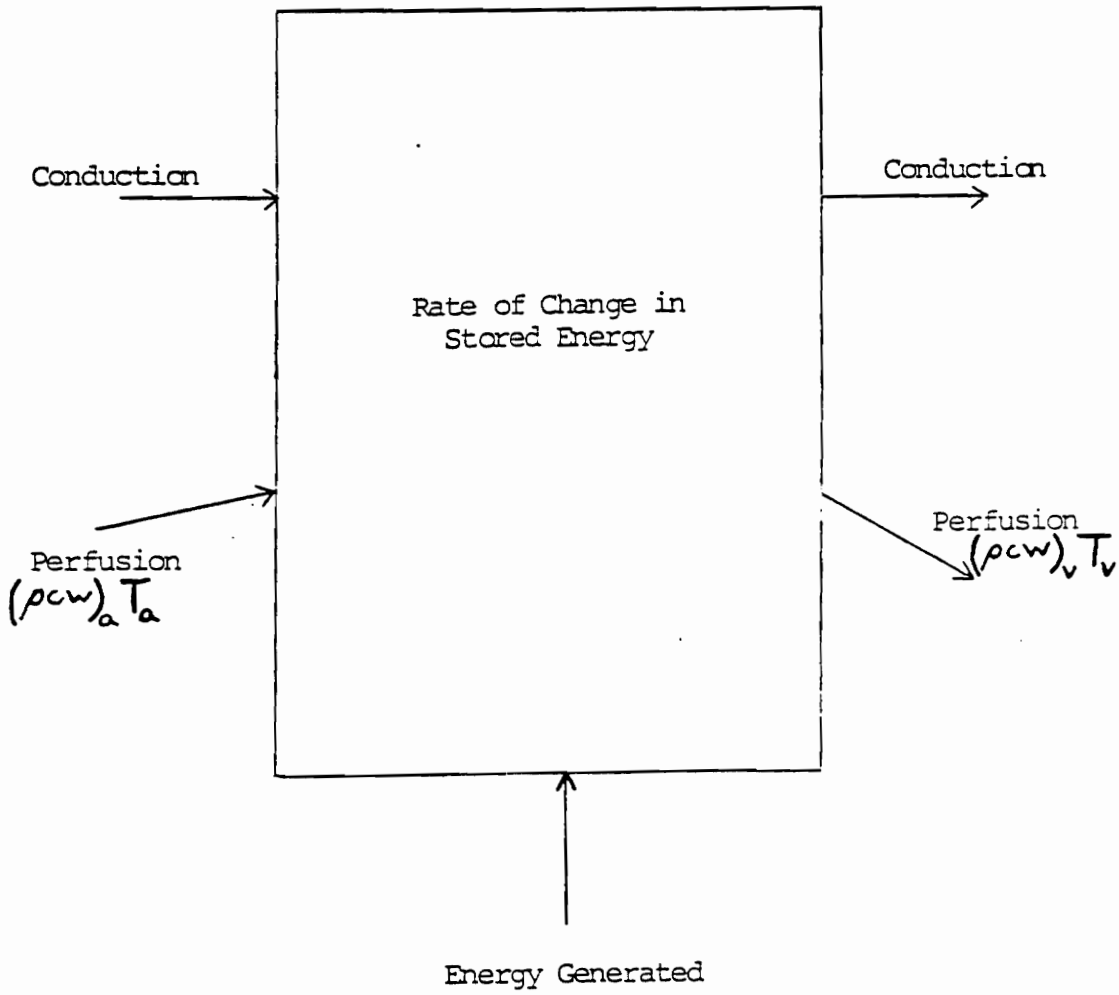

Fig. 4. Control Volume for Pennes Equation Derivation

temperature of the blood flowing in the veins was assumed equal to the tissue temperature ($T=T_v$). This assumption is useful in nondimensionalizing the equation, and should be accurate since capillary blood will approach an equilibrium temperature with the surrounding tissue. Finally, internal heat generation was also neglected. This is valid since the probe will be used on the skin surface only, and the tissue here is not highly metabolic.

The remaining equation consists of (from left to right) a transient term, a radial conduction term, an axial conduction term, and a perfusion term only

$$(\rho c)_T \frac{\partial T}{\partial t} = k_T \frac{1}{r} \frac{\partial}{\partial r}\left(r \frac{\partial T}{\partial r}\right) + k_T \frac{\partial^2 T}{\partial y^2} - (\rho c w)_b (T - T_a) \qquad (3.2)$$

This was nondimensionalized to simplify the analysis. The nondimensional variables are defined

$$\Theta = \frac{(T - T_a)}{(T_p - T_a)}, \eta = \frac{r}{R}, \xi = \frac{y}{R}, t' = t/\tau \qquad (3.3)$$

Substituting theta and the independent variables yields

$$\frac{\partial \Theta}{\partial t'} = \left(\frac{k}{\rho c}\right)_T \left(\frac{\tau}{R^2}\right) \frac{1}{\eta} \frac{\partial}{\partial \eta}\left(\eta \frac{\partial \Theta}{\partial \eta}\right) + \left(\frac{k}{\rho c}\right)_T \left(\frac{\tau}{R^2}\right) \frac{\partial^2 \Theta}{\partial \xi^2} - \frac{\tau (\rho c w)_b}{(\rho c)_T} \Theta \qquad (3.4)$$

Tissue thermal diffusivity is defined as $(k/\rho c)_T$. This has the same dimensional units as the inverse of τ/R^2. To further simplify the equation, τ was defined as R^2/α . The coefficients of the conduction terms now simply equal one. The only term that remains to be simplified is the perfusion term. By substituting R^2/α for τ and by using a volumetric definition for perfusion, w_b, the coefficient of the perfusion term can be simplified to

$$M=\left(\frac{\rho_b k_b w_b}{k_T}\right)R^2 \tag{3.5}$$

The coefficient of the perfusion term, M, is now dimensionless. The final form of the energy balance equation for a section of tissue is

$$\frac{\partial\Theta}{\partial t'}=\frac{1}{\eta}\frac{\partial}{\partial\eta}\left(\eta\frac{\partial\Theta}{\partial\eta}\right)+\frac{\partial^2\Theta}{\partial\xi^2}-M\Theta \tag{3.6}$$

3.2.2 Method Of Solution

The perfusion term, $M\Theta$, is the term that makes this equation applicable to biological tissue. Without this term, the equation can be applied to any homogeneous solid material.

The perfusion term makes this problem too complicated to solve analytically for the prescribed geometry. A numerical technique is therefore required.

A finite element method was considered for modeling the tissue and probe, but available code was not capable of modeling perfusion. It would have been necessary to write new code or modify existing code which would become very involved.

A finite difference program was determined to be the best method of solution. With this technique perfusion can be included without much difficulty. Several finite difference methods were investigated. An implicit technique was desired to give flexibility in the time steps used for this solution. Using the Crank-Nicolson method would result in five unknown values for θ in each finite difference equation. A pentadiagonal matrix solver could be used to solve this set of equations. An additional method would be to divide each matrix up into sub-matrices that are each tridiagonal in form. This would be time consuming and impractical. It was decided that the most efficient method of solution was the Alternating Direction Implicit (ADI) method [21].

The ADI method is actually a factorization of the Crank-Nicolson equations. It involves setting up two different finite difference equations, one for each spatial direction. First, each derivative term is expressed as an analog, an approximation of the actual derivative. This allows the

problem to be broken up into a finite number of time and spatial steps. The two finite difference equations are alternately used in every other time step. Because of this, the time steps can be better understood as double time steps. In each double time step the first finite difference equation is used followed by the second equation. Answers are only accurate after a complete double time step.

In the first time step, the analog for the radial direction (η) was written implicitly, and the analog for the axial direction (ξ) was written explicitly. In the second time step, the analog for the axial direction was written implicitly while the analog for the radial direction was written explicitly (see Appendix C). Rearranging these terms to put the unknowns on the left side of the equation and the knowns on the right side of the equation presents the general finite difference equations (see Appendix C). These equations are applicable at every node in the mesh except those along the boundary of the mesh.

3.2.3 Boundary Conditions

Imaginary node techniques allow the boundary conditions to be changed without changing the basic matrix. Figure 5 shows some sample nodes on the boundary of the mesh. In this

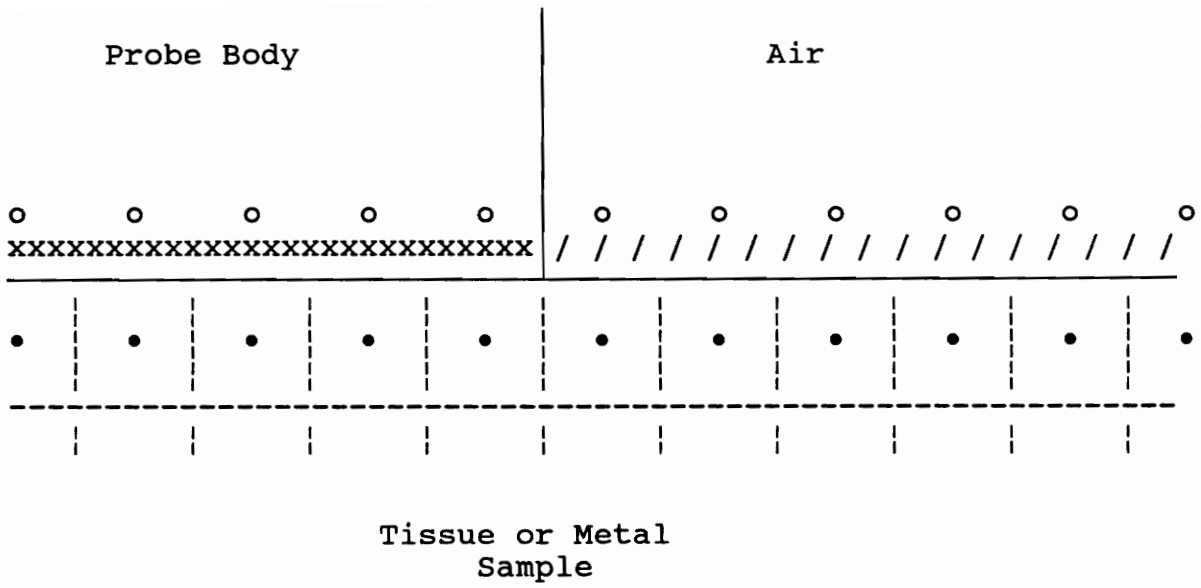

Symbols

• = Element Node

o = Imaginary Node

// = Insulated Boundary

xx = Constant Temperature or Heat Flux Boundary

Fig. 5 Sample Elements on the Boundary of the Mesh

solution the whole boundary is insulated except for the interface between the probe and the tissue. This boundary is best modeled by a constant temperature condition. The probe will be maintained at approximately 15 °C by a water cooling system and the tissue is initially at 37 °C. The center axis of the probe and the tissue is assumed to be axisymmetric. This can be represented by an insulated boundary in the radial direction at $\eta = 0$.

At the insulated boundaries the imaginary node temperature, θ_0, is equal to the edge node temperature, θ_1, by the relation

$$\frac{\Theta_1-\Theta_0}{\Delta l}=\left(\frac{\partial\Theta}{\partial l}\right)_b \tag{3.7}$$

$$\left(\frac{\partial\Theta}{\partial l}\right)_b=0 \tag{3.8}$$

By simple algebra $\theta_1 = \theta_0$, and θ_0 is eliminated from the boundary finite difference equations by substitution.

The constant temperature boundary condition is slightly more complicated. The equation relating the imaginary and edge nodes is

$$\Theta_b=\frac{\Theta_1+\Theta_0}{2} \tag{3.9}$$

where Θ_b is the temperature at the interface. According to the definition of Θ, Θ_b can also be written:

$$\Theta_b = \frac{T_p - T_a}{T_p - T_a} = 1 \tag{3.10}$$

Therefore

$$\frac{\Theta_1 + \Theta_0}{2} = 1 \tag{3.11}$$

$$\Theta_0 = 2 - \Theta_1 \tag{3.12}$$

Again substitute for Θ_0 in the boundary finite difference equations. This results in a $2/(\Delta\xi)^2$ term (in addition to the Θ terms) on the right hand side of the equation. This will be the driving term, the term which will cause the values of Θ to change, in the finite difference scheme.

A third boundary condition of interest is that of a constant heat flux. If the boundary of the tissue-probe interface were changed to constant heat flux, the solution could be compared to the circular analytical solution of section 3.1. The two-dimensional accuracy of the program could be proven. Fourier's Law, $q''=-k(\partial T/\partial x)$, can be nondimensionalized to

$$q'' = -\frac{k(T_p - T_a)}{R}\frac{\partial\Theta}{\partial\xi} \tag{3.13}$$

The derivative term can be approximated as before and solving for Θ_0 yields

$$\Theta_0 = -\frac{q''R\Delta\xi}{k(T_p - T_a)} + \Theta_1 \tag{3.14}$$

Once again Θ_0 is eliminated from the equations. After substitution, the driving term for the constant heat flux condition is

$$-\frac{q''R}{k(T_p - T_a)\Delta\xi} \tag{3.15}$$

3.2.4 Writing the Program

The finite difference program was written in double precision Fortran (see Appendix D). All terms dependent on location in the mesh are stored as two dimensional arrays.

All geometric and tissue properties are defined at the beginning of the program and are constant for a given solution. The size and number of time steps are also specified.

Coefficients for the unknown θ's are solved at the beginning of the program. These are constant for a given mesh size and set of tissue properties, and do not depend on time. Theta values on the left hand side of the finite difference equations (Appendix C) are at the new, unknown time, and theta values on the right hand side are at the known time step. Initially, theta at every point equals zero. The driving boundary condition at the tissue-probe interface is what changes theta values from zero.

After defining the properties and coefficients, the program goes through a large DO LOOP for every double time step. Constants for the right hand side are obtained based on the current values for theta and boundary conditions. The new values for theta are solved for in a tridiagonal matrix solver. The equations in the second time step are given these new values of theta, which are substituted into the right hand side of the equations. The tridiagonal matrix solver is again used to obtain new values for theta. This process will continue for the number of time steps defined at the beginning of the program.

The program itself is very versatile. Time was spent

organizing and writing the program in such a way that enables the variables to be easily changed. Nondimensionalizing the energy balance equations eliminated units from the main body of the program. It also reduced the number of variables in the program and made the program easier to understand.

The boundary conditions were done using imaginary node techniques. This allows the use of the same basic finite difference equations for all node points next to the boundaries. The boundary conditions were easily changed from constant temperature to constant heat flux in order to perform some checks on the program.

The program can model any number of elements in any size or ratio, although care must be taken to choose a mesh pattern that converges to the correct answers. The time step size and length of time can be specified to any value. The time step can also be increased exponentially during a solution to get small time steps initially and larger ones later in the program. This enables the initial, quickly changing heat flux to be modeled accurately, but saves run time later when the heat flux is almost at steady state. All of the tissue properties (conductivity, diffusivity, perfusion, density) are specified at the beginning of the program, and can be easily changed.

4. HEAT FLUX MICROSENSOR

The Heat Flux Microsensor is produced using thin film sputtering techniques. This allows an intricate pattern of 40 pairs of thermocouple junctions to be deposited in a 3mm x 4mm area (see Fig. 6). The total gage thickness is less than two μm. The gage consists of a top and bottom thermocouple layer separated by a thermal resistance layer of SiO. The thermocouples in each layer are connected in series forming a thermopile. The top and bottom thermopiles are connected in parallel which forms a differential thermopile. The thermocouples measure the temperature on both sides of the resistance layer in the form of a voltage signal. The voltage signal is directly proportional to the heat flux. Currently the metal combination being used for the thermocouples is nichrome-platinum. Other metal combinations previously used were copper-nickel and nichrome-tantalum [22].

The gage has several characteristics making it superior to previous heat flux measuring devices. The gage is so small and thin that it will not disturb or alter the environment in which it is placed. This quality, its negligible thickness, also makes the frequency response of the gage extremely high. Tests have shown the ability of the gage to measure changes in heat flux at a frequency of 50 kHz [22]. The small size also enables the gage to pinpoint the heat flux over a specific

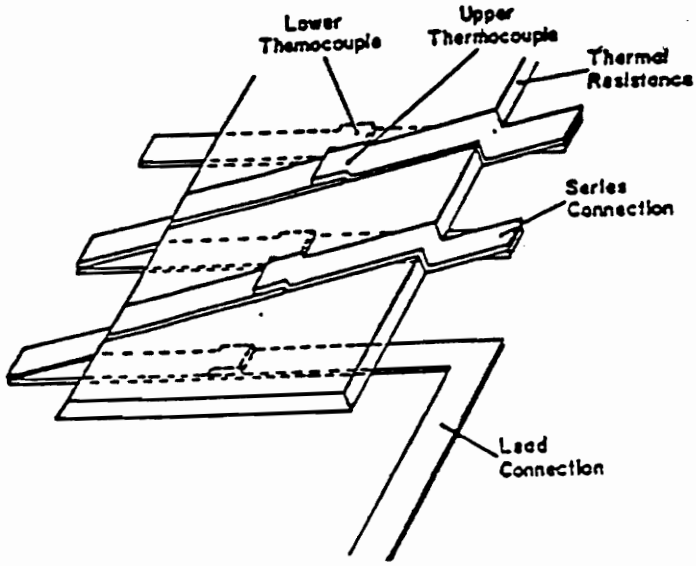

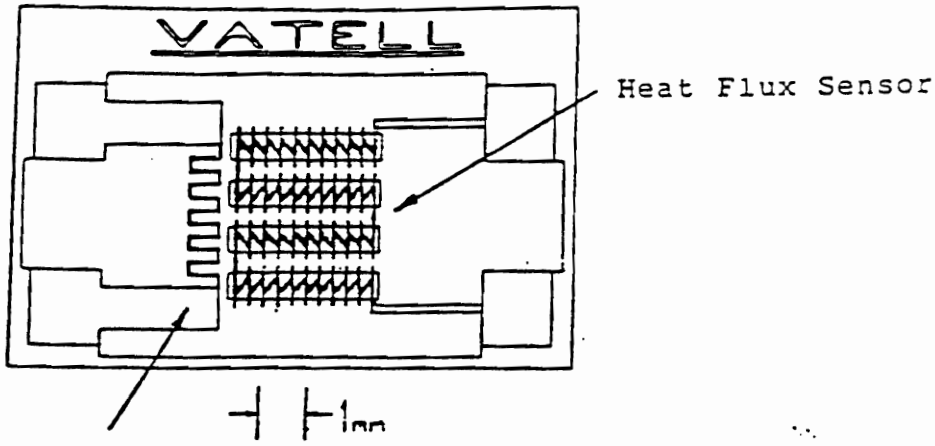

Resistance Temperature Sensor (RTS)

Fig. 6. Heat Flux Microsensor

area. The method of gage production allows it to be deposited directly onto areas of interest, such as turbine blades, engines, exhaust nozzles, etc.

The gages are versatile and can measure a large range of heat fluxes accurately. Since the gage is a passive transducer it can measure heat flux to and from a surface. Its potential applications therefore include medicine, engines, industrial machinery, rocketry, and propulsion devices.

4.1 Recent Improvements in Gage Design

Several improvements in the Heat Flux Microsensor have recently been made. One of the biggest areas of improvement is in the through connection method. The Heat Flux Microsensor has two leads coming from the heat flux gage for the heat flux signal and two leads coming from the surface thermocouple or RTS for the surface temperature. These leads are also sputtered onto the substrate surface and must make an ohmic connection to the signal analyzing instrumentation. Originally the "clips" shown in Fig. 7 were used. These were adjusted until reliable contact was made with the metal lead pads and then tightened to restrict movement. The problem arose when they were subjected to the cool jet in the calibration setup (see Fig. 8). This blower produced a

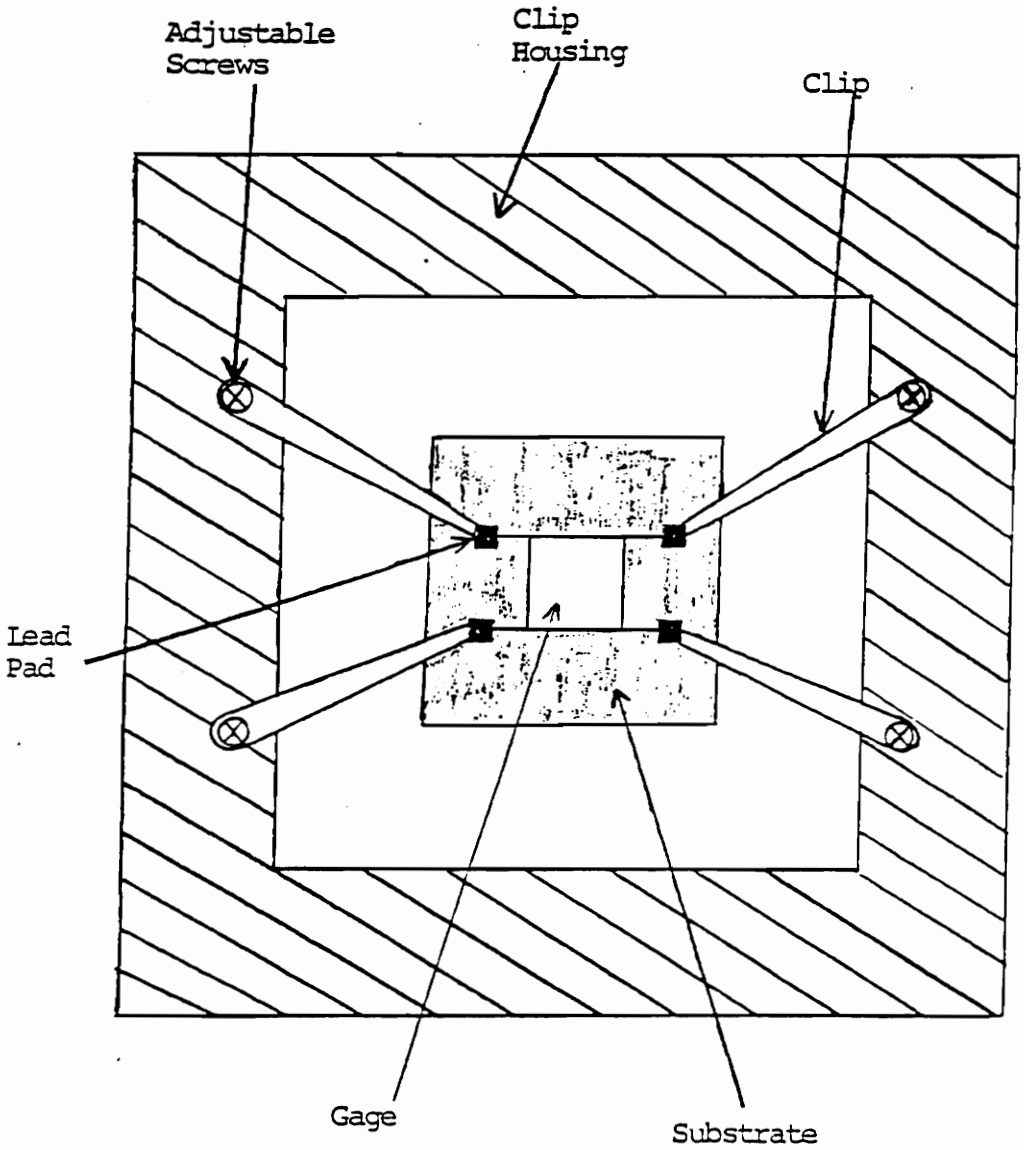

Fig. 7. Clip Design for Gage Operation

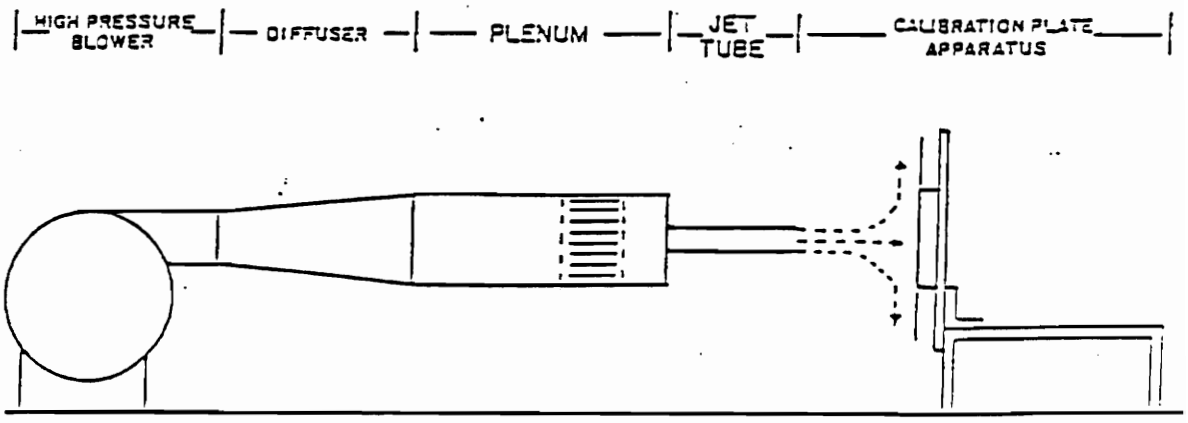

Fig. 8. Calibration Setup

sufficient air flow to cause the clips to vibrate slightly and lose contact with the pads. The signals under these conditions were obviously irregular. Even with silver paint applied to the pads to improve the connection, the problem still persisted. Eventually the design would have proved impractical anyway because the clips and gage holder would have made it impossible to do the conduction tests.

An alternative was to use through connections. When fabricating the gage, four holes were drilled in the substrate, pins were inserted and the gage was sputtered onto the substrate. This showed significant improvement in providing a more reliable signal. The gage surface was now flush which enables the gage to be used for the transient conduction applications. A problem still occurred, however, when the gage was heated above 100°C and cooled several times. The thermal stress caused the pins to pull away from the pads resulting in loss of connection.

The newest design now incorporates a conical pin with a curved hole cut in the surface of the substrate as shown in Fig. 9. This results in greater surface area of contact between the pin and the sputtered pad. Furthermore, the pin is inserted after the sensor is fabricated. This allows the metal leads to be sputtered down into the pin holes. There is much more lead pad area for the pins to contact with this procedure. Additionally, the other end of each pin is held

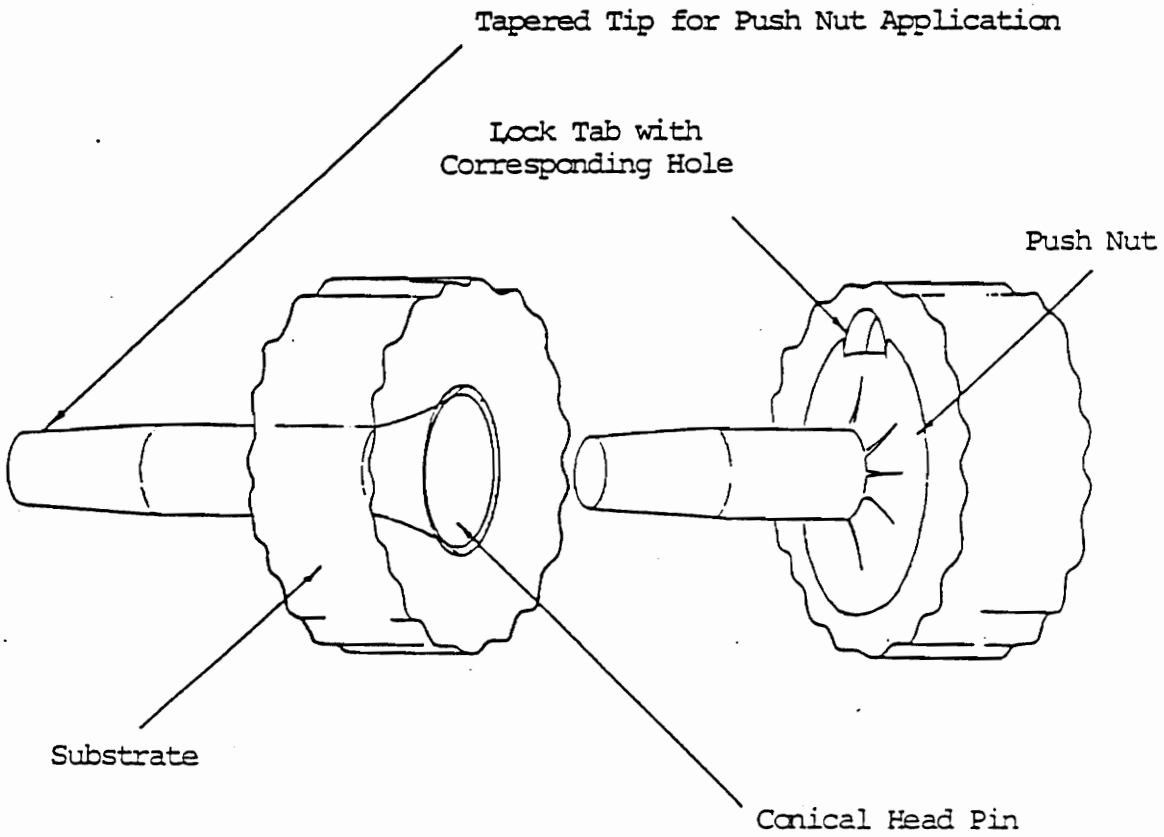

Fig. 9. Conical Pin and Push Nut

firmly in place by a push nut. The push nut prevents small movements of the pin, and also enforces compressive contact between the film and the pin. This will reduce the chance of breaking the surface pad connections. The latest gages have these types of connections and they have shown excellent results.

Additional steps were taken to reduce the signal noise level. This is critical since the voltage output levels are quite small (microvolts before amplification). The lead wires are connected to twisted-shield pairs to reduce the noise. Also a differential amplifier was built that has high common mode rejection to produce a clear signal.

Initially the gages were made on 2.54 cm x 2.54 cm glass or aluminum nitride squares. These were then mounted on a larger flat plate with the previously discussed clips attached shown in Fig. 7. The new through connection method was developed for new substrates, 2.54 cm diameter, 0.64 cm thick aluminum nitride disks. This size was accepted as a standard, and all devices used for testing were designed so that the disks could be mounted in the device and then removed after the testing was performed. Therefore, one disk could be used in several different types of tests. Because aluminum nitride has a high thermal conductivity, the disk surface temperature remained uniform for most conditions tested. Thermal imaging showed that the disk surface was at a uniform surface temperature

even when heated or cooled rapidly.

4.2 Microsensor Calibration and Testing

Before a Heat Flux Microsensor can be used for any of its innovative applications, it must be calibrated and put through some standard tests. The gage produces a voltage output proportional to heat flux. The purpose of the calibration tests is to determine the gage sensitivity--how many microvolts represent a W/cm^2, the standard unit for heat flux. Additionally, these preliminary tests ensure that the microsensor is giving signals characteristic of a working gage. Once these tests have been successfully completed, the gage can be used reliably for numerous other tests of greater interest.

The calibrations have been accomplished using several different methods. Steady-state convection and conduction methods have been tried. Transient convection methods have to this point been most reliable. In the future steady-state or transient conduction may prove to be the best method for calibration.

In the convection tests the gage is located at the stagnation point of an air flow of a different temperature from the gage. If the air flow is cool (room temperature),

then the gage is heated. The gage can also be left at room temperature and subjected to a hot air flow.

For the cool air tests the gage is mounted on the face of the calibration plate shown in the calibration setup (refer to Fig. 8). The front of the box is an aluminum plate with a small hole for the disk holding the gage. Several strip heaters are located on the backside of the plates and disk in order to produce a uniform temperature and ideally one-dimensional heat flux when the cool air is turned on.

The first class of tests are the steady-state convection tests. In these tests the cool air is turned on for the duration of the experiment. The temperature of the heaters are raised in 5°C increments, and the apparatus is allowed to reach a thermal equilibrium with the air flow. Then 100 instantaneous readings of the heat flux are made using an HP 3468A Digital Multimeter. The average of these readings is obtained at each set temperature from 35 - 85°C.

The main problem with this setup is that the actual gage temperature is not high enough to produce large signals. Because the air flow is continually running throughout the entire experiment, the gage is constantly cooled. As a result the gage never gets above 50°C although the heaters are as high as 85°C. The gages can survive up to at least a few hundred degrees celsius; obviously the full capability of the gage is not being tested. When trying to obtain an accurate

calibration the desired heat flux is much greater than can be obtained at steady state in this setup.

Transient convection tests allow the gage response to be studied at temperatures and heat fluxes much higher than the steady-state tests. The gages produce much larger heat flux signals if the air is kept off and the gage is heated to a high temperature, ~125°C, by a more powerful Variac heater. The fan is turned on, but the flow is blocked by a large shutter for a few seconds to allow the fan to reach full flow rate. The shutter is then opened and a heat flux and temperature time-history like the one in Fig. 10 is recorded. Data from these curves can be used to obtain a calibration coefficient for the gage. The following equation is used to calculate the coefficient

$$S=\frac{Emf_{gage}}{h_{gardon}(T_{probe}-T_{air})} \tag{4.1}$$

Simultaneous heat flux and temperature data can be picked off of the curves at several different times to obtain an average coefficient. Table 1 shows the corresponding data and results from analyzing the curves in Fig. 10. The value for h_{gardon} is determined by steady-state tests with a Gardon gage in exactly the same flow conditions. For these tests it was found to be 306 $W/m^2 \cdot K$.

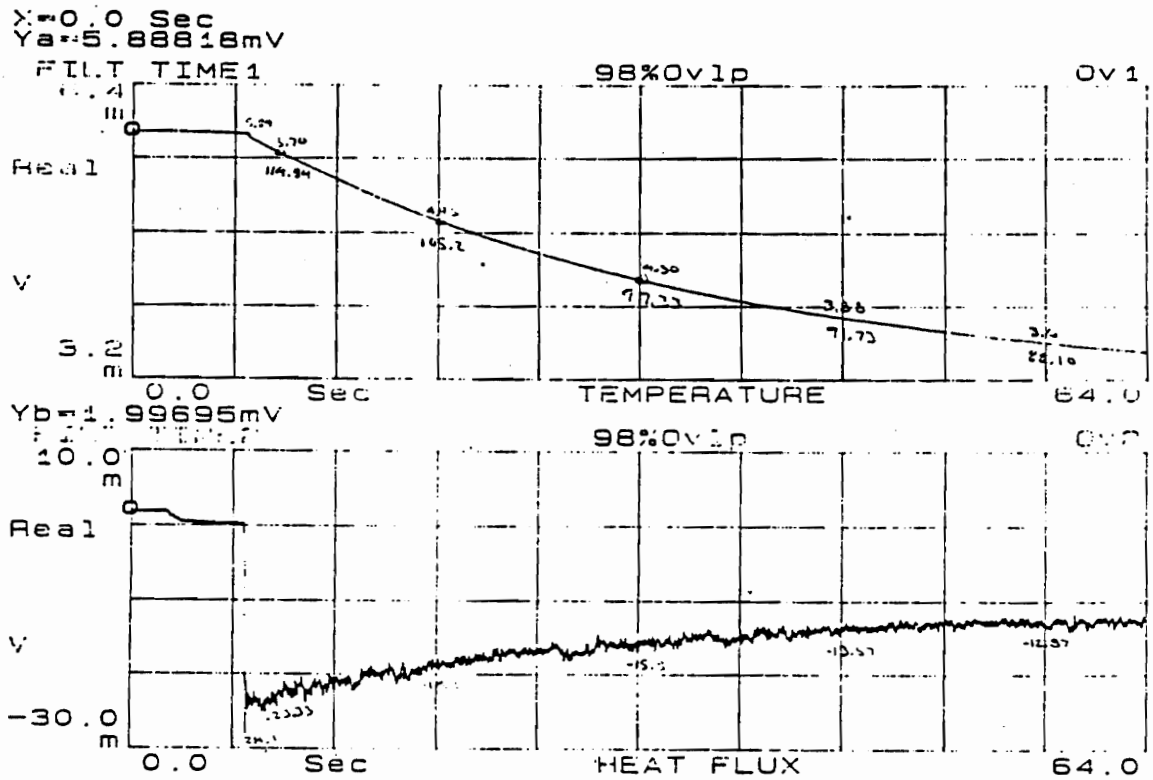

Fig. 10. Cool Air Transient Calibration Test

Table 1. Calibration Coefficient Data

time (sec)	Emf (μv)	T (mv)	T (°C)	ΔT (°C)	S (μv/W/cm^2)
2	23.3	5.7	114.8	89.8	8.4
12	18.9	4.9	105.2	80.2	7.6
24	15.8	4.3	97.3	72.3	7.1
36	13.6	3.9	91.7	66.7	6.6
48	12.9	3.6	88.1	63.1	6.6

Another class of tests that falls into the transient category is the heat gun tests. A power stripper that blows hot air at 250°C was set up 7.6 cm from the gage as shown in Fig. 11. After the heat gun is turned on a shutter device shields the gage from the hot air until the heat gun is up to full power. Then the shutter is released and a blast of hot air hits the cool gage producing the signal in Fig. 12.

Comparing the two heat flux curves in transient flow (figures 10 and 12) leads to several important points. When cool air is blown on a heated gage, the heat flux signal is negative. Heat is flowing out of the gage into the flow, which is negative by convention. Conversely, when hot air is blown on a cool gage, the heat flux is positive since heat is flowing into the gage.

Some additional differences can be noted as well. The signal in cool air jumps to a large negative peak, but then decays exponentially quite rapidly down to about 30% of the initial peak within 15 seconds. The hot air signal jumps quickly to a large heat flux, but holds at virtually that value for the duration of a 10-15 second test with no decay.

This difference can be explained by examining the physical setup. The air flow rate of the hot air is much smaller than that of the cool air. Therefore, the hot air will not bring the whole system to a "uniform" temperature as quickly as the cool air does. The peak heat flux in the hot

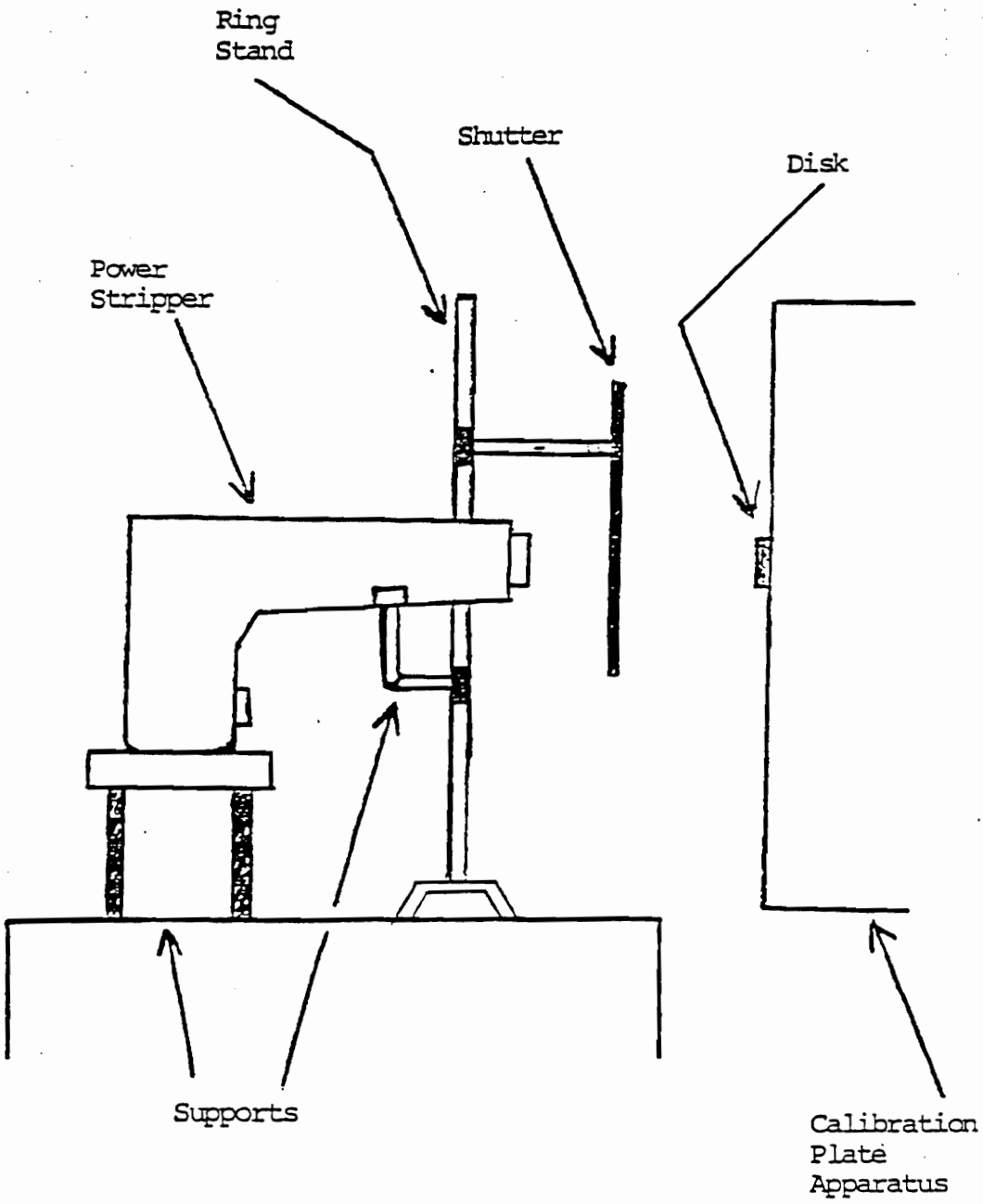

Fig. 11. Hot Air Convection Test Setup

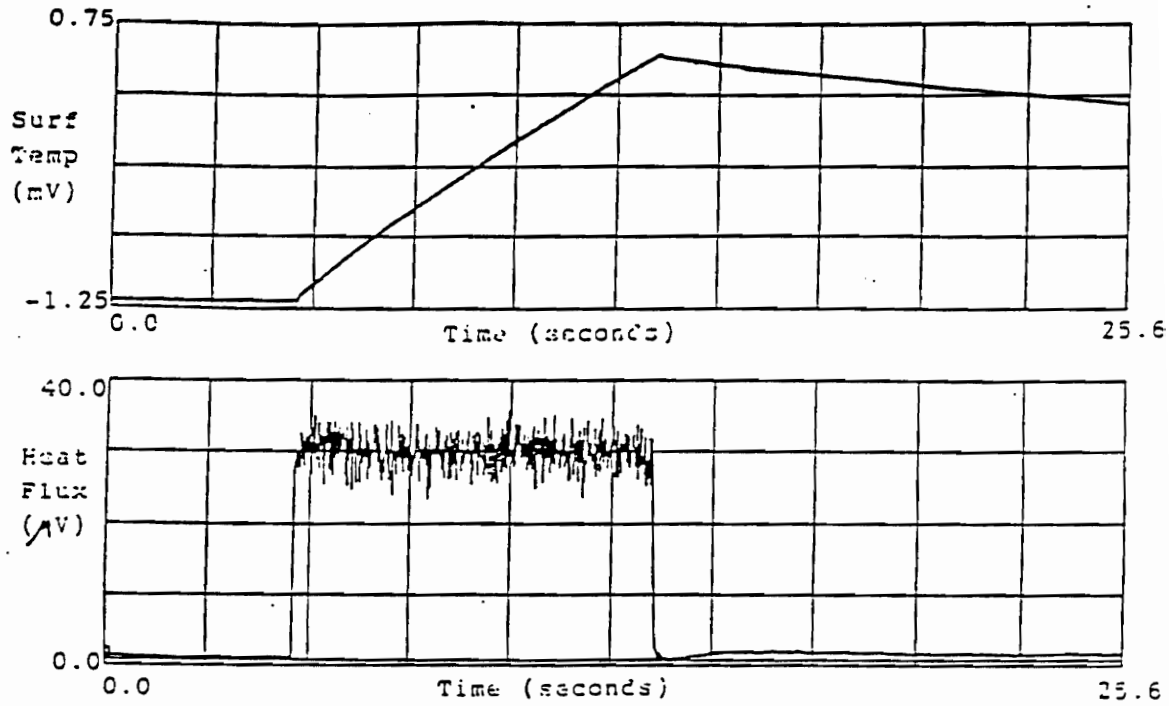

Fig. 12. Transient Hot Air Test

air tests is so drawn out that it appears as a large steady-state response.

A second explanation is that in the hot air test the whole system is at room temperature except for the hot air. Therefore, there is a lot of mass at room temperature that will tend to keep the gage at a low temperature, and, in turn, produce larger heat fluxes than if the temperature rose quickly. In the cool air test, only a small heater is raising the gage temperature and much of the mass in the system remains quite cool. When the jet is turned on, the small heated area is quickly consumed by the cool air since not much mass needs to be cooled. The result is a quick peak followed by much smaller heat flux output.

It is also interesting to look at the hot air curve when the shutter is closed. Sometimes there is a small overshoot where the heat flux is negative. This is due to the fact that the gage has been heated during the test, and is now hotter than the surrounding air. Although there is no forced flow over it, a small amount of heat is convected out to the air.

5. Thermal Conductivity and Diffusivity Probe

It is useful to know the thermal properties of metals and other materials for several reasons. When designing engines, cooling systems, or any apparatus where heat dissipation is critical, the thermal properties of the materials must be known accurately. Then the heat transfer in the system can be correctly predicted, and the device can be optimally designed. Thermal properties can also be used to characterize the molecular structure of metals.

The Heat Flux Microsensor can be used to find thermal properties of materials. When placed in contact with a metal of different temperature a transient heat flux will be produced. In addition, the changing temperature of the metal is monitored at some distance from the gage metal interface by an isolated thermocouple. A time-history record of the heat flux and isolated thermocouple is made. From this data the thermal conductivity (k) and the thermal diffusivity (α) can be extracted. A specialized device to make these measurements was designed and built by the Vatell corporation. This device is called the thermal conductivity probe.

5.1 Theoretical Study

The two-dimensional time-dependent analytical heat flux

model discussed in chapter three was used to help design the apparatus. The proposed design was to mount one of the disks on a device which could bring the gage into contact with the metal of interest. The gage was heated by a band heater to approximately 40°C above the metal temperature. A thermocouple was located at some distance from the disk-material interface. This isolated thermocouple measured the initial material temperature and the change in temperature after contact was established. The purpose of the analytical study was:

- To determine an optimal distance from the probe-material interface for the isolated thermocouple to be located.
- To determine the required temperature difference between the probe and material needed to get measurable heat transfer.
- To get an idea of how big of a contact area was required in the system and how to size the apparatus.
- To help show that the variables k and α are separable from the heat flux and temperature data and to provide insight on how to accomplish this task.
- To predict and compare the experimental results of the actual test apparatus.

5.1.1 Thermocouple Location

The thermal properties of carbon steel ($k = 60.5$ W/m K, $\alpha = 17.7 \times 10^{-6}$ m^2/s) were used to run some initial tests in order to check the proposed design. Steel was chosen because it is a metal with relatively low thermal conductivity and diffusivity which would provide conservative values for heat transfer on which to base the initial design.

Of greatest importance initially was how fast and to what magnitude the heat flux effects would be observed at points outside of the contact area. The change in temperature throughout the test is measured by an isolated thermocouple located outside of the area of contact. The change in temperature history at the isolated thermocouple must be accurately known in order to eventually separate out the thermal properties.

The circular analytical program from section three was run for several distances from the contact area. The thermocouple must obviously be located close enough to the probe-metal interface to detect a significant temperature change. Equally important, the thermocouple must be located far enough from the contact area so that its temperature is effected only by conduction through the metal and not radiation from the probe body. In addition, there must be

enough material between the contact area and the thermocouple for the thermal diffusivity to play a significant role in the heat transfer. In other words the thermocouple must be far enough from the probe so that when the probe and material are brought into contact there is a measurable amount of time before any change is detected by the thermocouple.

Temperature vs. time curves are shown in Fig. 13 for distances $r/a = 1.2$, 1.5, 2.0, and for a typical heat flux magnitude. These tests showed that detectable temperature differences occur at $r/a < 2.0$, less than 1.27 cm from the probe. According to these tests, locating the thermocouple between 0.64 cm to 1.27 cm from the probe would meet all above criteria.

5.1.2 Separate Effects of k and α

The analytical program was also used to study the individual effects of k and α on the heat flux and temperature responses. Learning how the thermal properties influence the signals suggests methods of separating the two properties from heat flux and temperature data.

Under constant heat flux conditions, decreasing k increased the change in temperature over the same period of time. Decreasing α decreased the change in temperature over the same period of time as seen in Fig. 14. This test

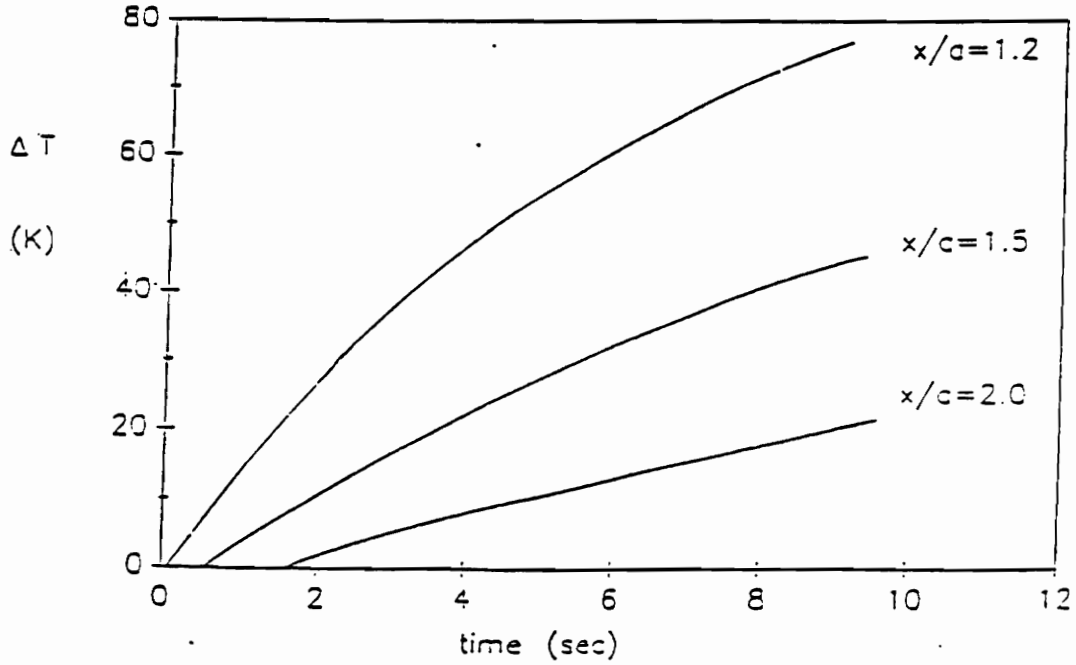

Fig. 13. ΔT at Isolated Thermocouple

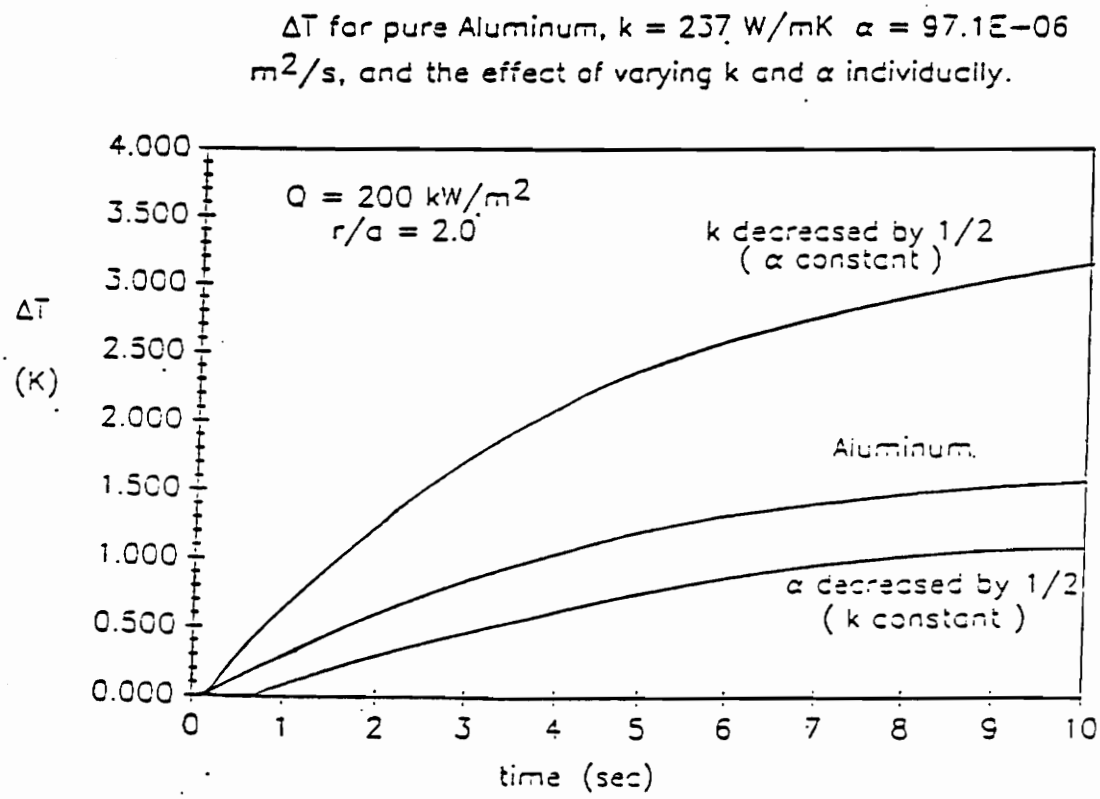

Fig. 14. Effect of Changing k or α of Aluminum

suggests that changes in a thermal property have characteristic effects on the heat transfer curves which can be attributed specifically to that property.

But where is the best place on the heat flux and temperature change curves to isolate k and α? Thermal conductivity can be most accurately extracted from the heat flux response a few seconds after the initial peak in heat flux. Thermal diffusivity is most readily apparent in the length of time between probe-material contact and the first detectable change in temperature at the isolated thermocouple.

An additional idea was tested that is believed to indicate that k and α are separable. The term $k\rho c$ is kept constant based on the one-dimensional relation

$$q'' \propto \sqrt{k\rho c}\,\Delta T \qquad (5.1)$$

The terms k and ρc were varied in a compensating manner. For example, to keep $k\rho c$ constant k was halved and ρc was doubled. This makes α 1/4 of its original value from the relation $\alpha = k/\rho c$. The separate effects of k and α could not be observed by examining equation 5.1 since it is a one-dimensional equation. However, applying these new properties to the two-dimensional circular heat source analytical program resulted in no change or a very small change in the heat flux and temperature at the probe center, but a significant change

in these quantities at a distance outside of the probe (see figures 15 and 16). This indicates that k and α are separable because the effect of k is seen at the probe center, and the effect of $k/\sqrt{\alpha}$ is seen at a distance from the probe. Therefore, k can be isolated from the heat flux information measured by the gage, and α can be isolated by the temperature data at the isolated thermocouple.

5.1.3 Sensitivity Analysis

The analytical programs used to model the thermal conductivity probe were also used to determine the accuracy with which the measurements must be made. With a basic copper-constanten thermocouple the temperature measurement has an uncertainty of ± 0.1 °C . If the isolated thermocouple is located 1.27 cm from the probe face, then after 1 second the temperature change is still under 0.3 °C even for high α materials if a constant 2.0 W/cm^2 heat flux is assumed. The magnitude of uncertainty is on the same order as the output. This will lead to a huge range of possible values for k and α when calculating these properties from the ΔT data. However, after 10 seconds the change of temperature has increased to over 1.0°C for all metals. Since the error now is an order of magnitude smaller than the change in temperature, k and α can

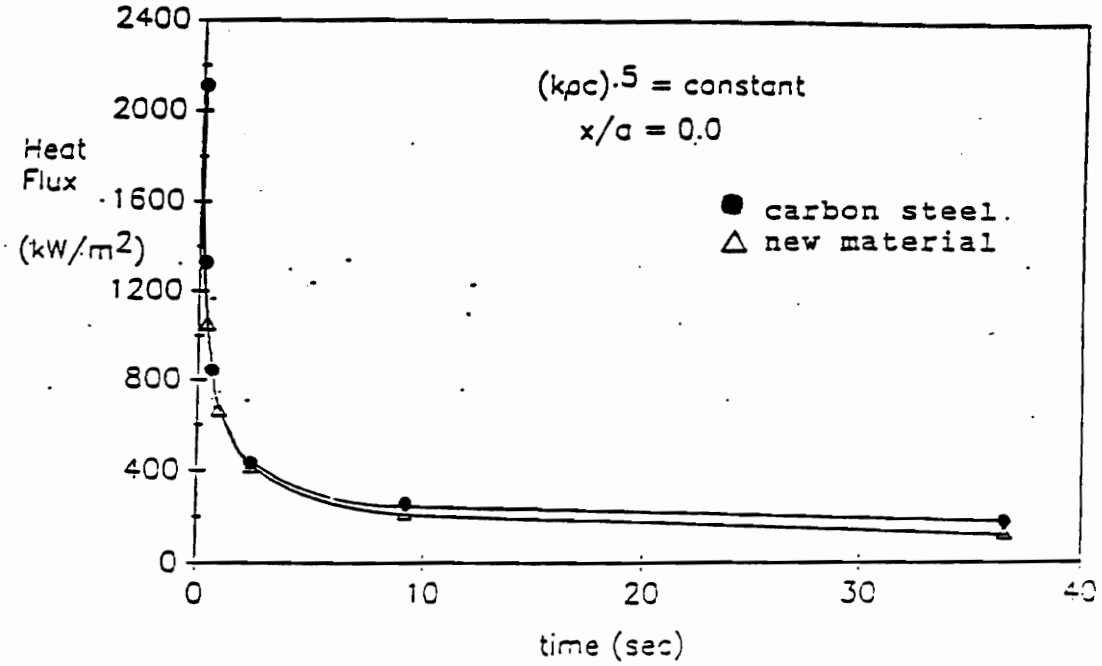

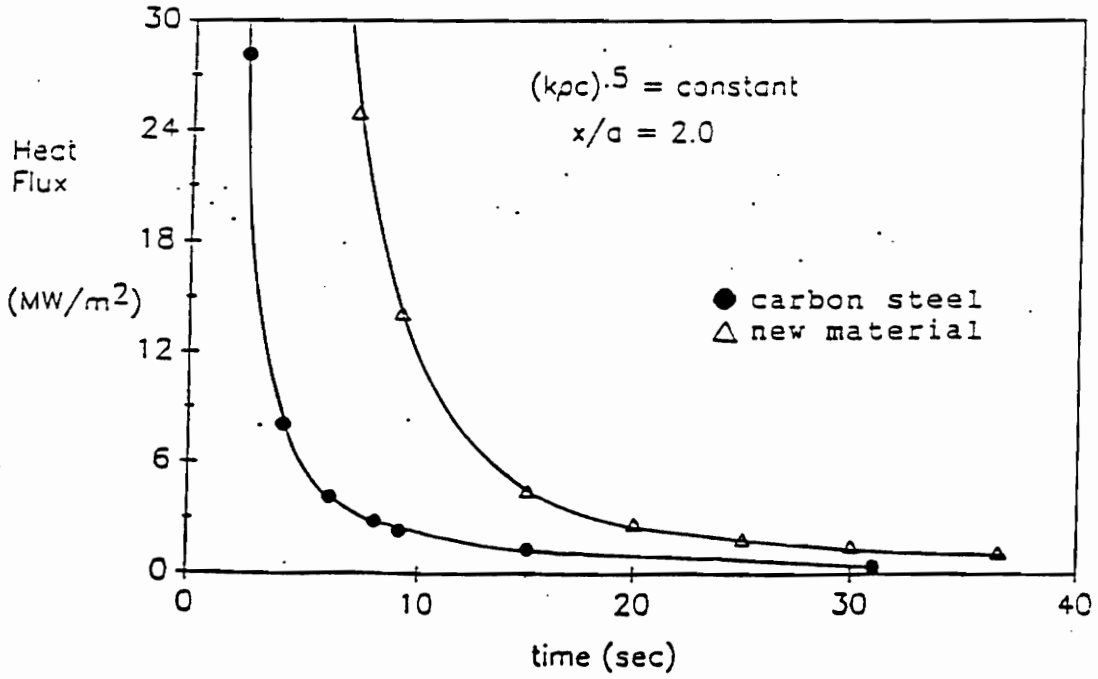

Fig. 15 Heat Flux vs. Time with kρc Constant

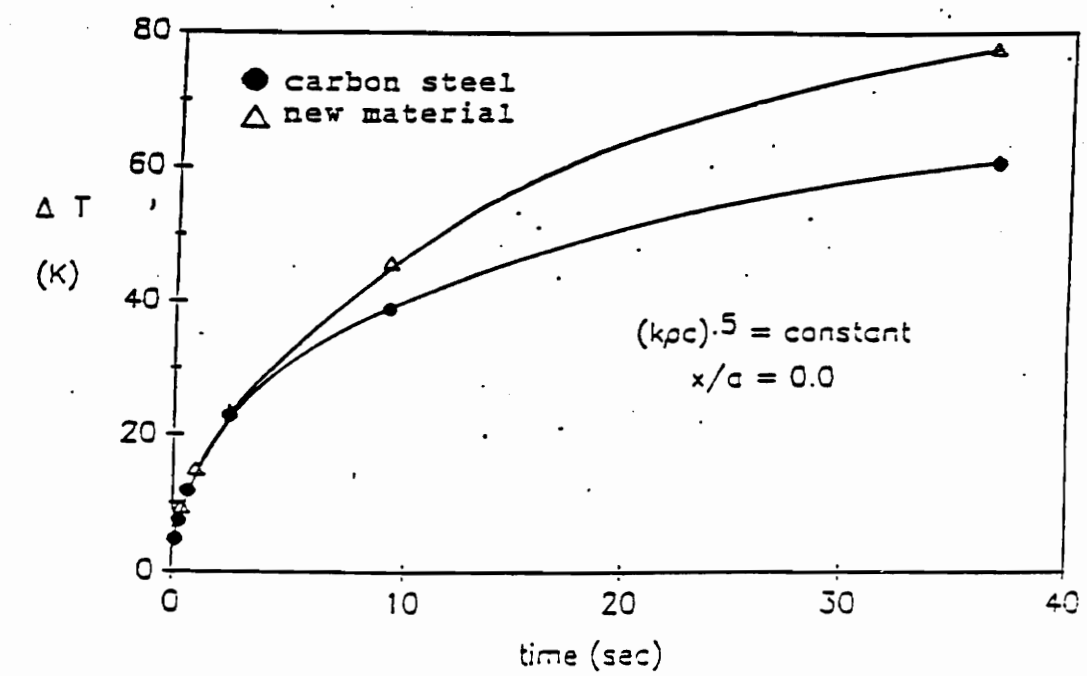

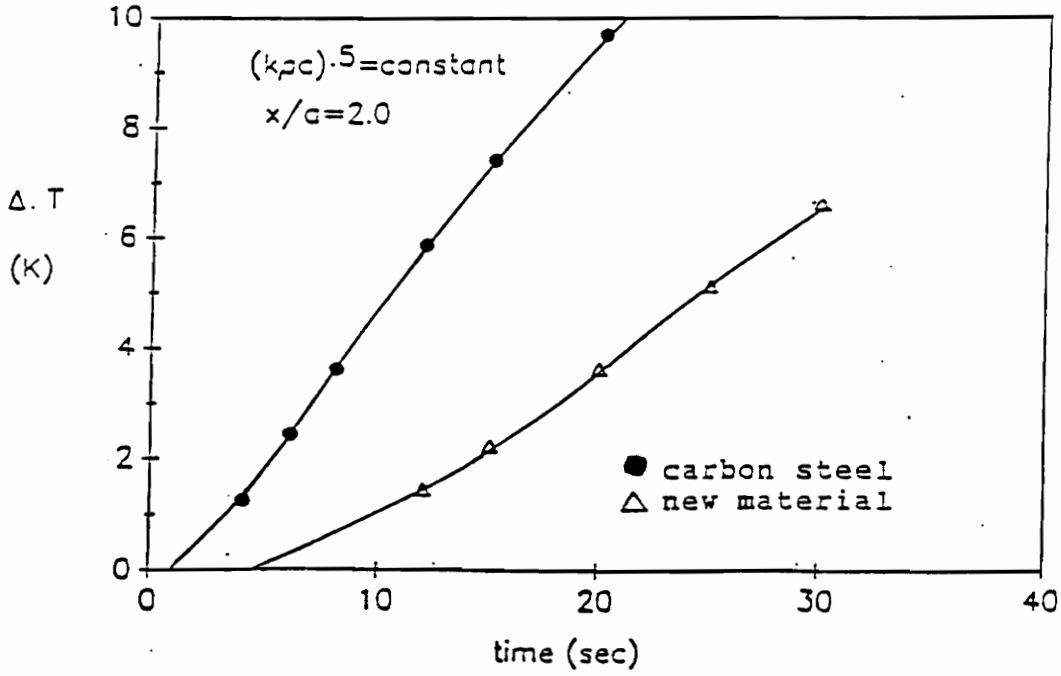

Fig. 16 Temperature vs. Time with kρc Constant

now be found to within 10% or better. This test suggests that if a temperature value is needed to calculate k and α it would be best to examine a value after 10 seconds. Increasing ΔT could be achieved by increasing the heat flux or by moving the isolated thermocouple closer to the probe. Both of these would have the same ultimate effect of helping to achieve a higher certainty for k and α.

Similar calculations were done assuming that the heat flux is known to $\pm$ 0.025 W/cm^2. The heat flux starts off large (ideally infinity if no contact resistance existed) when the probe and material are brought into contact. The heat flux gradient levels off significantly in 5-10 seconds, but will continue to decrease slowly to zero if given enough time. The highest level of heat flux and, therefore, theoretically the time when the 0.025 W/cm^2 uncertainty would be most insignificant occurs in the first couple of seconds. However, it is the longer time response that will reveal reliable information about k and α.

Under one second the heat flux is mostly a function of the contact resistance rather than k or α. The heat flux curves of different materials are difficult to differentiate at this time. Therefore, the heat flux will provide the most dependable data for calculating the thermal properties at times greater than a few seconds after initial contact.

5.2.1 Experimental Tests

The thermal conductivity probe apparatus is shown in Fig. 17. The probe is attached to the top plate and is heated to 65 °C before each test. The test begins as the probe free falls guided by four support bars. A damper catches the probe about 1 cm above the test material and eases it into contact with the material surface. Materials are slid in and out of the apparatus through the slot in the front. The isolated thermocouple is clipped into place before releasing the probe. It can be adjusted to almost any distance from the probe up to 1.2 cm. The thermocouple was protected from radiation effects by a wood splint. The test apparatus was used with three specially machined metal specimens designed to fit into the 7.62 cm x 7.62 cm x 1.27 cm slot in the apparatus. The materials were chosen to fit the wide range of thermal properties existing in metals: stainless steel, aluminum and copper (see table 2). Data from the analytical circular program was obtained for all three of these metals.

5.2.1 Isolated Thermocouple Comparison

The temperature change at the isolated thermocouple shows good agreement between experimental and analytical results. With the thermocouple located 0.5 cm from the probe,

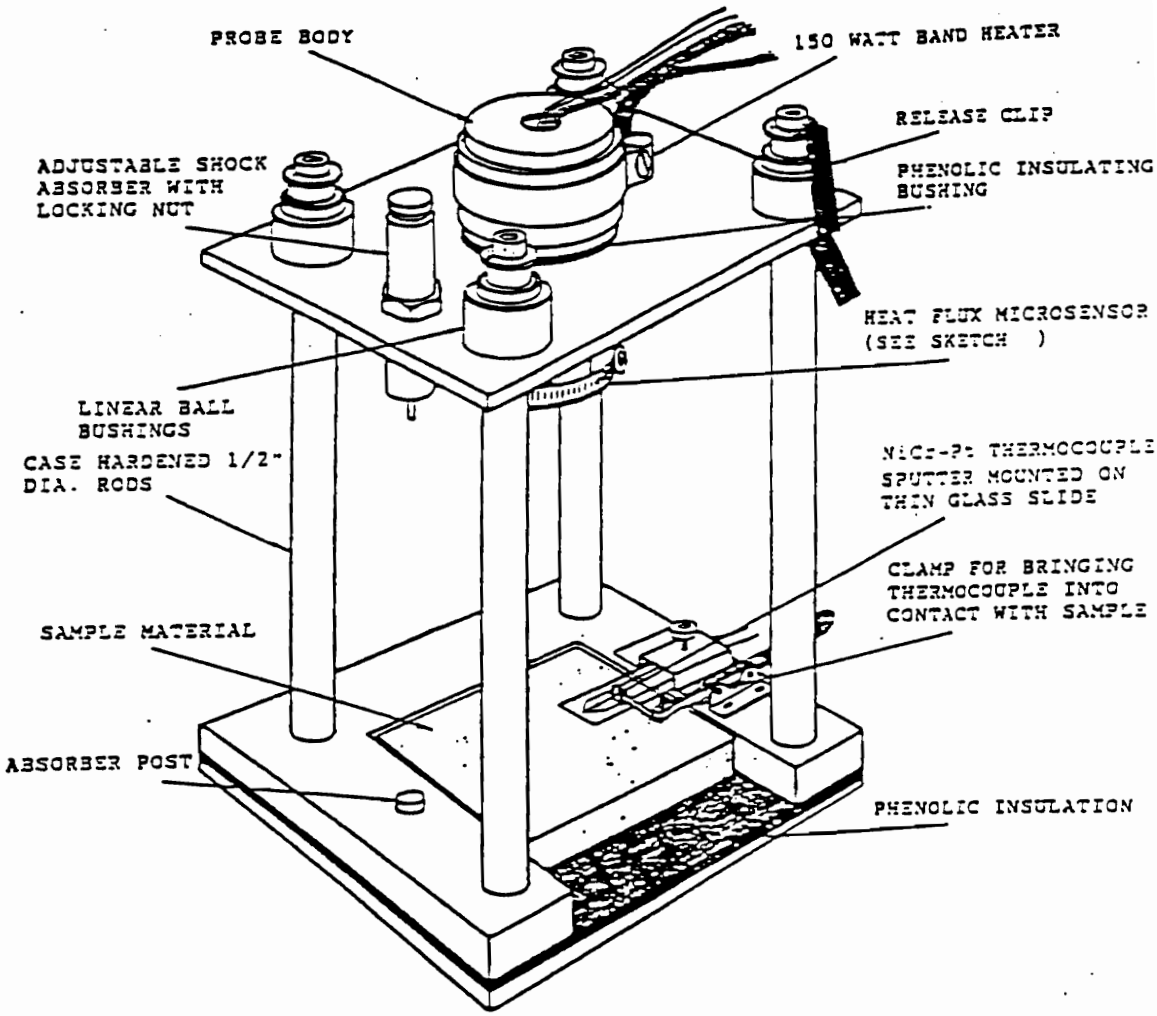

Fig. 17. Thermal Conductivity and Diffusivity Apparatus

Table 2. Material Property Data

Material Prop.	stainless steel 304	hard bus-bar copper	6061 T-6 aluminum	pure copper	pure aluminum
k (W/m-K)	14.9	390.9	154.8	401.0	237.0
α $(m^2/s) \times 10^{-6}$	3.9	113.9	65.6	117.0	97.1
c_p (J/kg-K)	477.0	385.2	870.0	385.0	903.0
ρ (kg/m^3)	7900.0	8912.9	2712.6	8933.0	2702.0

the program predicted that Al and Cu would start to show a ΔT almost immediately upon contact between probe and material (see Fig. 18). This is explained by the high thermal diffusivity of the two materials. Stainless steel was predicted to have about a 1 second delay before the change in temperature occurs due to its extremely low, for metals, thermal diffusivity. It also shows an obvious period where the ΔT vs. time curve is concave upwards. This pattern exists for the other two metals, but occurs an order of magnitude faster on the time scale (between 0 - 1 second rather than 0 - 10 seconds), and is therefore not as apparent. For $q = 20.0$ W/cm^2, copper reaches a nearly steady value for ΔT of about 2 °C, aluminum of about 3 °C, and stainless steel is still rising sharply at 13.5 °C after 14 seconds according to the analytical program.

The experimental results match these trends, if not the exact magnitudes, closely (see Fig. 19). Aluminum and copper rise almost immediately and have very close to the same shape as the analytical curves. The ΔT for aluminum is also about 1.5 times bigger than ΔT for copper, also predicted analytically. Stainless steel shows about a 1 second delay, a slightly concave upward area, but does not rise as steeply as analytically predicted. After 14 seconds it only barely surpasses copper in magnitude. Similarly aluminum and copper

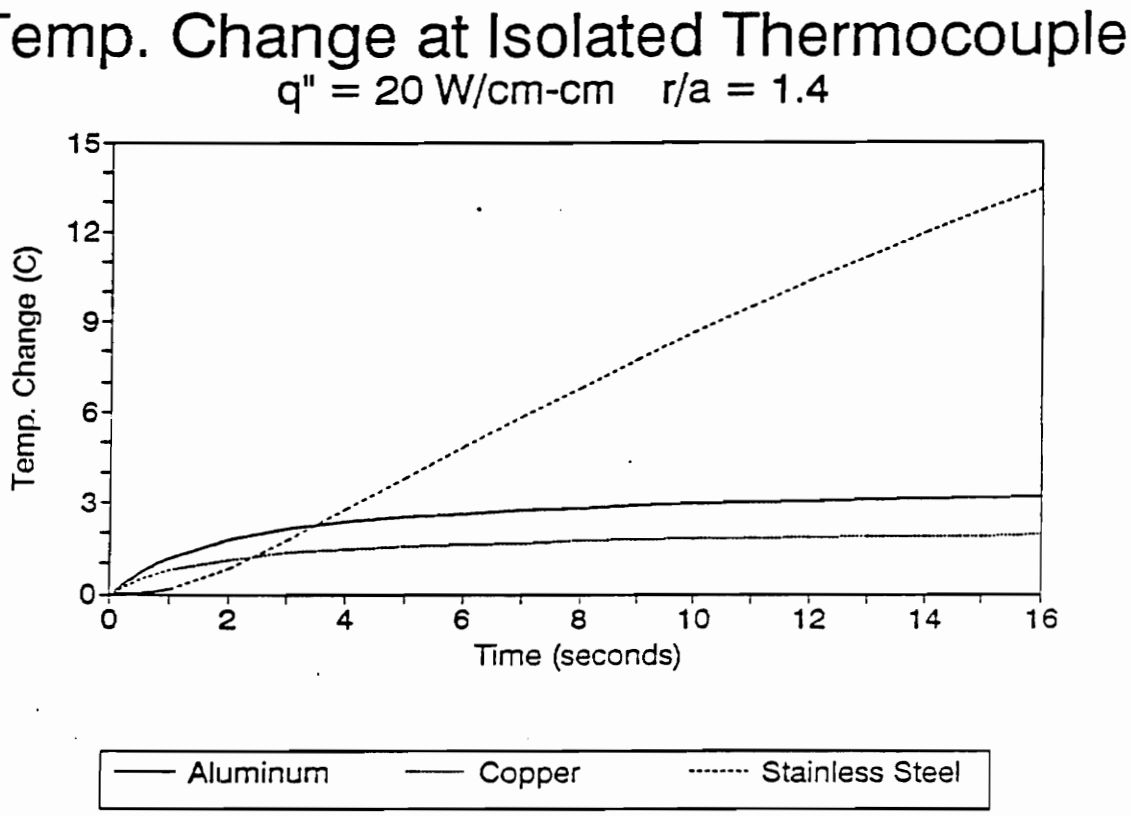

Fig. 18. Analytical Isolated Thermocouple Data

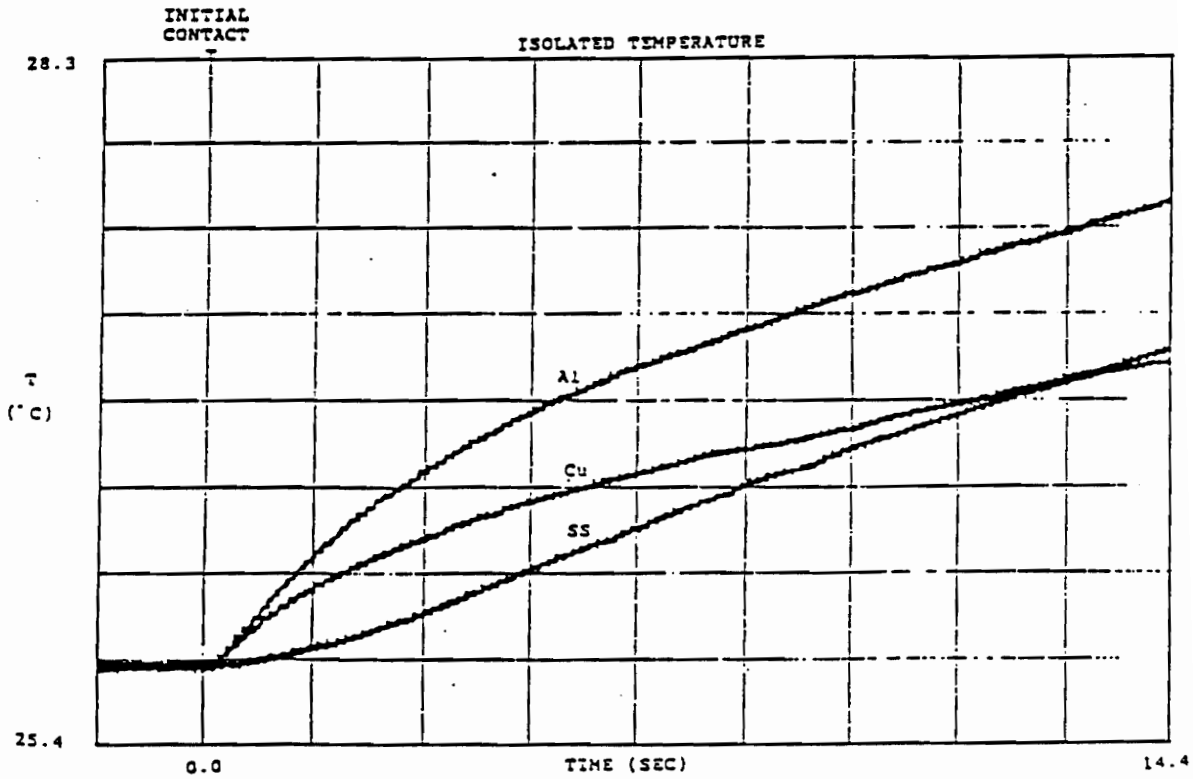

Fig. 19. Experimental Isolated Thermocouple Data

don't quite reach the magnitudes predicted after 14 seconds. The curves for aluminum and copper are rising at a faster rate experimentally than analytically at the end of the 14 second test.

Several explanations can be provided for these discrepancies. The biggest source of difference between the analytical model and the experimental testing is that the analytical solution assumes constant heat flux. Experimentally, however, the heat flux is actually decaying. Over the 14 second test period, therefore, the average heat flux in experimental tests will be lower than the constant analytical heat flux. More heat transfer would be expected in the analytical solution than in actual test results. A larger ΔT therefore would be logical in the analytical results. This, in fact, does occur for all three metals.

Another possibility is that there was an error in the placement of the isolated thermocouple. The analytical solution was done for a distance of 0.5 cm from the probe edge. Near the probe edge the temperature gradients are very high. Even a small error in placement of the thermocouple will have significant effects on the ΔT readings. If the thermocouple had been located as much as 0.254 cm further out, that would significantly contribute to the lower temperatures observed experimentally. It is important to note that the thermocouple location was held constant for all three samples.

Although the apparatus was designed and built as a highly precise instrument, there were some problems in obtaining good contact between the probe and sample. On some of the trials the probe would bind on one of the bearings, and the result would be poor coplanar contact at the probe-metal interface. The resulting air gap would significantly reduce the heat transfer to the sample since air is a good insulator.

This problem was partly solved by adding a layer of thermal paste to the probe face. This reduced the problem of poor contact by filling the air gap. The paste also served the dual purpose of isolating the gage from the metal samples and preventing the gage from shorting out. The problem of poor contact, however, was believed to be the main reason for the low repeatability of these experiments.

The finite difference model was used to test a constant temperature boundary condition between the metals and probe face (see Fig. 20). For this boundary condition, copper shows the highest ΔT at the isolated thermocouple, followed by aluminum and stainless steel. In reality, the actual boundary condition will be neither constant temperature nor constant heat flux. Therefore, the actual response at the isolated thermocouple should be some combination of the theoretical responses obtained for constant heat flux and constant temperature boundaries.

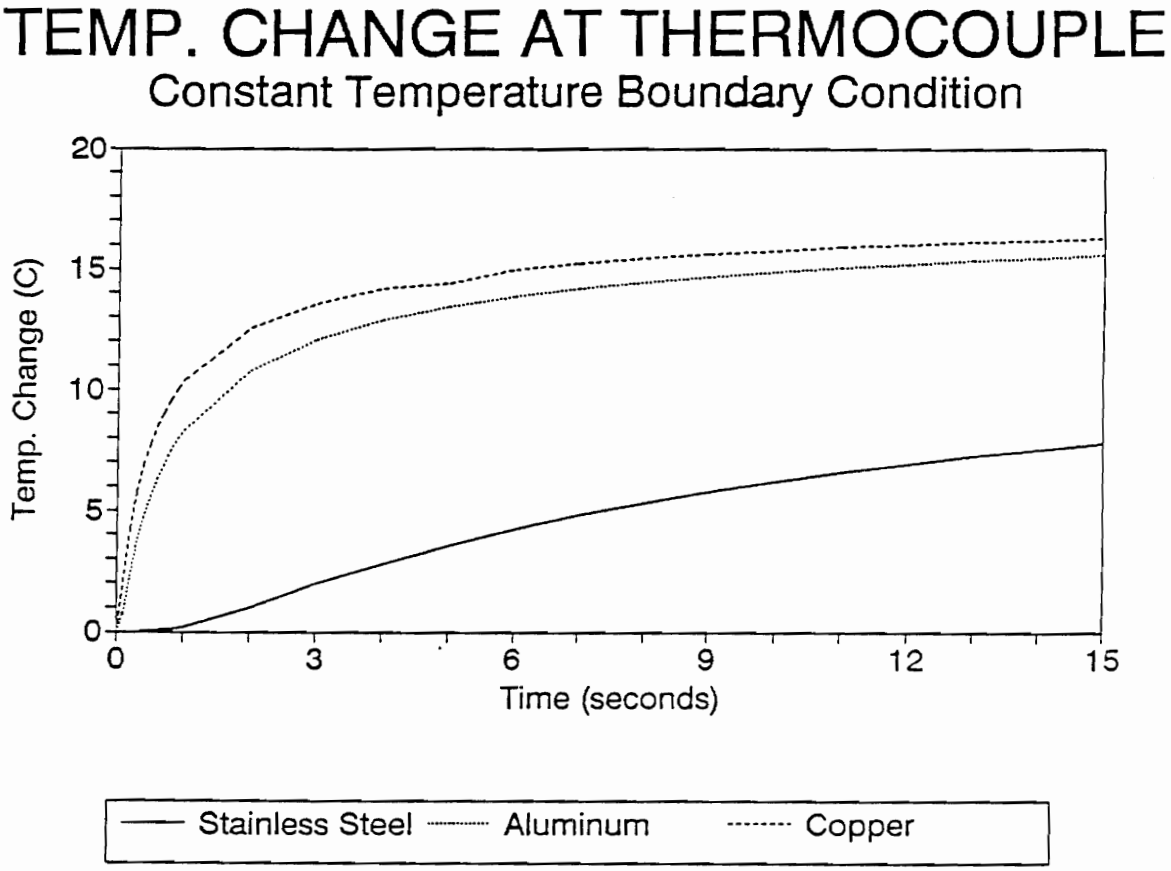

Fig. 20. Isolated Thermocouple Response for Constant Temp.

5.2.3 Heat Flux Comparisons

Although the analytical solution was developed for a constant heat flux source, the equation was reorganized so that a constant temperature difference could be specified, and the equation solved for the heat flux. This was done initially for the purpose of obtaining approximate results to help design the thermal conductivity probe. Once the finite difference program was completed, it was used to provide theoretical data to compare to the experimental data. In the finite difference program the probe-metal boundary was specified as a constant temperature difference boundary equal to 40°C. This was used since the probe was heated to 65°C and the metal sample was at ambient temperature, 25°C.

The experimental heat flux followed the trends of the finite difference solution. Contact resistance is not accounted for in this solution, and therefore the initial theoretical heat flux is infinite. This will not occur physically, but the program correctly predicts that the heat flux will start high and reduce to an almost flat curve at the end of the 16 second test. Fig. 21 shows the finite difference heat flux curves obtained for the three metals for a constant temperature difference of 40°C. Copper has the highest heat flux, followed by aluminum and then stainless steel. These trends are expected due to the decreasing

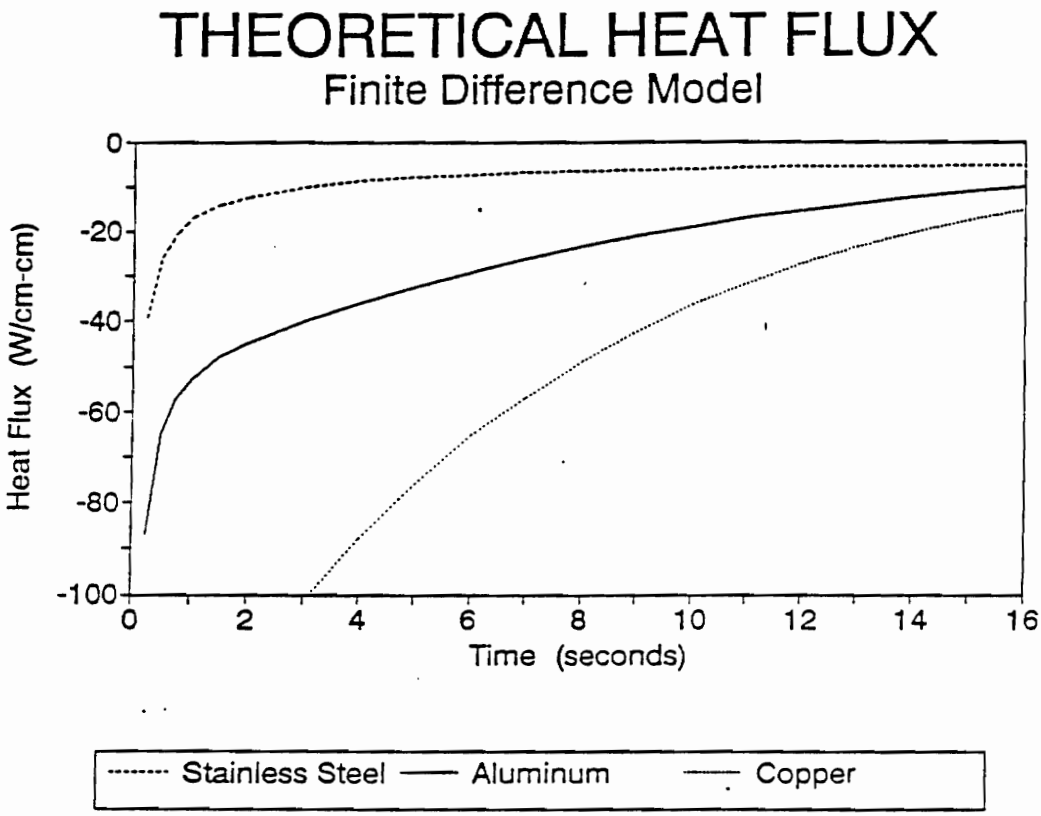

Fig. 21. Finite Difference Heat Flux Curves

thermal properties of these three metals.

The experimental results were not as clear cut. The initial peak was extremely dependent on how well and how quickly good contact was achieved. Weights were added to the plate holding the probe to try to improve the contact pressure with only satisfactory results. When good contact was established there was still an inherent contact resistance between the probe and the sample. The initial peak in heat flux is characteristic of the two materials in contact, and their respective surface finishes rather than the thermal properties of the metal.

In the experimental tests all metals showed heat flux peaks between 8 and 10 W/cm^2 (Fig. 22). The peaks all occurred under 1 second. It was difficult to differentiate between the different metals from the peak data alone. This may indicate that the contact resistance between the probe and the three metals is almost the same. Nevertheless, the experimental heat flux values are much smaller than the finite difference heat flux values due to the contact resistance.

After about 14 seconds all three experimental heat flux curves had reached a state where they were almost level as the finite difference curves had. Stainless steel reaches a value after 14 seconds of about 2.5 W/cm^2. This is significantly lower than aluminum and copper's value of about 4.0 W/cm^2

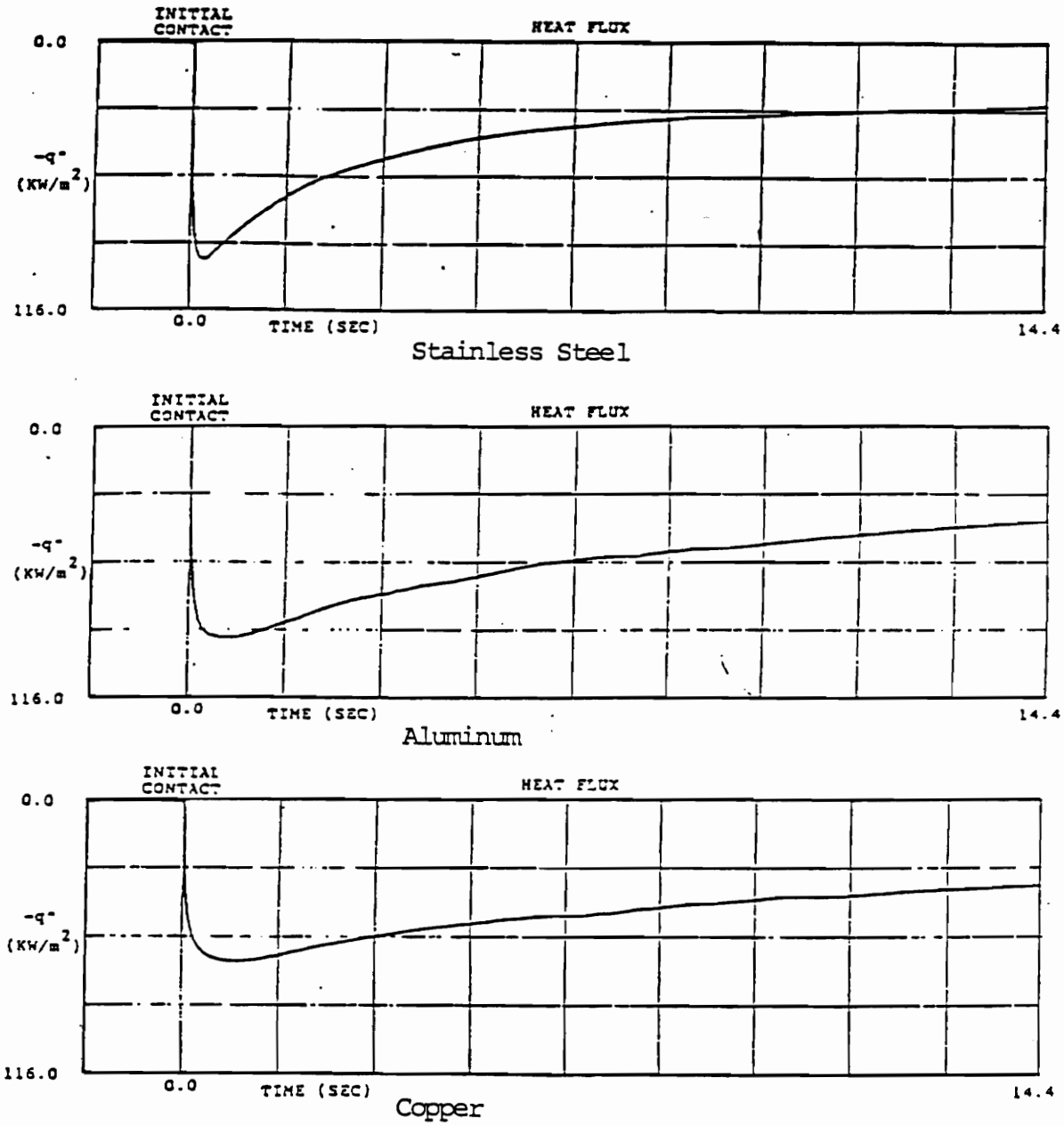

Fig. 22. Experimental Heat Flux Response

after 14 seconds. This is a surprising result since the thermal conductivity of copper is 391 W/m·K and of aluminum is 155 W/m·K. According to the finite difference solution, copper's heat flux curve should be larger than that of aluminum.

Although the heat flux curves appear to reach a condition where they are not changing after the test period of 14 seconds, this should not be mistaken as a steady-state heat flux. If given enough time the heat flux will reduce to zero.

Although the magnitudes of the finite difference heat flux curves are much higher than the experimental curves, the decay rates of the heat flux curves compare well. In both cases, copper decays at the slowest rate followed by aluminum and stainless steel. The differences in magnitude are attributed to the high contact resistance between the probe and metal.

5.3 Conclusions and Recommendations

Based on the detailed analytical and experimental study of the thermal conductivity apparatus, the following conclusions can be drawn:

- Thermal conductivity and thermal diffusivity can be extracted from the transient temperature and heat flux records.

- Due to assumptions used in the analytical model (no contact resistance, boundary condition differences) there are some discrepancies with the experimental data. However, both follow the same trends lending support to the solution validity and the probe accuracy.

- Good signals were obtained using the thermal conductivity and diffusivity probe although contact resistance and alignment problems with the apparatus affected repeatability.

The following recommendations are made for the future development of the thermal conductivity probe:

- If dependable values for k and α are to be obtained from heat flux and temperature data, precise instrumentation will be required to measure exactly the heat flux and temperature response. Algorithms for getting k and α from this data must be developed.

- The effects of contact resistance, temperature change of the probe, and finite sample size must be characterized and modeled in the analysis.

- As much of the measurement process as possible should be computerized and run automatically in order to avoid human errors.

- An insulative layer should be sputtered directly on the gage surface or another more repeatable method should be found to protect the gage from the metal sample

and to improve contact. This would avoid the mess and uncertainties of using thermal paste.

6. BIOPROBE

The finite difference model discussed in chapter 3 was used to perform a thermal analysis of the heat transfer between our specialized bioprobe and biological tissue. Theoretical knowledge of the heat transfer system was required to assist in designing the bioprobe and to predict experimental results.

Heat transfer from parts of the body are an important indicator of the health of the tissues in that area. Certainly no one would dispute the importance of a similar quantity, body temperature, to an individual's health. An irregular body temperature is a primary signal of sickness. Heat transfer can also be an indicator of disease. Abnormally high heat transfer from the skin surface could signal the location of a cancerous tumor. By monitoring the heat transfer from a damaged or diseased part of the body the recovery rate and process can be understood. Circulation patterns could even be determined since the gage is potentially sensitive to heat transfer differences due to changing blood flow. Changing blood perfusion to an area could indicate how well a transplanted organ is adapting, and how well a patient is doing during surgery. Eventually the gage could help detect disease, help in understanding the healing process, or help better condition athletes. All of

this will be determined noninvasively, without breaking the skin surface.

The finite difference program discussed in chapter three was applied to this problem. This provided a theoretical comparison for touching the specialized bioprobe to the skin surface. The theoretical and experimental results are presented in this section.

6.1 Validation of the Numerical Program

Several checks were performed on the program to ensure that it was being used correctly for this application, and that the data from the program was accurate. Even if all of the equations are correct the program can yield inaccurate results if the time step size or element size are chosen poorly. The steepest heat flux gradients as well as the highest heat flux occurs under one second. The time steps in this period must be small enough to accurately model this period. Moreover, it takes at least 10 steps through the program before accurate results are assumed. The time steps must be initially small, but can be increased with time once the heat transfer gradient decreases.

An additional factor to be controlled is the element size. Since tissue has low thermal diffusivity ($\alpha = 1.5 \times 10^{-7}$

m^2/s) and thermal conductivity (k = 0.5 W/m K), the heat transfer effects will not travel quickly through the tissue. The elements must be small enough so that several are in the region effected by the constant temperature boundary in order to give accurate results. Originally, square elements of side length = 0.3 - 1.2 mm were used. The length of the tissue-probe interface is 12.7 mm. These elements proved to be too large. They did not create a fine enough mesh in the axial direction, into the depth of the tissue, and the temperature and heat flux data was inaccurate. This occurred because after several seconds the cooling effect of the probe had only penetrated about a millimeter of tissue. Thus only two or three elements in the axial direction had been effected and this is not nearly enough to get accurate results.

If the square shape was maintained, but decreased in size to create the required number of elements in the axial direction, then so many elements would have been used that run time would be too long. The mesh needed to be refined only in the axial direction. The radial direction had a sufficient number of elements with just 10 elements in each row under the probe surface and equally sized elements outside the probe. This was determined by doubling and then tripling the number of elements in the radial direction. When refined in such a way the temperature values at each node converged to the same

value.

The problem was solved by making the element length in the axial direction some fraction of the radial length. For most times of interest simply making the axial side 1/10 of the radial side was sufficient (see table 3). For extremely small times, .01 seconds or smaller, an even greater aspect ratio was required. For many cases there are several different possible combinations of number of elements and ratio of sides that converge correctly. To determine an optimal element size the mesh was refined several times until the nodal values had converged, and further refining of the mesh had no effect. This technique provided accurate results without increasing the run time.

To further ensure that the model was giving accurate results, it was compared to the one dimensional semi-infinite body solution for time dependent heat flux. This solution is given by:

$$q=\frac{k(\Delta T)}{\sqrt{\pi \alpha t}} \tag{6.1}$$

The heat flux at the center of our model closely follows this equation up to approximately 30 seconds. The two dimensionality of our solution effects the heat transfer at the probe center for larger times.

A second check was performed by converting the constant

Table 3. Time Step and Element Size

TIME (seconds)	$\Delta t'$ time step size	# STEPS	MESH SIZE	RATIO radial: axial
0.001	2.5×10^{-8}	20	100 x 100	100:1
0.010	2.5×10^{-7}	20	80 x 80	10:1
0.100	2.5×10^{-6}	20	40 x 40	10:1
1.000	2.5×10^{-5}	20	20 x 20	10:1
10.000	2.5×10^{-5}	200	20 x 20	10:1
100.000	2.5×10^{-4}	200	20 x 20	1:1

temperature boundary condition in the numerical program to a constant heat flux. If zero perfusion is assumed in the model, then the two dimensionality of the model can be checked with the 2-D analytical solution discussed in chapter three. The finite difference model did closely follow the trends and magnitudes of the analytical model. The resulting temperature difference of both models at the center, edge, and 0.32 cm from the edge of the probe are very similar (see Figs. 23 - 25). The finite difference results in these figures were extrapolated from the elements near the skin surface to get the values at the surface. From these results the finite difference model accurately predicts 2-D heat flux.

6.2 Results of Model Solutions

Once the validity of the model had been proven, several tests were performed with the program. The effect of blood perfusion on the heat flux was the most important test. If changes in blood perfusion rates could be detected by the bioprobe in the form of changing heat flux rates then the bioprobe would truly be a breakthrough instrument.

Blood perfusion, blood flowing through biological tissue, maintains the tissue at approximately 37°C. The probe surface is approximately 15°C. When touched to the skin surface the tissue area will be cooled. A high blood flow rate will

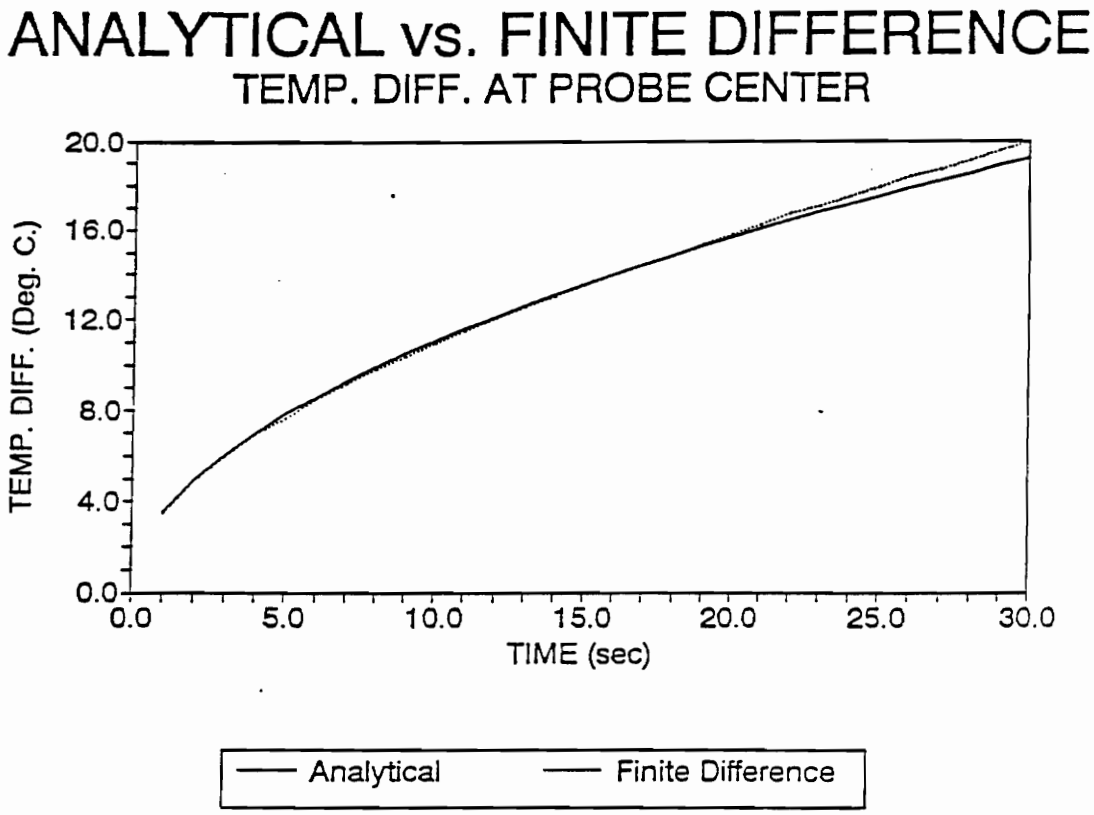

Fig. 23. ΔT Comparison at Probe Center

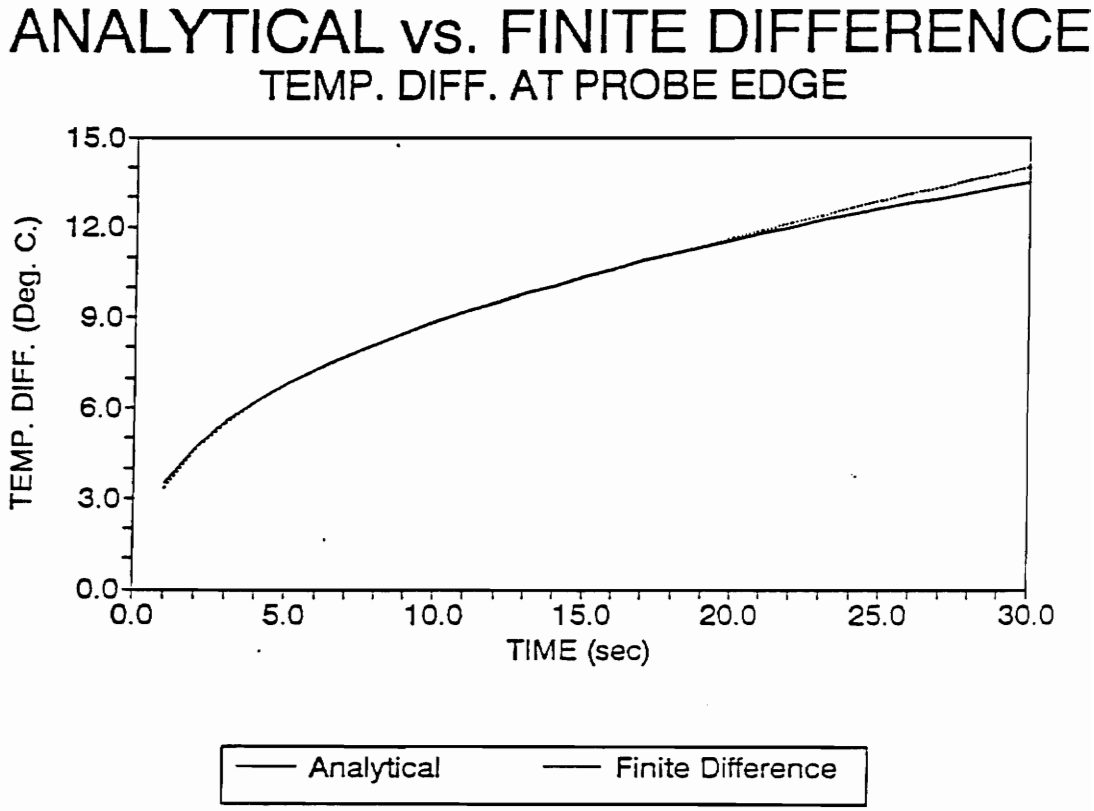

Fig. 24. ΔT Comparison at Probe Edge

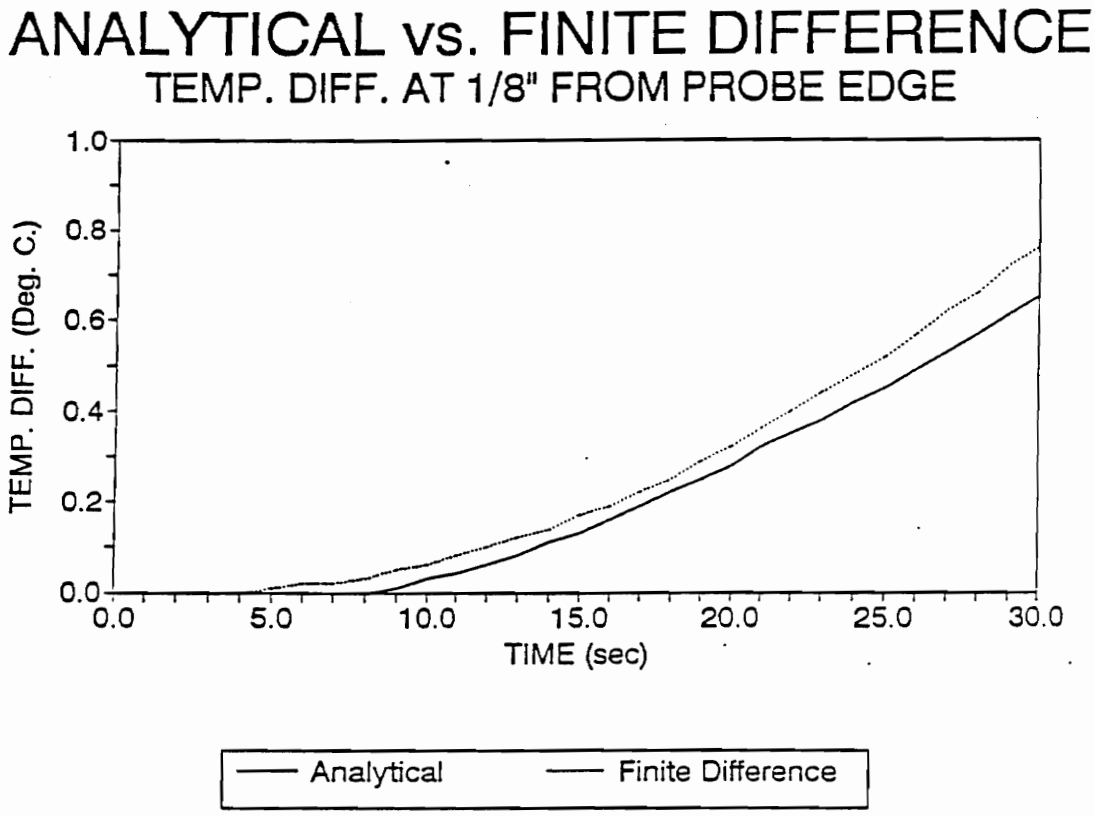

Fig. 25. ΔT Comparison 1/8" from Probe Edge

replace part of the volume of cooled tissue with warm blood from the rest of the body more often than a low blood flow rate. Tissue with high blood flow rates will tend to stay warmer than tissue with low blood flow rates. Therefore, higher heat fluxes will occur in tissue with higher blood flow rates.

Perfusion rates in humans range from 0.0005 - 0.05 ml/ml/sec. Blood perfusion at rest is approximately 0.002 ml/ml/sec. Several factors can effect this rate: exercise, disease, drugs, age, body part, and heating or cooling of the tissue.

One of our tests was to change the perfusion rate of the model and examine this effect on the resulting heat flux. Several perfusion rates from 0.0000 ml/ml/sec to 0.05 ml/ml/sec were tested (see Fig. 26). At times under three seconds it is nearly impossible to distinguish between the different perfusion rates. As time increases up to 30 seconds, the curves do spread out and show significant differences in heat flux for the different perfusion rates. Currently our gages can measure heat flux to an accuracy of 0.025 W/cm^2. Referring again to Fig. 26, it is apparent that the difference in heat flux between 0.000 and 0.002 ml/ml/sec perfusion rates is approximately 0.03 W/cm^2 after 30 seconds. The difference between 0.002 and 0.005 ml/ml/sec

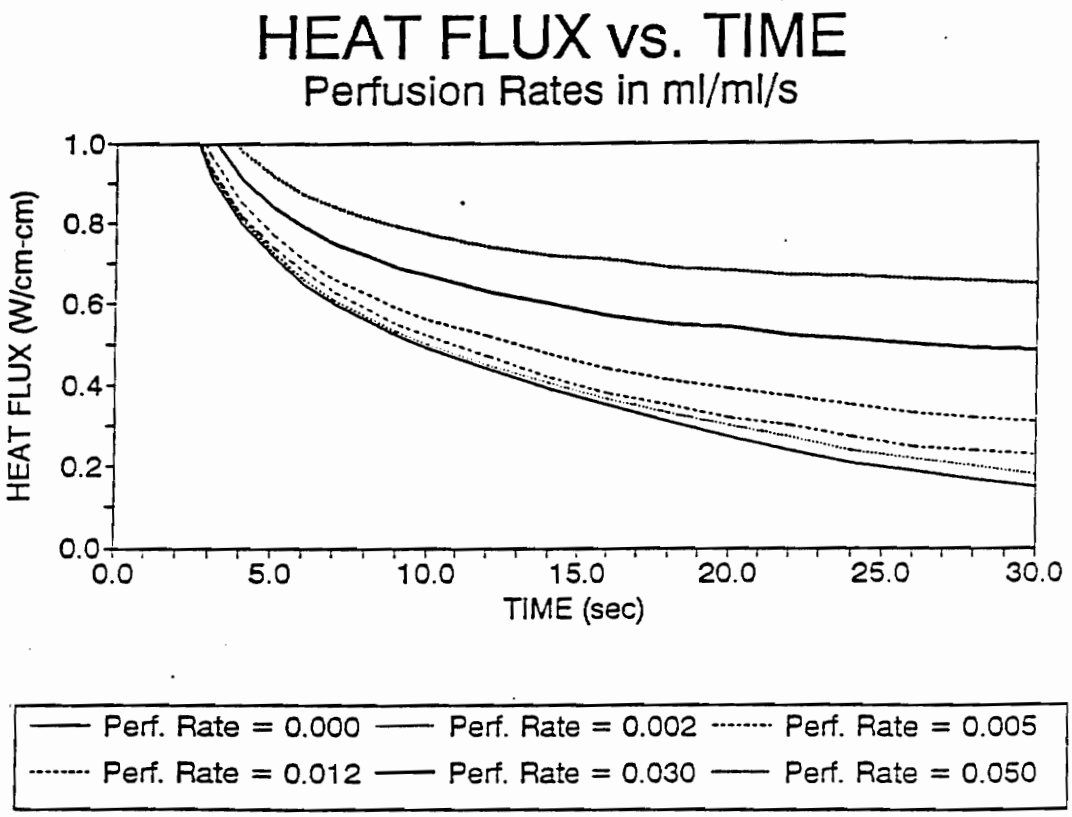

Fig. 26. Heat Flux for Different Perfusion Rates

perfusion rates is 0.04 W/cm^2 after 30 seconds. Although these differences are detectable, an increase in perfusion of 150% (from 0.002 to 0.005 ml/ml/sec) only results in an increase in heat flux of 25 %. Heat flux appears to be a relatively weak function of perfusion rate.

Rapid and large changes in blood flow rates are common. It would not be uncommon for blood flow to increase by as much as 10 - 15 times or more in a specific part of the body. According to the model this type of change could be detected.

Studying the heat flux trends for more than 30 seconds however would not be practical. At about this time the cool probe face will cause the blood vessels near the surface to contract and decrease the blood flow to this area.

Additionally, the model was used for a case of no blood flow for a period of time followed by a sudden impulse of a rather large perfusion rate. This would simulate for example blood flow in an arm being constricted by a tourniquet and then loosened to allow the blood flow to rush through. Figure 27 shows the response of the heat flux for three different periods of constriction. In actuality, the curves probably would not react so quickly due to physiological characteristics of blood vessels not included in the model. However, the change in heat flux appears to be great enough to be detected by the bioprobe.

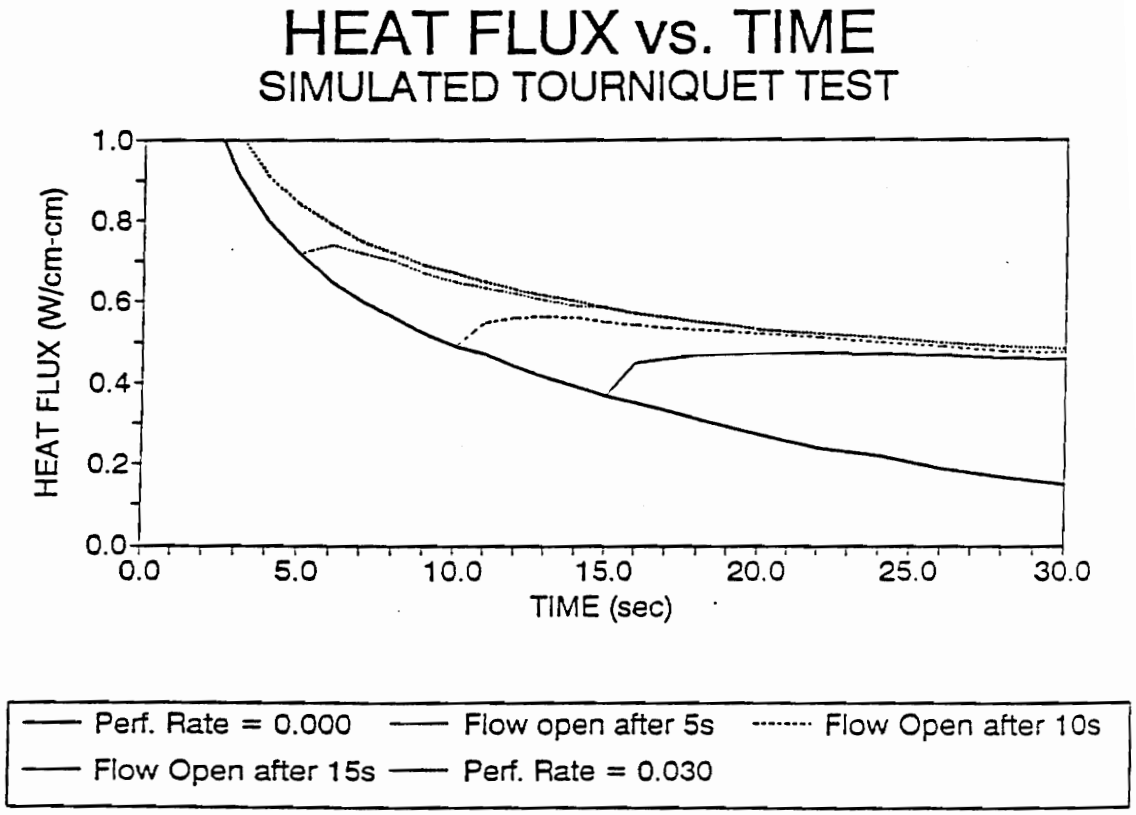

Fig. 27. Finite Difference Tourniquet or Pressure Cuff Test

6.3 Experimental Tests with the Bioprobe

The idea of determining blood flow rates by measuring heat flux was tested with the bioprobe. Two dogs were used for this testing. The first dog was significantly smaller than the second dog. The first dog did not have much muscle and soft tissue around the bones of its limbs. This made good contact between the probe face and the skin surface difficult. Good contact was obtained with the second dog because it was larger and more muscular. The second set of tests were also more successful because the experience of having already performed one set of tests proved very helpful. For these reasons only the tests on the second dog are presented.

Very little can be concluded about the different perfusion rates simply by looking at the heat flux curves. They must be analyzed for characteristics that are currently believed to be important indicators of perfusion. Much more detailed study of the heat flux curves will be necessary to pinpoint exact values for perfusion. Currently only trends in changing perfusion rates can be identified.

The slopes of the heat flux curves were calculated for the time interval from 2 to 5 seconds after the initial peak. This period was chosen because the natural log of this part of the curve was linear for all of the experimental tests. The slope in this region should be an indication of perfusion,

decreasing for increasing perfusion.

Additionally, the experimental curves were all integrated from 2 to 22 seconds after the initial peak. The areas under the curves should be larger for larger heat fluxes. Therefore, when blood perfusion is greater the integrated heat flux should be larger.

The peak of the heat flux curves is not given much attention in the analysis of the curves. At this time the heat flux is a function of how steadily and quickly contact is achieved with the skin and probe. Peak heat flux data is also largely dependent on the contact resistance between the probe and skin; blood perfusion is probably not a factor at this time.

6.3.1 Bioprobe Description

The bioprobe can be seen in Fig. 28. It consists of a 10.2 cm long solid aluminum cylinder 2.86 cm in diameter. One end is machined to hold the substrate with the heat flux gage. The gage leads are fed back through the length of the probe and emerge on the opposite end. Also machined into the aluminum probe body are two water-cooling pathways. These are simply holes which tap water (14 - 15°C) flows through. The holes criss-cross near the backside of the gage substrate. The holes are connected to plastic tubing outside of the probe

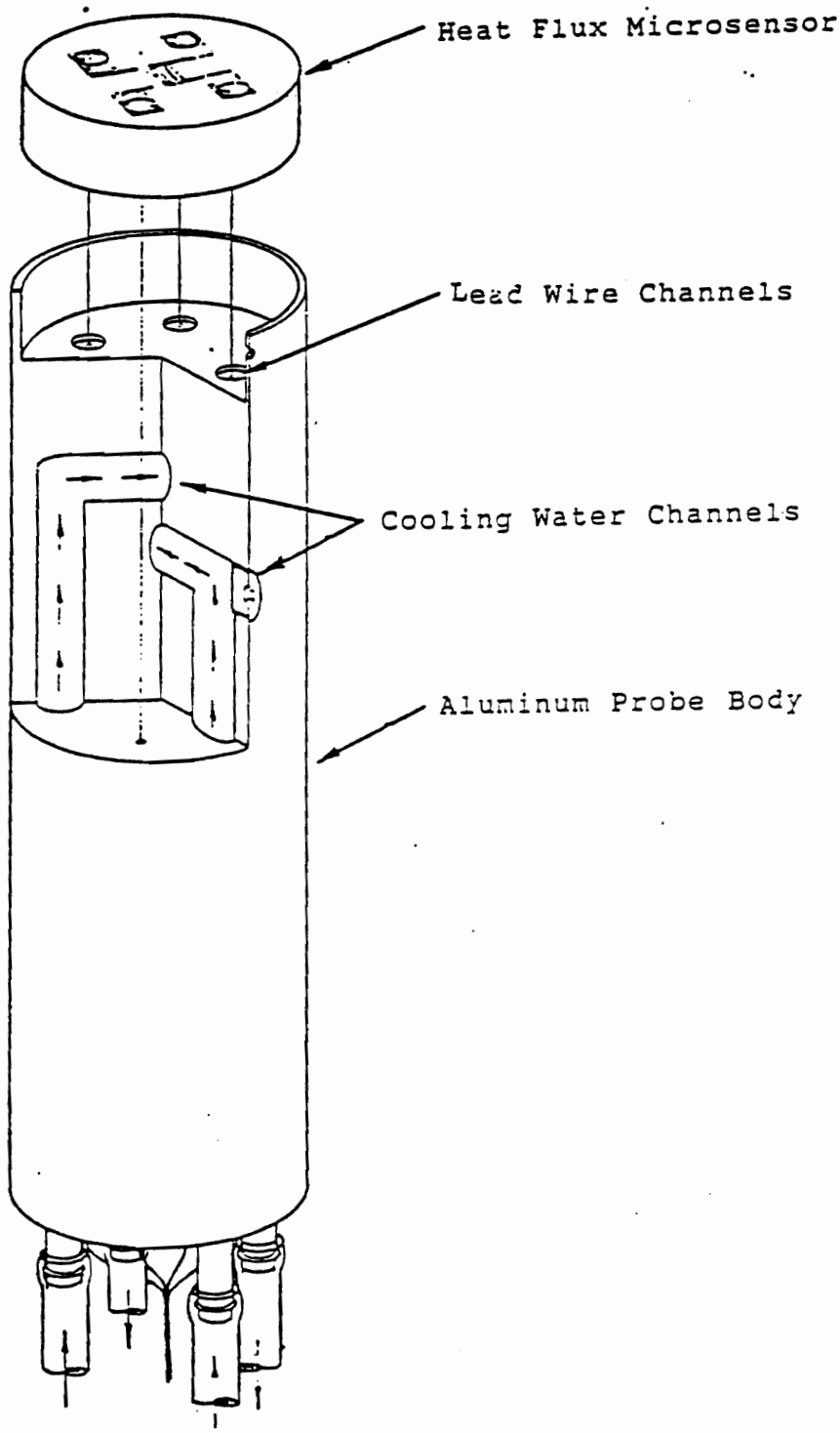

Fig. 28. Bioprobe

which run to a tap water source and a drain. This is an effective method as it cools the entire probe and gage to the water temperature within a minute. The water cooling system and the solid aluminum cylinder is what differentiates the bioprobe from previous microsensor probe devices.

6.3.2 Test Preparation and Procedure

The two dogs were tested on different days approximately a week apart. Since the probe requires very steady placement during a test, it was necessary to anesthetize the dogs.

The dogs were shaved in the test areas so that good contact with the skin surface could be obtained. Both forelimbs, part of the stomach and one hindlimb was shaved and cleaned thoroughly. Finally, Nair was applied to get the smoothest possible surface.

The procedure followed to run a test was fairly quick and simple. The cooling water was turned on to the desired flow rate. Usually it was just left on at a constant flow for all of the tests. About a minute was allowed for the probe to reach an equilibrium temperature with the water. The HP Digital Signal Analyzer was set in time capture mode. The duration of the tests was between 25 - 30 seconds.

To perform an actual test the probe is held as close to the base as possible to avoid raising the gage temperature due

to conduction from the experimenter's hand. The bioprobe must be placed swiftly yet very steadily in contact with the desired body location. The whole gage surface should be in contact with the skin surface. Enough pressure should be applied to get good contact, but no more than necessary. The pressure must be kept as constant as possible for the duration of each test, and from test to test as well.

Comparative tests were done in an attempt to find the ideal water flow rate and the ideal pressure with which to apply the bioprobe to the skin surface. Water flow was tested at the rates 0, 1.5, 3.0, and 6.0 liters per minute. The higher water flows should keep the gage cooler when touched to the warm tissue surface. The curves in Fig. 29 show that the temperature is lower with higher water flow rates. Figure 30 shows that the effect of different flow rates on the heat flux is not measurable. The flow rate chosen for the rest of the tests was 3 liters/minute.

A very critical factor in the tests was how hard the probe face should be pressed onto the skin. If too little pressure was applied then good contact between the two surfaces may not be obtained. Air could be between the gage and skin which would significantly effect the signal. It was also theorized that pressing too hard might decrease the blood flow to the test area. It is unacceptable to affect the blood flow in this manner since it is the quantity of interest.

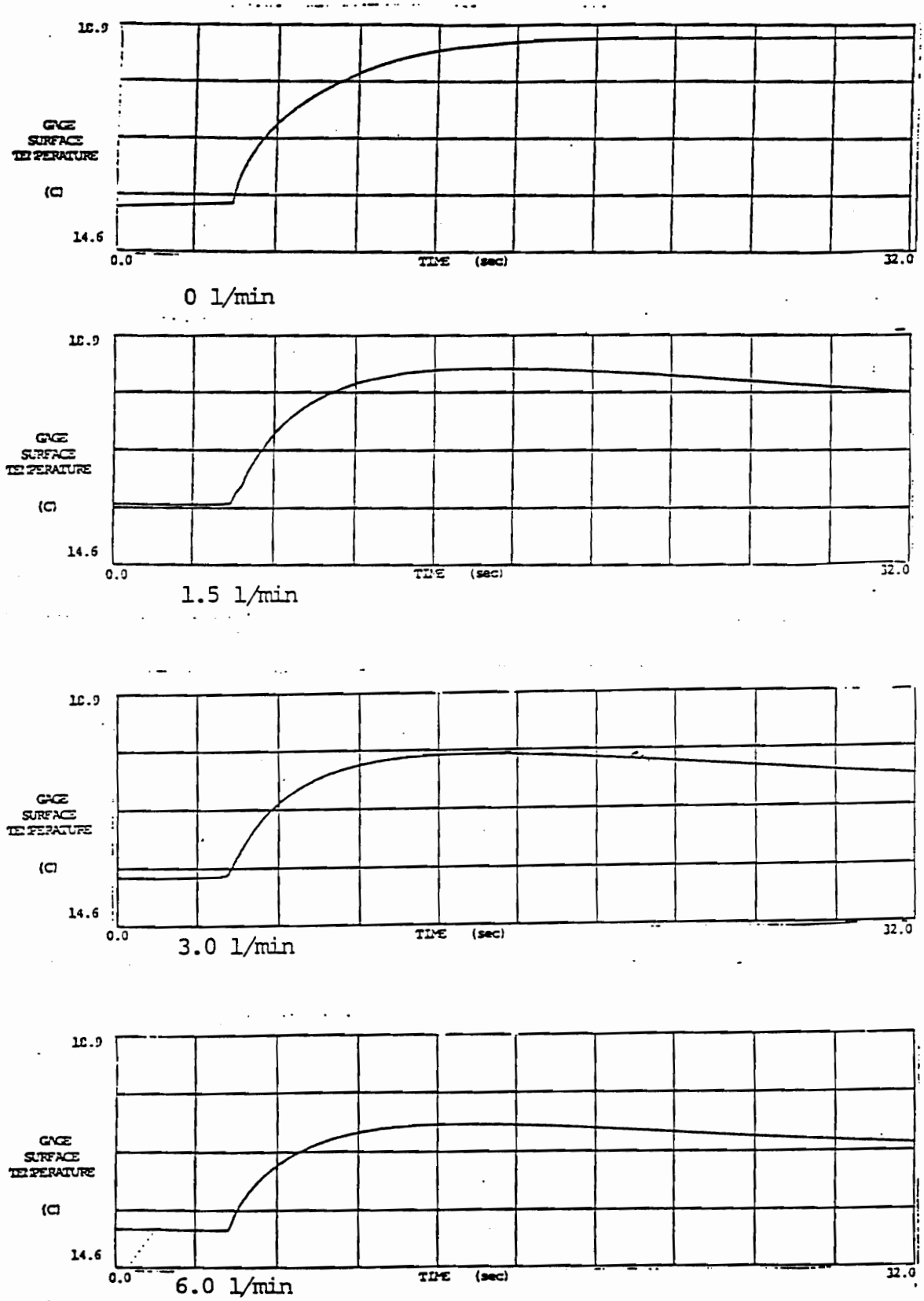

Fig. 29. Temperature Curves for Different Flow Rates

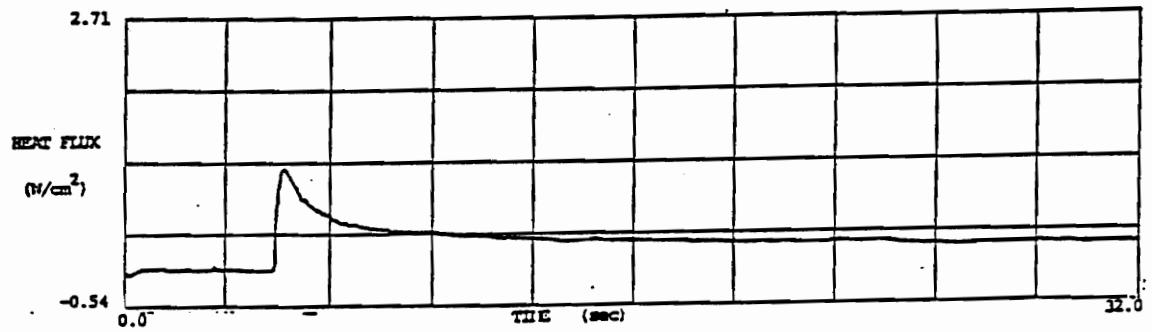

0 l/min

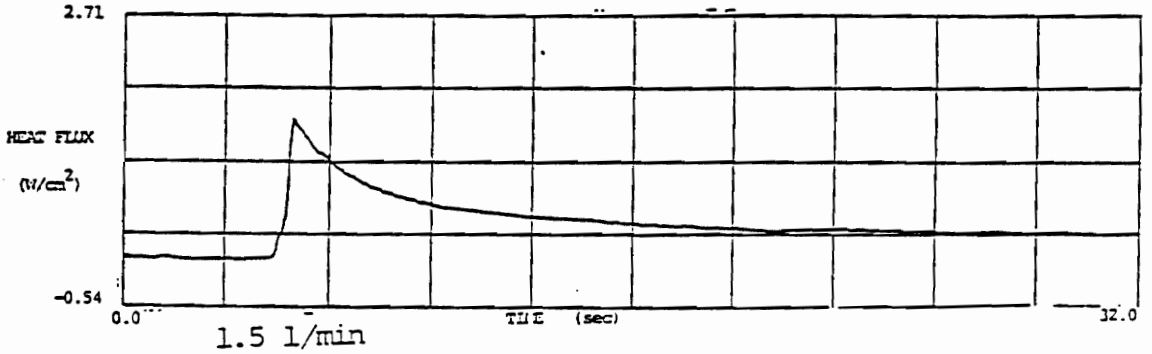

1.5 l/min

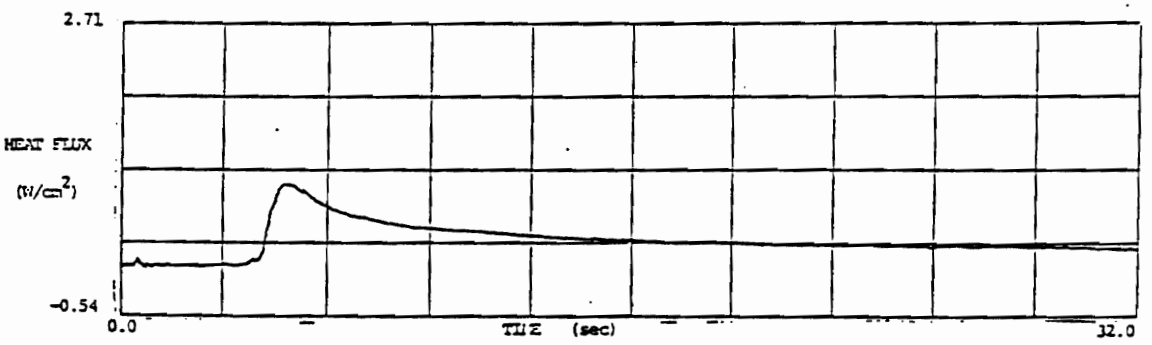

3.0 l/min

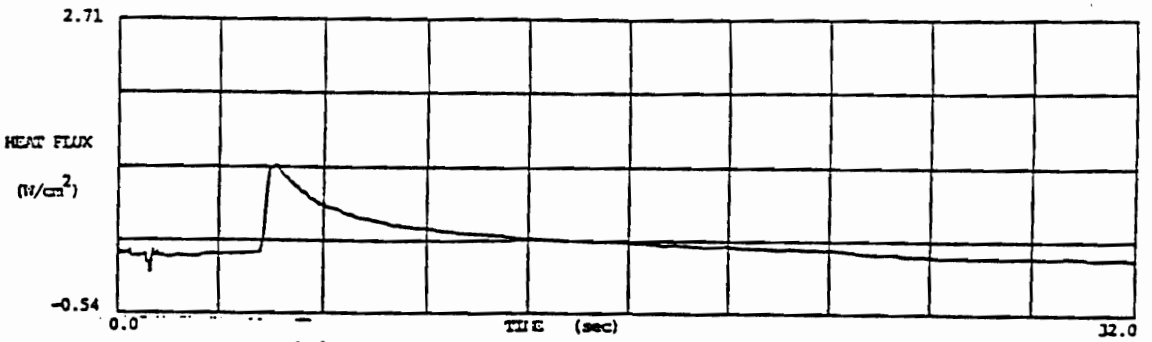

6.0 l/min

Fig. 30. Heat Flux Curves for Different Flow Rates

Additionally, there is a small possibility that the gage could start acting like a strain gage if it is pressed too hard to a surface. However, this is more likely to occur when testing a hard metal surface rather than soft tissue.

The curves in Fig. 31 show one test with high contact pressure and one test with low contact pressure. The remaining tests were done with a pressure about halfway between these two pressures. These figures suggest that the more dangerous case is applying too little pressure. The signal in this test is much lower than the normal or high pressure tests. Conversely, the normal and high pressure tests show close agreement in the heat flux signals. This seems to suggest that applying too much pressure may not have as drastic of an effect as initially expected. The temperature curves increase with increasing pressure as expected.

6.3.3 Tests on Different Body Parts

The majority of the tests were done on the right front leg of the dog about 5 cm below the "elbow". Different body parts were also tested to compare perfusion rates throughout the body. The other two test areas were the right hindlimb and the left lower stomach area. The heat flux and temperature signals of these two areas indicate that the

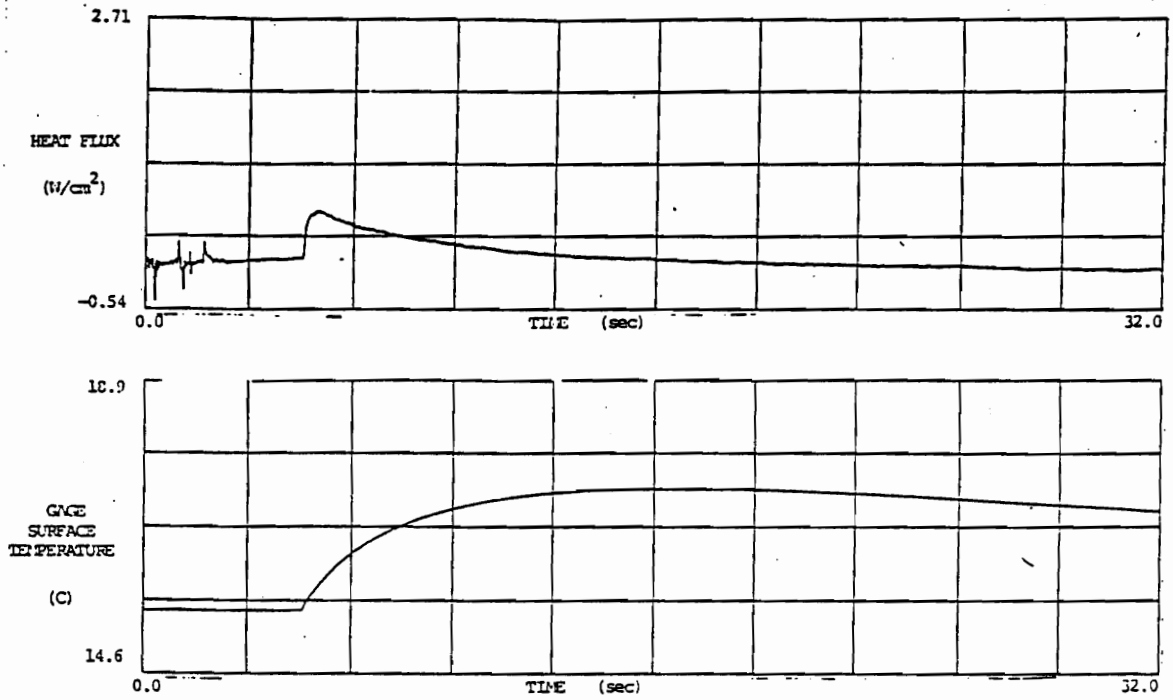

Low Pressure

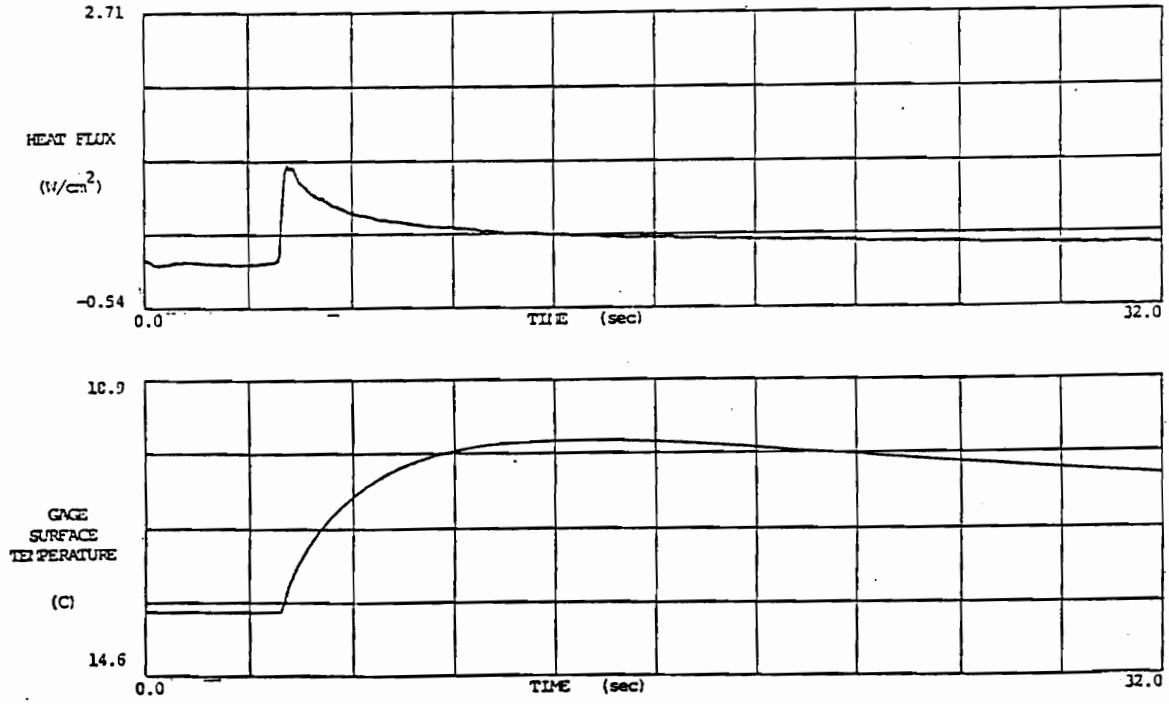

High Pressure

Fig. 31. High and Low Contact Pressure Tests

perfusion of the stomach and hindleg is similar to that of the front leg (see Fig. 32).

6.3.4 Pressure Cuff Tests

The pressure cuff consisted of an inflatable tube that was wrapped around the right forelimb of the dog just above the area where the heat flux was to be measured. The tube was inflated up to 200 mm Hg and was left on for five minutes. This was ideally supposed to cut off all blood flow to the region. At this time the probe was applied to the skin surface, and at about five seconds into the test the valve holding the air was opened. This released the pressure on the forelimb, and should have resulted in a large increase in blood perfusion in the skin under the probe surface. According to the finite difference program there should have been a detectable change in the heat flux due to the sudden change in perfusion (refer to Fig. 27). In actuality, Fig. 33 shows that the heat flux signal does not show any change due to the increase in blood perfusion.

This can be explained by several factors. The pressure cuff may not have been restricting blood flow as much as estimated. Additionally, the program does not account for the response of blood vessels to being constricted and released. Possibly the vessels take several seconds to expand and let

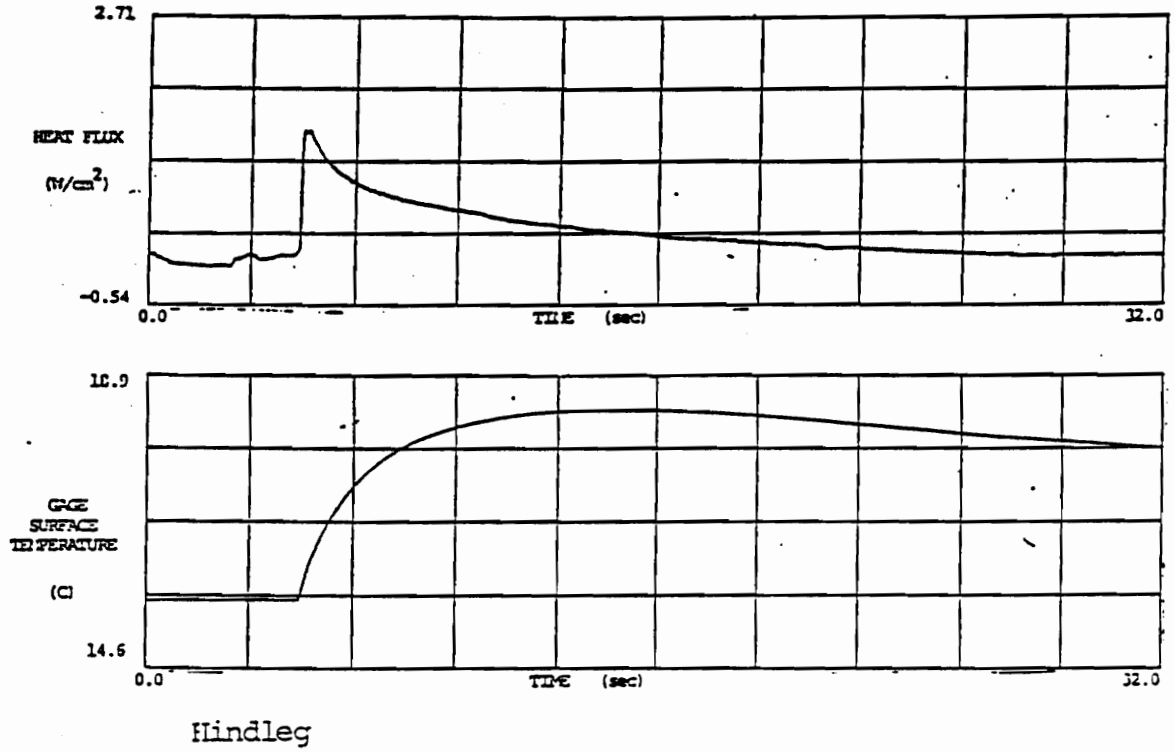

Hindleg

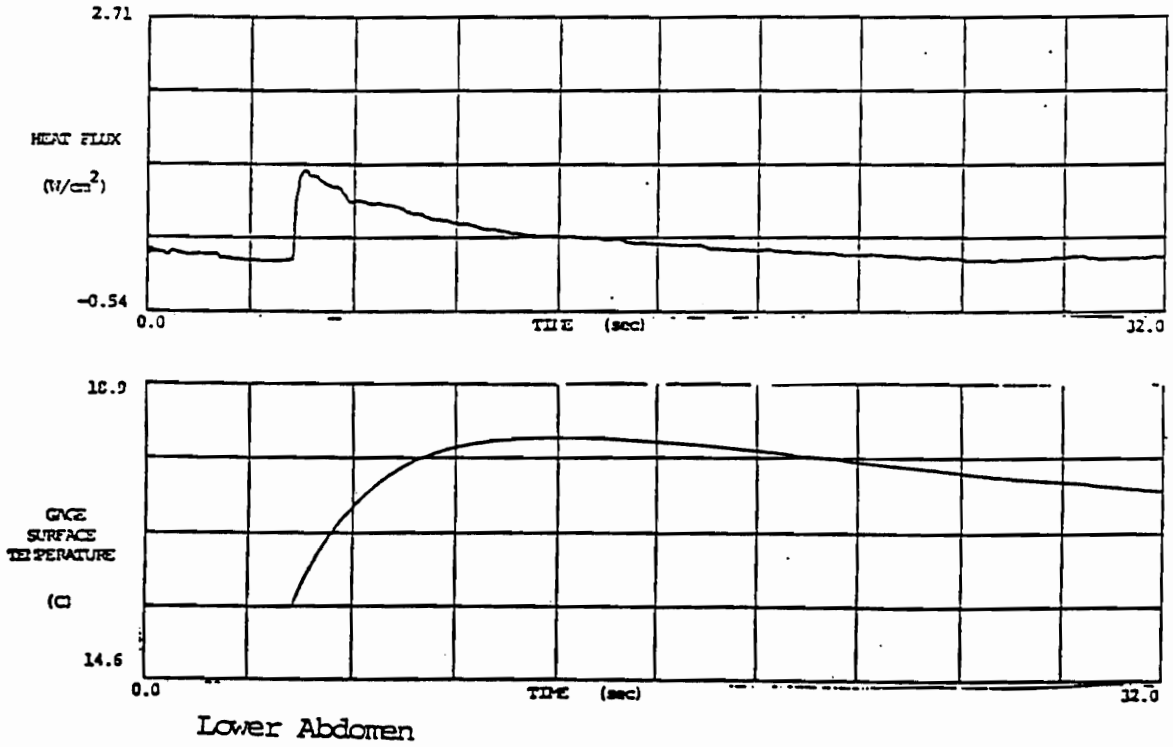

Lower Abdomen

Fig. 32. Tests on Alternate Body Parts

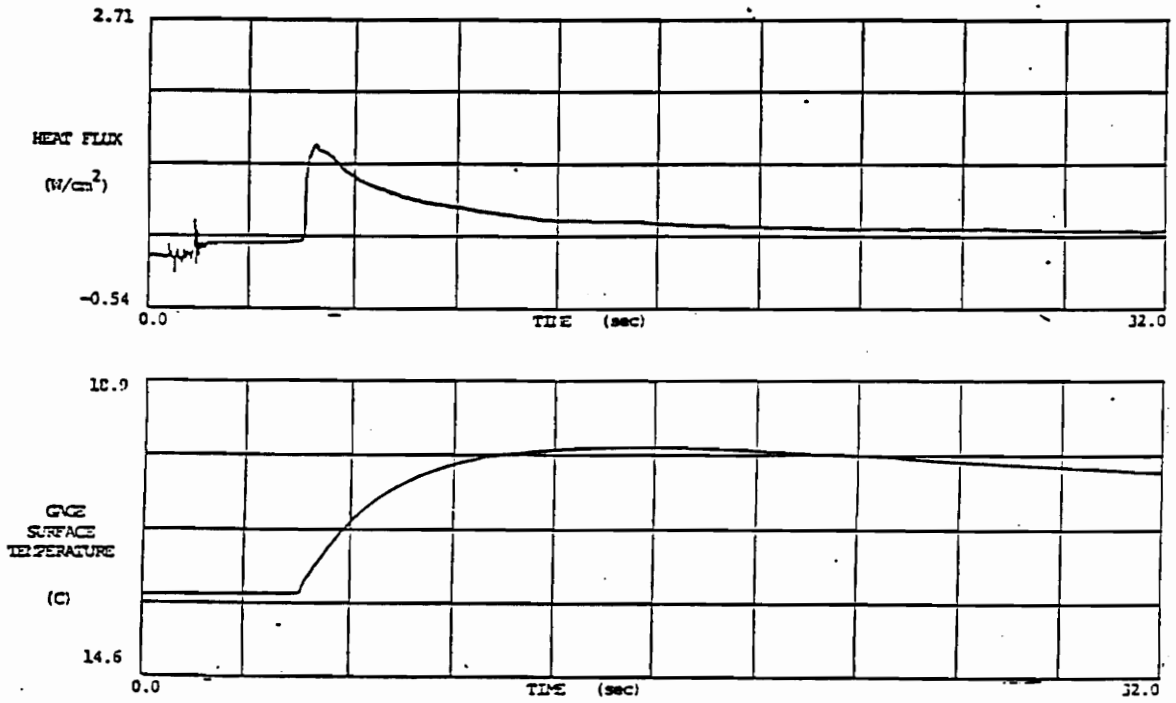

Fig. 33. Pressure Cuff Test

blood flow through, so that the rise in perfusion is gradual and not instantaneous as was modeled in the program. Another possibility may be that the location of the pressure cuff may have been chosen poorly. Recall that the cuff was located higher on the leg than the probe. Since arterial blood generally flows further from the surface than venal blood it is possible that the cuff only stopped venal blood. Therefore, during the five minutes that the cuff was on, blood continued to fill the front leg, but did not flow out. When the cuff was released there would be no sudden rush of blood to the skin under the probe because the veins near the surface were already full of blood. It would appear to be a wiser to locate the probe just above the cuff rather than just below it.

6.3.5 Vasodilator Test

The final set of tests performed involved injecting the dog with a 1.44 ml bolus of Verapamil. This drug expands the blood vessels and should increase the perfusion throughout the body. The drug has an estimated half-life of about 20 minutes, but takes about 4 minutes for the effects to start to occur.

Figures 34 to 37 show the heat flux and temperature for several times up to 30 minutes. Table 4 summarizes the

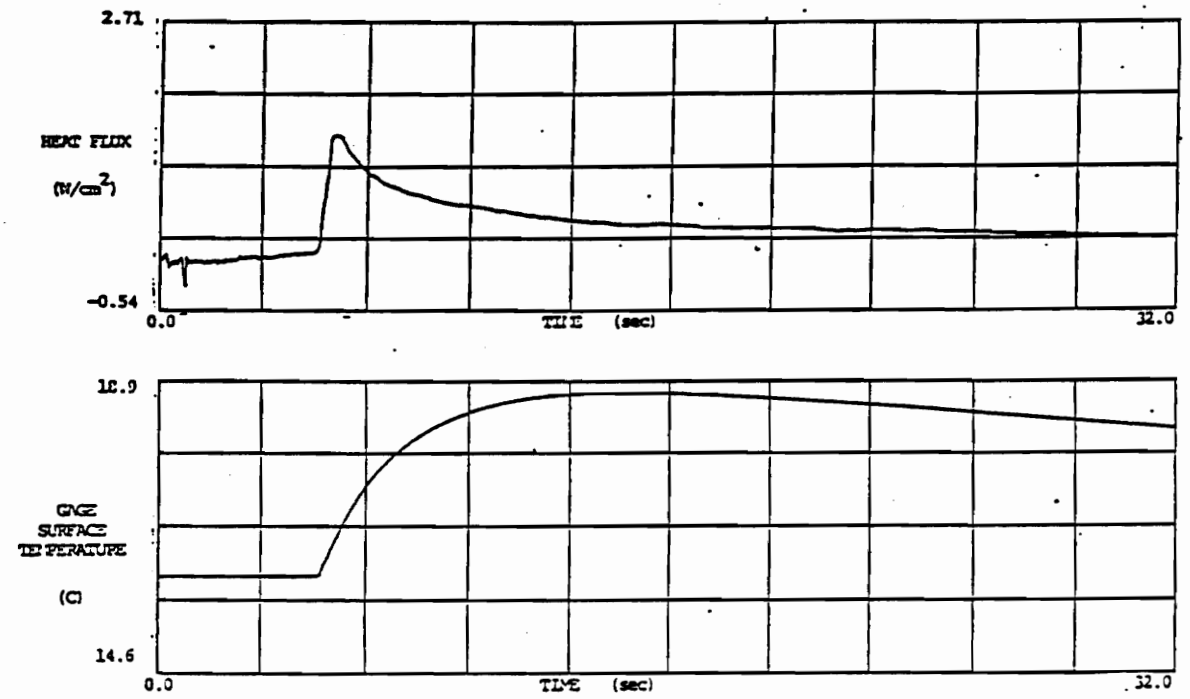

1 min. after injection

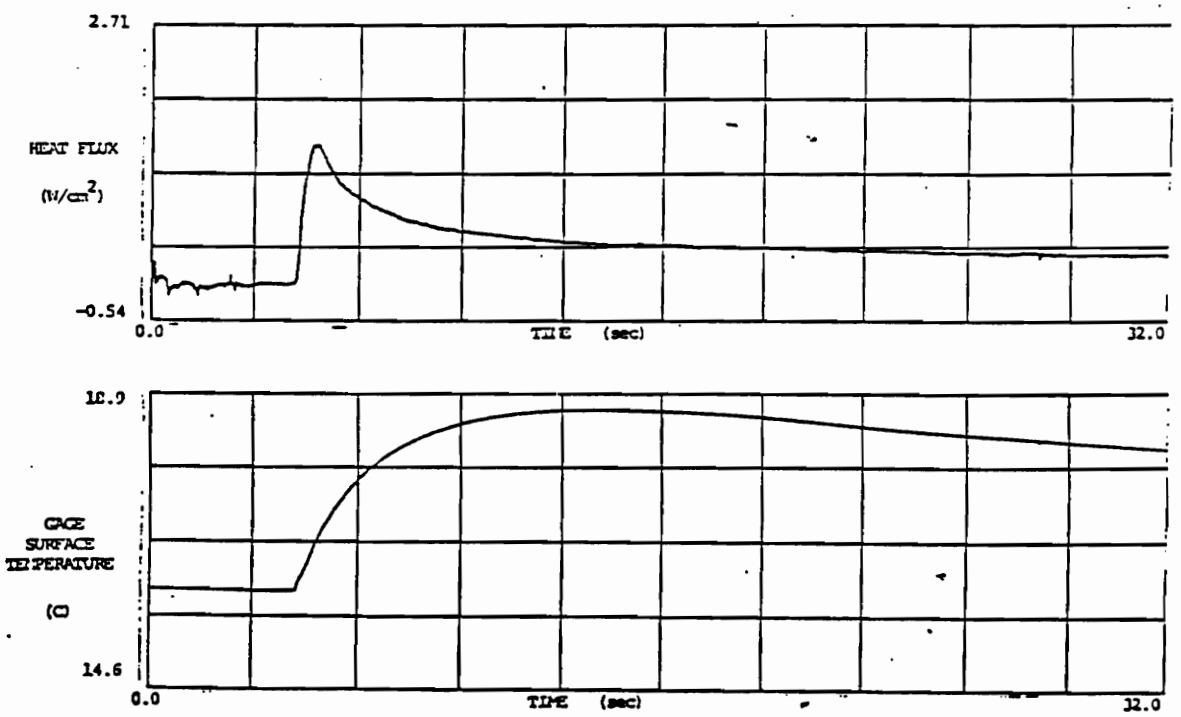

5 min. after injection

Fig. 34. Vasodilator Tests

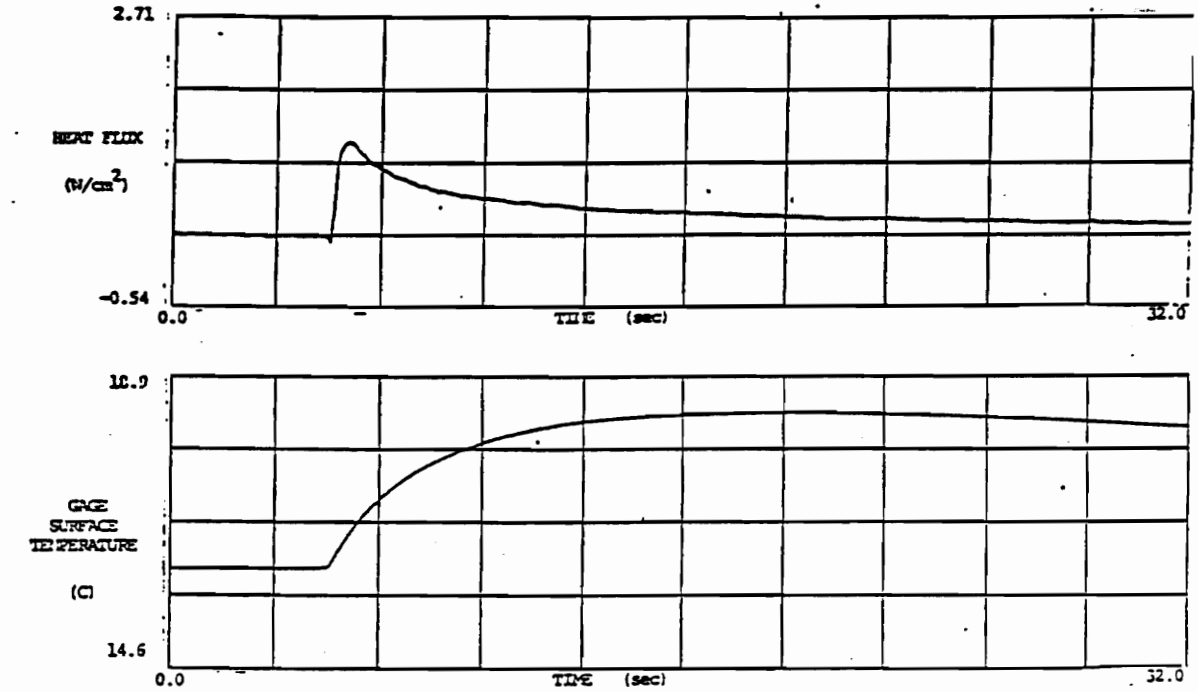

10 min. after injection

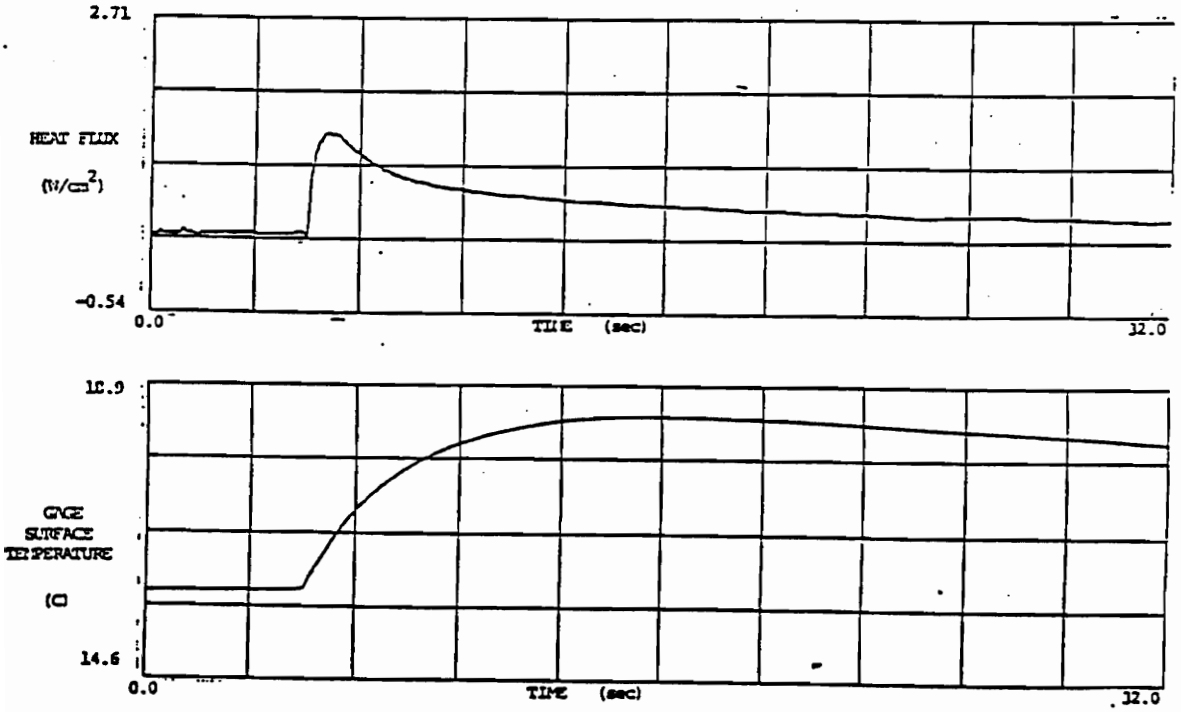

15 min. after injection

Fig. 35. Vasodilator Tests

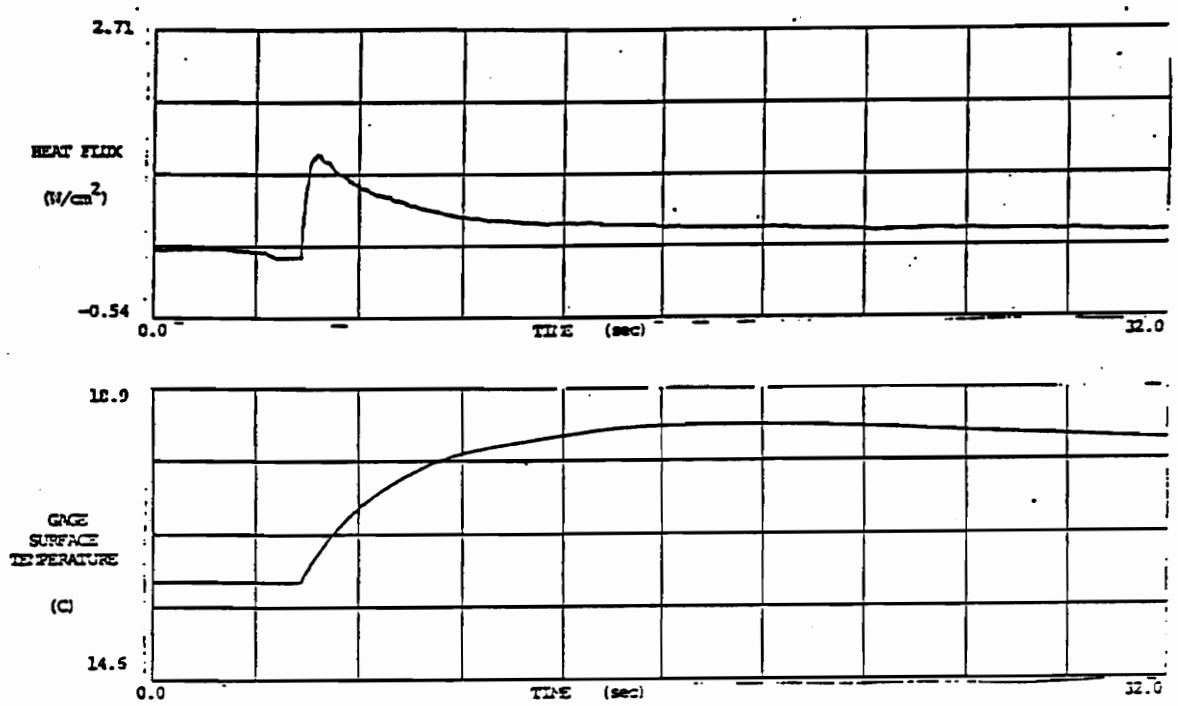

20 min. after injection

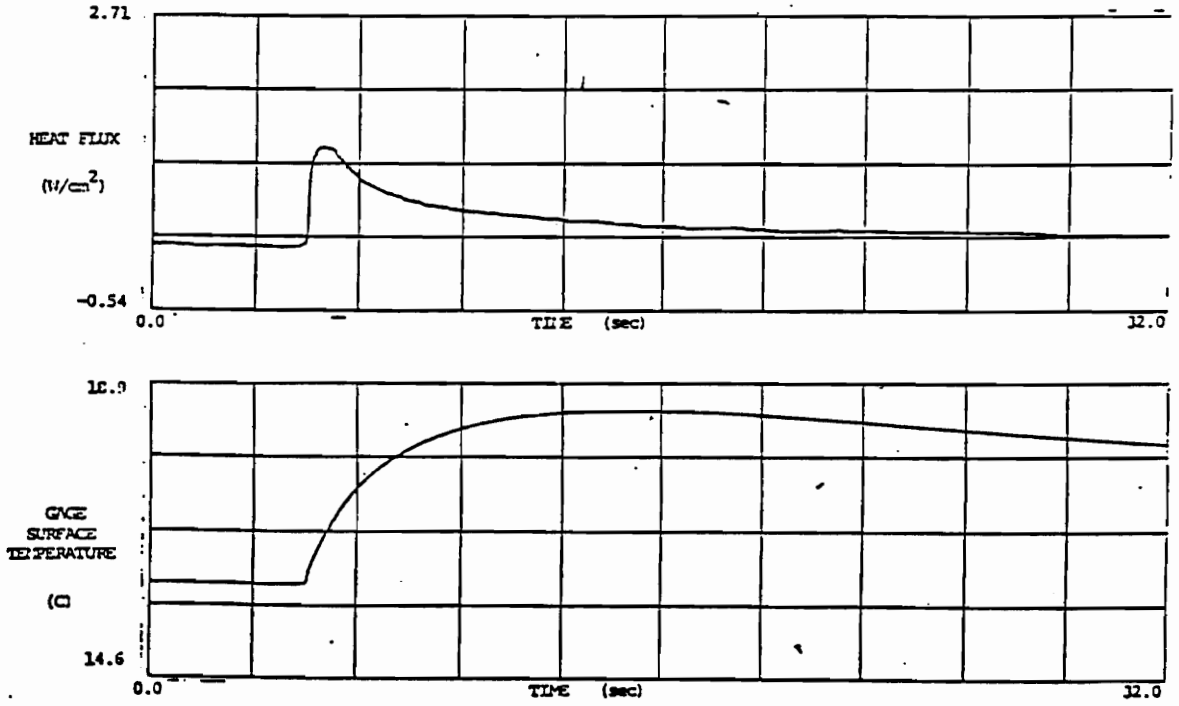

25 min. after injection

Fig. 36. Vasodilator Tests

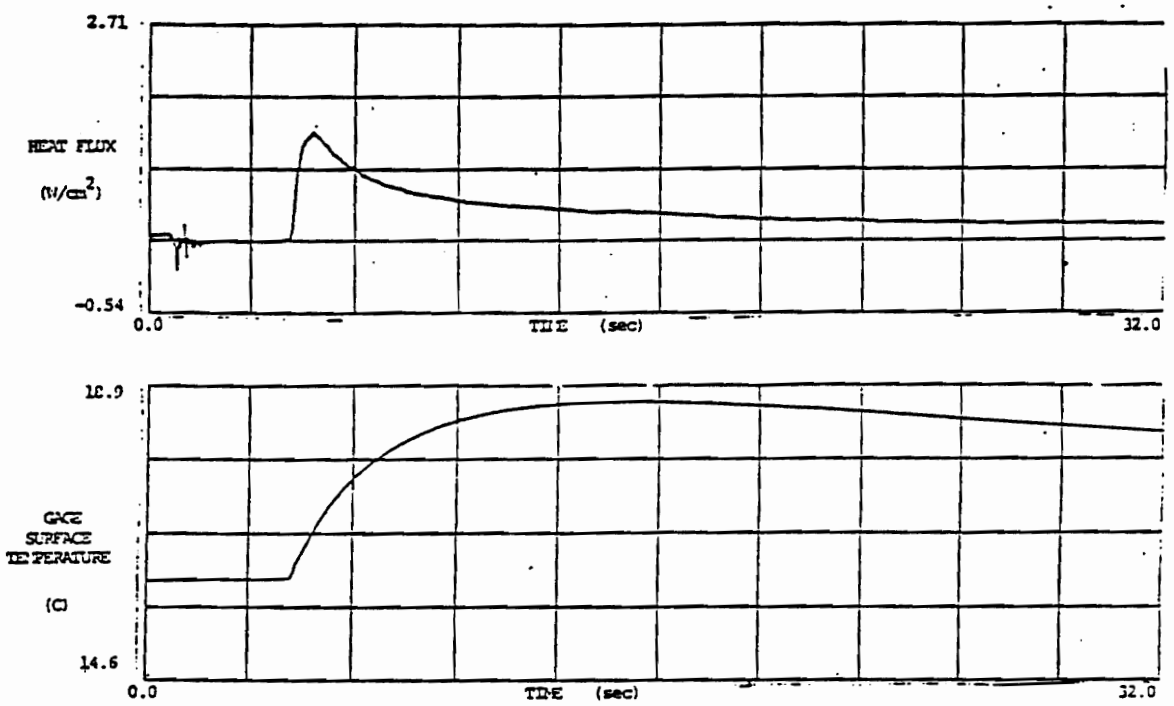

30 min. after injection

Fig. 37. Vasodilator Tests

Table 4. Slopes and Integrations of Experimental Curves

Test Description	Slope (2-5 s) ln(μv)/s	Integration (2-22s)
Flow Rate = 0.0 l/min	0.127	35.25
Flow Rate = 1.5 l/min	0.155	82.11
Flow Rate = 3.0 l/min	0.135	55.46
Flow Rate = 6.0 l/min	0.109	62.40
Light Pressure	-----	-----
Heavy Pressure	0.128	46.96
Hind Leg	0.126	54.76
Abdomen	0.197	46.03
Pressure Cuff	0.120	88.10
Vasodilator 1 min.	0.122	86.23
Vasodilator 5 min.	0.154	59.10
Vasodilator 10 min.	0.091	107.00
Vasodilator 15 min.	0.078	131.67
Vasodilator 20 min.	0.142	101.75
Vasodilator 25 min.	0.116	86.19
Vasodilator 30 min.	0.104	117.90

integration and slopes of these curves for the previously discussed time periods. The integrated heat flux at 10 and 15 minutes is particularly interesting. According to these numbers there is a significant increase in perfusion at these times, which corresponds to the time where the drug is supposed to have maximum effect. Based on the theoretical analysis the perfusion is estimated to have increased from .002 to .008 ml/ml/s during the vasodilator tests.

Table 5 shows the integration and slopes of the finite difference curves. These numbers are in the exact same range as the experimental values in Table 4. Figure 38 compares an experimental and a finite difference heat flux curve for a normal perfusion rate (0.002 ml/ml/sec). The two curves are similar in shape and magnitude. The approximately 0.1 W/cm^2 difference between the two is likely due to the contact resistance between the probe and skin which the finite difference program does not model.

Table 5. Slopes and Integrations for Theoretical Curves

Perfusion Rate	Slope of Curve	Integration
ml/ml/sec	2-5 s (ln(μv)/s)	2-22 s (ln(μv)·s)
0.0000	0.15	119.0
0.0020	0.15	124.6
0.0050	0.14	129.6
0.0080	0.14	134.4
0.0120	0.14	140.9
0.0167	0.13	147.4
0.0300	0.12	166.6
0.0500	0.11	192.7

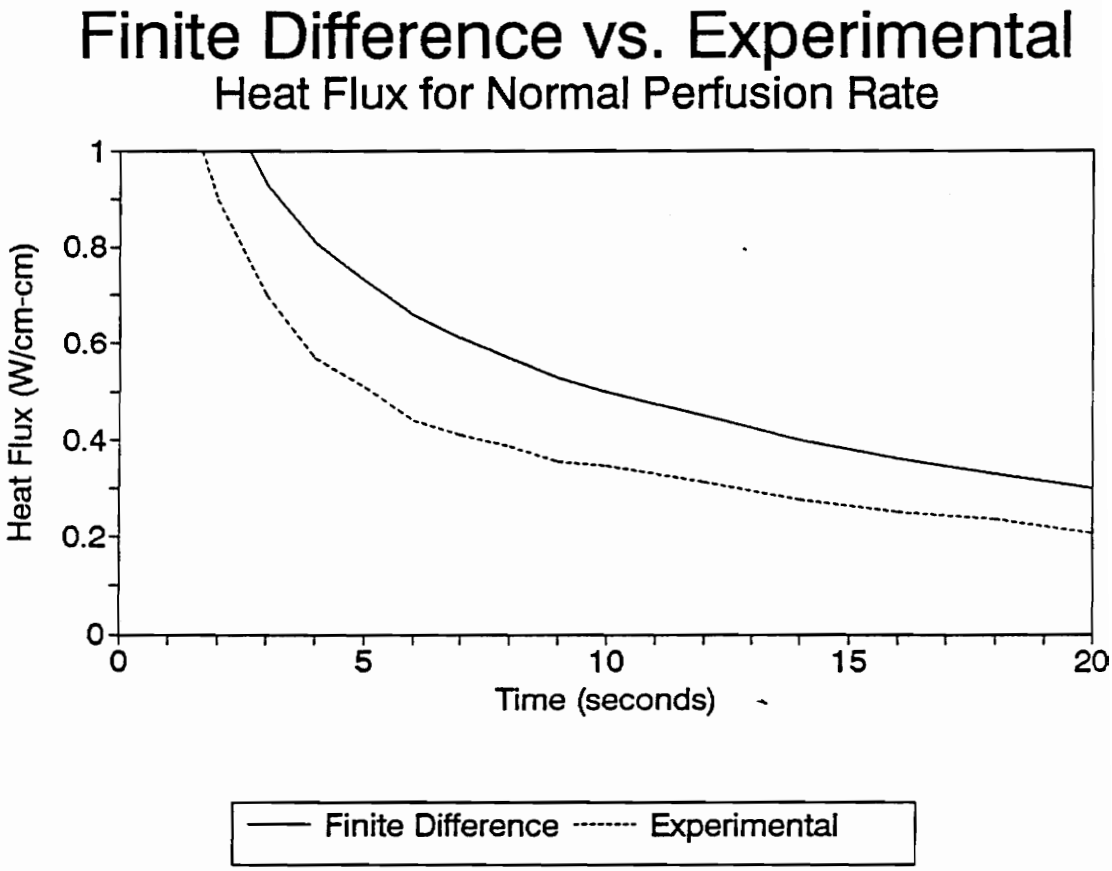

Fig. 38. Heat Flux for Normal Perfusion Rate

6.4 Conclusions and Recommendations

The agreement between the experimental data and the finite difference model solutions is good. Table 4 shows the slopes and integrations of all of the experimental tests, and table 5 shows the slopes and integrations of a range of chosen perfusion rates in the theoretical tests. The slopes and integrations of the experimental heat flux curves match the theoretical ones closely. The shapes of the curves are similar as well.

The relatively small differences in the experimental and theoretical results can be explained by several factors. First, the actual boundary between the tissue and probe is not a constant temperature as is assumed in the finite difference model. The constant temperature boundary is a good approximation after the first few seconds, but in those first few seconds the temperature difference at the boundary changes rapidly. Also the Pennes bioheat equation is only an approximation of the heat transfer that occurs in biological tissue. It assumes that the tissue is homogeneous. Finally, biological properties are not well known. The values used in the program are not exact for all biological tissue. From the analysis and experiments done on the bioprobe, the following conclusions can be made:

- The finite difference model accurately models two-

dimensional heat transfer and the perfusion effects.

- The bioprobe has trouble differentiating between changes in blood perfusion on the order of .001 ml/ml/s.
- The bioprobe can measure relatively large changes in blood perfusion induced by a vasodilator.

Based on the experimental tests the following recommendations are also made:

- The sensitivity of the Heat Flux Microsensor should be increased for this particular application. This can be accomplished by making the thermal resistance layer thicker (up to 3 times the current thickness), adding more thermocouples, or by changing the metals used for the thermocouples. Making these modifications will increase the signal to noise ratio of the gage and should enable it to measure even small perfusion changes. The sensitivity must be improved for the bioprobe to be a widely accepted medical instrument.
- The method of applying the probe to the tissue should be automated. A device that steadily lowered the probe until the desired tissue contact pressure was achieved would be ideal. Additionally, a pressure gage should be added to the probe face so that the same pressure can be achieved in every test. This would be an optimum pressure that would achieve good contact without affecting the blood flow. This method would allow for

more repeatable and reliable tests.

- When permission is obtained to do more tests on the dogs, the pressure cuff test should be redone with the heat flux being monitored above the point of constriction. This should be a more successful location for detecting a sudden change in blood perfusion.

- A method for analyzing the curves to obtain actual values for perfusion must be developed. The solution will certainly be complicated, and will be based on analysis of peak heat flux, heat flux decay rate, steady-state heat flux, and temperature.

7.0 REFERENCES

1. Hager, J. M., Onishi, S., Langley, L. W., and Diller, T. E., 1991, "High Temperature Heat Flux Measurements", AIAA Paper No. 91-0165, 1991.

2. Leidenfrost, W., "Measurements of Thermophysical Properties", in Measurements in Heat Transfer, 1976, Ed. by Eckert, E. R. G. and Goldstein, R. J., pp. 475-522.

3. Hoch, M., Nitti, D. A., Gottschish, C. F., and Blackburn, P. E., 1962, "New Method for the Determination of Thermal Conductivities between 1000 C and 3000 C", in Progress in International Research and Transport Properties, Eds. Masi, J. F. and Tsai, D. H., ASME Second Symposium on Thermophysical Properties, pp. 512-518.

4. Takegoshi, E., Hirasawa, Y., and Imura, S., "Thermal Conductivity Measurements of High Conductivity Materials by a Transient Hot-Wire Method", Japanese Research-Heat Transfer, Vol. 19, 1990, pp. 366-375.

5. Danielson, G. C. and Sidles, P. H., "Thermal Diffusivity and Other Non-Steady Methods", in Thermal Conductivity, 1969, Ed. by Tye, R. P., pp. 149-201.

6. "Fast Measurements of Thermal Diffusivities of Ceramics", NASA Tech Briefs, ARC-11705, pp. 1-6.

7. Kobayasi, K., 1988, "Recent Developments in Measuring Techniques for Thermal Conductivity and Thermal Diffusivity", JSME International Journal, Vol. 31, No. 1, pp. 1-8.

8. Takehashi, I., Sugawara, A., Igawa, H., and Mifune, H., 1988, "Precise Measurement of Thermophsical Properties by a Direct Electrical Heating Method", JSME International Journal, Vol. 31, No. 2, pp. 320-328.

9. Fukai, J., Simizu, Y., Miura, T., and Ohanti S., 1988, "Simultaneous Extimation of Thermal Properties by Periodic Heating Method of Hot Wire", in Experimental Heat Transfer, Fluid Mechanics, and Thermodynamics, Eds. by Shah, R. K., Ganic,E. N., and Yang, K.T., pp. 1279-1285.

10. Patel, P. A., Valvano, J. W., Pearce, J. A., Prahl, S. A., and Denham, C. R., 1987, "A Self-Heated Thermistor Technique to Measure Effective Thermal Properties from the Tissue Surface", Journal of Biomedical Engineering, Vol. 109, pp. 330-335.

11. Chato, J. C., 1985, "Measurements of Thermal Properties of Biological Materials", Ch. 8 in Heat Transfer in Medicine and Biology, Vol. 1, Eds., A. Shitzer and R. C. Eberhart, Plenum Press, NY, pp. 167-192.

12. Valvano, J. W., Nho, S., and Anderson, G. T., 1990, "A Weinbaum-Jiji Model of Steady-State Heated Thermistors in the Canine Kidney Cortex", in Advances in Measuring and Computing Temperatures in Biomedicine: Thermal Tomography Techniques, Bioheat Transfer Models, Eds. by Roemer, R. B., Valvano, J. W., Hayes, L., and Anserson, G. T., Vol. 147, pp. 51-58.

13. Bowman, H. F., "Estimation of Tissue Blood Flow", in Heat Transfer in Medicine and Biology, 1985, Eds. Shitzer, A., and Eberhart, R. C., pp. 193-230.

14. Anderson, G. T., and Burnside, G., 1990, "A Noninvasive Technique to Measure Perfusion Using a Focused Ultrasound Heating Source and a Tissue Surface Temperature Measurement", in Advances in Measuring and Computing Temperatures in Biomedicine: Thermal Tomography Techniques, Bioheat Transfer Models, Ed. by Roemer, R. B., Valvano, J. W., Hayes, L., and Anderson, G. T., Vol. 147, pp. 31-36.

15. Walsh, J. T., and Bowman, H. F., 1984, "A Noninvasive Technique for Quantifying Tissue Perfusion", in Advances in Bioengineering, Ed. by Spilker, R. L., pp. 5-6.

16. Castellana, F. S., Skalek, R., Cho J. M., and Case, R. B., 1983, "Steady-State Analysis and Evaluationof a New Thermal Sensor for Surface Measurements of Tissue Perfusion", Annals of Biomedical Engineering, Vol. 11, pp. 101-115.

17. Diller, T. E., 1989, "Heat Flux Microsensors for Biological Measurements", in Bioheat Transfer - Applications in Hyperthermia, Emerging Horizons in Instrumentation and Modeling, Ed. by Roemer, R. B., McGrath, J. J., and Bowman, H. F., pp. 115-119.

18. Jaeger, J. C., 1952, "Approximations in Transient Surface Heating", Austrailian Journal of Scientific Research, Vol. 5, pp. 1-9.

19. Pennes, H. H., 1948, "Analysis of Tissue and Arteriol Blood Temperatures in the Resting Human Forearm", Journal of Applied Physiology, Vol. 1, pp. 93 -122.

20. Song, W. J., Weinbaum, S., and Jiji, L. M., 1987, "A Theoretical Model for Peripheral Tissue Heat Transfer Using the Bioheat Equation of Weinbaum and Jiji", Journal of Biomechanical Engineering, Vol. 109, pp. 72-78.

21. von Rosenberg, D. U., Methods for the Numerical Solution of Partial Differential Equations, 1969, pp. 84-89.

22. Hager, J. M., Simmons, S., Smith D., Onishi, S., Langley, L. W., and Diller T. E., "Experimental Performance of a Heat Flux Microsensor," ASME Paper No. 90-GT-256, 1990.

23. Shepherd, J. T., Physiology of the Circulation in Human Limbs in Health and Disease, 1963.

8. APPENDIX A.

The following three equations give transient temperature change for a constant heat source applied to the prescribed geometries. These analytical solutions were taken from Jaeger [18]. The programs in Appendix B were used to evaluate the solutions for the infinite strip and circular models.

infinite strip

$$\dot{v} = \frac{qaT^{\frac{1}{2}}}{K\pi^{\frac{1}{2}}}\left\{\operatorname{erf}\frac{a+z}{2aT^{\frac{1}{2}}} + \operatorname{erf}\frac{a-z}{2aT^{\frac{1}{2}}} - \frac{a+z}{2a(\pi T)^{\frac{1}{2}}}\operatorname{Ei}\left(-\frac{(a+z)^2}{4a^2T}\right) - \right.$$
$$\left. - \frac{(a-z)}{2a(\pi T)^{\frac{1}{2}}}\operatorname{Ei}\left(-\frac{(a-z)^2}{4a^2T}\right)\right\}.$$

square model

$$= \frac{2q}{k}\left(\frac{z^2}{\pi}\right)^{\frac{1}{2}}\frac{1}{4T^{\frac{1}{2}}}\int_0^{\infty}\operatorname{erf}\frac{1}{u}\left\{\operatorname{erf}\frac{(1-\xi)}{u} + \operatorname{erf}\frac{(1+\xi)}{u}\right\}du.$$

circle model

$$= \frac{aq}{k}\int_0^{\infty} J_0(\lambda r)J_1(\lambda a)\operatorname{erf}\{\lambda(zt)^{\frac{1}{2}}\}\frac{d\lambda}{\lambda}.$$

The following figures represent graphical solutions of the equations on the previous page. The graphical solutions are for a limited number of times and locations.

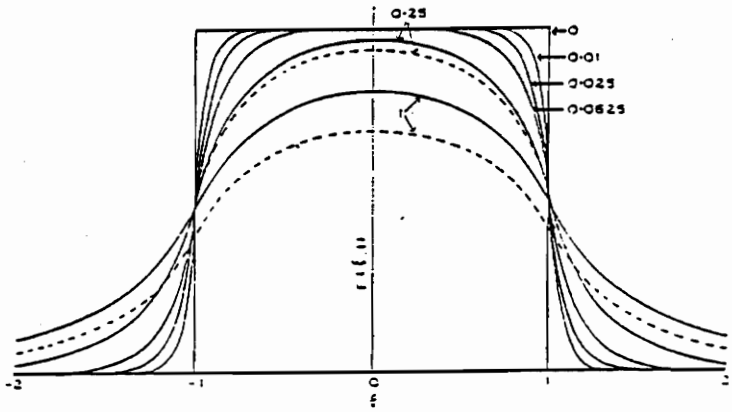

—Temperature distribution across a strip (full lines) and a square (dotted lines) for various values of the time. The numbers on the curves are the values of $T = \varkappa t/a^2$.

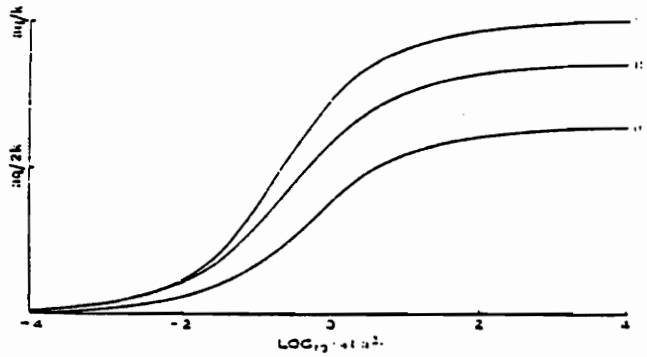

—Centre, average, and circumferential temperature for heating over a circle of radius a: curves I, II, and III.

These graphical solutions were obtained from the paper by Jaeger [18].

9. APPENDIX B

The following two programs were written by Michael Michener. The first uses Jaeger's infinite strip solution and the second uses Jaeger's circle solution. The program was solved at several different locations and times to obtain many of the graphs presented in chapter 5. The results were used to compare experimental and numerical results.

```
C-----------------------------------------------------------------------
C       MICHAEL MICHENER
C       MAY 21, 1990
C
C       PROGRAM WILL CALCULATE A TEMPERATURE DIFFERENCE FOR A
C       SPECIFIED HEAT FLUX OVER AN INFINITE STRIP WIDTH -A TO
C       +A.  THERMAL DIFFUSIVITY, CONDUCTIVITY, DISTANCE FROM
C       CENTER OF STRIP AND TIME MUST ALSO BE GIVEN.
C
C-----------------------------------------------------------------------
C       A=HALF THE WIDTH OF THE STRIP (M)
C       Q=HEAT FLUX IN W/M¢2
C       ALPHA= THERMAL DIFFUSIVITY (M¢2/S)
C       TK=THERMAL CONDUCTIVITY (W/MK)
C       Z=RATIO OF DISTANCE X TO A
C       TIME GIVEN IN SECONDS

        IMPLICIT REAL*8 (A-H,O-Z)
        A=.0127D0
        ALPHA=17.7D-06
        TK=60.5D0
        Q=1.0D06
        Z=2.0D0
        X=A*Z
        TIME =4.0000D0
        T=(ALPHA*TIME)/((A)**DFLOAT(2))
        X1=(A+X)**DFLOAT(2)/(DFLOAT(4)*T*(A)**DFLOAT(2))
        X2=(ABS(A-X))**DFLOAT(2)/(DFLOAT(4)*T*(A)**DFLOAT(2))
C
C       THIS PART OF THE PROGRAM CALCULATES THE EXPONENTIAL INTEGRAL
C       USING THE INFINITE SERIES SOLUTION.
C
        E1=.5772D0+LOG(X1)
        E2=.5772D0+LOG(X2)
        I=0
        SIGN=-1.D0
        B=1.D0
        FACT=1.D0
        DO 20 J=1,200
        I=I+1
        B=SIGN*B
        FACT=1.D0
        DO 70 N=I,1,-1
        FACT=FACT*DFLOAT(N)
   70   CONTINUE
        Z1=B*((X1)**DFLOAT(I))/(DFLOAT(I)*FACT)
        Z2=B*((X2)**DFLOAT(I))/(DFLOAT(I)*FACT)
        E1=E1+Z1
        E2=E2+Z2
        IF(ABS(Z1) .LE. 1.0D-06)THEN
        GO TO 100
        END IF
   20   CONTINUE

  100   X3=(A+X)/(2.D0*A*(T)**.5D0)
```

```
      X4=(A-X)/(2.D0*A*(T)**.5D0)
      X5=(A+X)/(2.D0*A*(3.1415D0*T)**.5D0)
      X6=(Q*A*(T)**.5D0)/(TK*(3.1415D0)**.5D0)
      X7=(A-X)/(2.D0*A*(3.1415D0*T)**.5D0)
      DELT=X6*(ERF(X3)+ERF(X4)-X5*(E1)-X7*(E2))
      WRITE(6,51)X1,X2,Z1,Z2,E1,E2
51    FORMAT(1X,6(E10.3,2X))
      WRITE(*,*)'TEMP    HEAT FLUX   ALPHA      K       X/A    TIME'
      WRITE(*,*)'(K)      (W/M¢2)    (M¢2/S)  (W/MK)          (S)'
      WRITE(6,50)DELT,Q,ALPHA,TK,Z,TIME,I
50    FORMAT(1X,F8.2,2X,E8.2,2X,E8.3,2X,F5.1,2X,F3.1,2X,F7.4,2X,I2)
      STOP
      END
```

```
C       ------------------------------------------------------------
C
C       MICHAEL MICHENER
C       MAY 29, 1990
C
C       THIS PROGRAM WILL CALCULATE THE TEMPERATURE
C       DIFFERENCE FOR A SPECIFIED TIME AND LOCATION FOR
C       THE CASE OF A CONSTANT HEAT FLUX SUPPLIED OVER
C       A CIRCULAR AREA.
C       ------------------------------------------------------------

        IMPLICIT REAL*8 (A-H,O-Z)
        CALL ERRSET (209,300,-1,-1,0,0)
        A=0.0127D0
        TK=0.50D0
        Q=4.0D03
        ALPHA=0.15D-06
        R=0.012065D0
        N=500000
        DO 99 ITIME=30,30
        TIME=DFLOAT(ITIME)/1.D0
        SUM=0.D0
         DO 10 LAMBDA=0,N,1
         Z=DFLOAT(LAMBDA)/100.D0
         X=Z*A
         X0=X*(R/A)
         X1=X
         X2=X*(((ALPHA*TIME)/(A**2.D0))**0.5D0)
         OJ=DBSJ0(X0)
         PJ=DBSJ1(X1)
         ERF=DERF(X2)
         F=(OJ*PJ*ERF)/Z
          IF(Z .EQ. 0.D0)THEN
          GO TO 30
          END IF
         SUM=SUM +2*F
         GO TO 10
   30    SUM = SUM +F
   10    CONTINUE
        SUM=SUM-F
        AINTG=(Z/(2.D0*N))*(SUM)
        TEMP=((A*Q)/TK)*AINTG
        WRITE(6,20)TEMP,TIME
   20   FORMAT(3X,'THE TEMPERATURE IS:',F12.4,2X,'K',F6.2,'SEC')
   99   CONTINUE
        STOP
        END
```

10. APPENDIX C

The equations on the following two pages are the finite difference representations of equation [3.6].

First Time Step:

$$\frac{\Theta_{i,j,n+1}-\Theta_{i,j,n}}{\Delta t'}=\frac{\Theta_{i-1,j,n+1}-2\Theta_{i,j,n+1}+\Theta_{i+1,j,n+1}}{(\Delta\eta)^2} \qquad \textbf{(10.1)}$$

$$+\frac{1}{\eta(I)}\left[\frac{\Theta_{i+1,j,n+1}-\Theta_{i-1,j,n+1}}{2(\Delta\eta)}\right]+\frac{\Theta_{i,j+1,n}-2\Theta_{i,j,n}+\Theta_{i,j-1,n}}{(\Delta\xi)^2}$$

$$-M\Theta_{i,j,n+1}$$

Second Time Step:

$$\frac{\Theta_{i,j,n+2}-\Theta_{i,j,n+1}}{(\Delta t')}=\frac{\Theta_{i-1,j,n+1}-2\Theta_{i,j,n+1}+\Theta_{i+1,j,n+1}}{(\Delta\eta)^2} \qquad \textbf{(10.2)}$$

$$+\frac{1}{\eta(I)}\left[\frac{\Theta_{i+1,j,n+1}-\Theta_{i-1,j,n+1}}{2(\Delta\eta)}\right]+\frac{\Theta_{i,j+1,n+2}-2\Theta_{i,j,n+2}+\Theta_{i,j-1,n+2}}{(\Delta\xi)^2}$$

$$-M\Theta_{i,j,n+2}$$

Equations reorganized with unknowns on left, and knowns on right (Forms of equation used in program).

First time step:

$$\Theta_{i-1,j,n+1}\left[\frac{1}{\eta(I)(2(\Delta\eta))}-\frac{1}{(\Delta\eta)^2}\right]+\Theta_{i,j,n+1}\left[\frac{1}{\Delta t'}+\frac{2}{(\Delta\eta)^2}+M\right]$$

$$+\Theta_{i+1,j,n+1}\left[-\frac{1}{(\Delta\eta)^2}-\frac{1}{\eta(I)(2(\Delta\eta))}\right]=\Theta_{i,j-1,n}\left[\frac{1}{(\Delta\xi)^2}\right] \quad \textbf{(10.3)}$$

$$+\Theta_{i,j,n}\left[\frac{1}{\Delta t'}-\frac{2}{(\Delta\xi)^2}\right]+\Theta_{i,j+1,n}\left[\frac{1}{(\Delta\xi)^2}\right]$$

Second Time Step:

$$\Theta_{i,j-1,n+2}\left[-\frac{1}{(\Delta\xi)^2}\right]+\Theta_{i,j,n+2}\left[\frac{1}{(\Delta t')}+\frac{2}{(\Delta\xi)^2}+M\right] \quad \textbf{(10.4)}$$

$$-\Theta_{i,j+1,n+2}\left[\frac{1}{(\Delta\xi)^2}\right]=\Theta_{i-1,j,n+1}\left[\frac{1}{(\Delta\eta)^2}-\frac{1}{\eta(I)(2(\Delta\eta))}\right]$$

$$+\Theta_{i,j,n+1}\left[\frac{1}{(\Delta t')}-\frac{2}{(\Delta\eta)^2}\right]+\Theta_{i+1,j,n+1}\left[\frac{1}{(\Delta\eta)^2}+\frac{1}{\eta(I)(2(\Delta\eta))}\right]$$

11. APPENDIX D

The following program was written by Michael Michener. It is a finite difference program modeling the Pennes Bioheat Equation [3.1]. The boundary equations used were specified in equations [3.8] and [3.12].

```
C234567
C     ------------------------------------------------------------
C                     MICHAEL MICHENER
C                     AUGUST 1990
C     ------------------------------------------------------------
C
C     THIS PROGRAM USES A FINITE DIFFERENCE FORMULATION TO SOLVE
C     A TWO DIMENSIONAL ( RADIAL COORDINATES ) TRANSIENT HEAT
C     TRANSFER PROBLEM.  THE SOLUTION ACCOUNTS FOR BLOOD PERFUSION
C     AND IS INTENDED TO MODEL BIOLOGICAL TISSUE.  THE TISSUE IS
C     INITIALLY ISOTHERMAL AT A TEMPERATURE OF 37 DEG. C.  ONE
C     BOUNDARY IS SUBJECTED TO A CONSTANT TEMPERATURE CONDITION
C     AND ALL OTHER BOUNDARIES ARE DEFINED AS HAVING ZERO HEAT
C     FLUX.
C
C
C     DEFINE RANGE OF ARRAYS FOR VARIABLES
C
      IMPLICIT REAL*8 (A-H,O-Z)
      REAL*8 M,KT
      DIMENSION THETA(100,100),A(100,100),B(100,100),C(100,100)
     $,D(100,100),E(100,100),F(100,100),G(100,100),H(100,100),
     $ETA(100),BETA(100,100),GAMMA(100,100),TEMP(100,100),Q(100,100)
      CALL ERRSET (208,300,-1,-1,0,0)
C
C     DEFINE TISSUE AND BLOOD PROPERTIES
C
      ALPHT=0.150D-06
      RHOB= 1000.D0
      SHB= 4000.D0
      WB= 0.0020D0
      KT= 0.5D0
      R= .0127D0
      M=((RHOB*SHB*WB)/(KT))*R**2.D0
C
C     DEFINE GEOMETRIC PROPERTIES
C
      NEDGE=10
      DH=1.0D0/DFLOAT(NEDGE)
      DZ=1.0D0*DH
      TIME = 0.D0
      XTIME = 0.D0
      DT=2.5D-05
      NTSTP=600
      N=20
      L=20
C
C     INITIALIZE THETA(I,J) MATRIX
C
      DO 1 I=1,N,1
      DO 2 J=1,L,1
      THETA(I,J)=0.D0
      A(I,J)=0.D0
      B(I,J)=0.D0
      C(I,J)=0.D0
```

```
      D(I,J)=0.DO
      E(I,J)=0.DO
      F(I,J)=0.DO
      G(I,J)=0.DO
      H(I,J)=0.DO
      ETA(I)=0.DO
      BETA(I,J)=0.DO
      GAMMA(I,J)=0.DO
      TEMP(I,J)=0.DO
      Q(I,J)=0.DO
    2 CONTINUE
    1 CONTINUE
C
C     COMPUTE ETA(I) VALUES
C
      DO 50 I=1,N,1
      ETA(I)=((2.DO*DFLOAT(I)-1.DO)/2.DO)*DH
   50 CONTINUE
C
C     DEFINE COEFFICIENTS OF 1ST TIME STEP MATRICES
C     A(I,J),B(I,J),C(I,J)
C     1ST COLUMN
C
      I=1
      DO 3 J=1,L,1
      A(1,J)=0.DO
      B(1,J)=1.DO/(ETA(I)*(2.DO*DH))+1.DO/((DH)**2.DO)+1.DO/DT+M
      C(1,J)=-1.DO/((DH)**2.DO)-1.DO/(ETA(I)*(2.DO*DH))
    3 CONTINUE
C
C     MIDDLE COLUMNS
C
      DO 4 I=2,N-1,1
      DO 5 J=1,L,1
      A(I,J)= 1.DO/(ETA(I)*(2.DO*DH))-1.DO/(DH)**2.DO
      B(I,J)=1.DO/DT+2.DO/(DH)**2.DO+M
      C(I,J)=-1.DO/(DH)**2.DO-1.DO/(ETA(I)*(2.DO*DH))
    5 CONTINUE
    4 CONTINUE
C
C     FINAL COLUMN
C
      I=N
      DO 6 J=1,L,1
      A(N,J)= 1.DO/(ETA(I)*(2.DO*DH))-1.DO/(DH**2.DO)
      B(N,J)= 1.DO/DT+1.DO/(DH)**2.DO-1.DO/(ETA(I)*(2.DO*DH))+M
      C(N,J)=0.DO
    6 CONTINUE
C
C     DEFINE E(I,J),F(I,J),G(I,J)
C     COEFFICIENTS OF 2ND TIME STEP MATRIX
C     FIRST ROW
C
      J=1
      DO 7 I=1,NEDGE,1
```

```
      E(I,1)=0.D0
      F(I,1)=1.D0/DT+3.D0/(DZ**2.D0)+M
      G(I,1)=-1.D0/(DZ**2.D0)
    7 CONTINUE
C
      DO 8 I=NEDGE+1,N,1
      E(I,1)=0.D0
      F(I,1)=1.D0/DT+1.D0/(DZ**2.D0)+M
      G(I,1)=-1.D0/(DZ**2.D0)
    8 CONTINUE
C
C     DEFINE MIDDLE ROWS
C
      DO 9 J=2,L-1,1
      DO 10 I=1,N,1
      E(I,J)=-1.D0/(DZ**2.D0)
      F(I,J)=1.D0/DT+2.D0/(DZ**2.D0)+M
      G(I,J)=-1.D0/(DZ**2.D0)
   10 CONTINUE
    9 CONTINUE
C
C     BOTTOM ROW
C
      J=L
      DO 11 I=1,N,1
      E(I,L)=-1.D0/(DZ**2.D0)
      F(I,L)=1.D0/DT+1.D0/(DZ**2.D0)+M
      G(I,L)=0.D0
   11 CONTINUE
C
C     FIRST TIME STEP CALCULATIONS
C     DEFINE RHS COLUMN   D(I,J)
C
      DO 29 NT=1,NTSTP,1
      J=1
      DO 12 I=1,NEDGE,1
      D(I,1)=2.D0/(DZ**2.D0)+THETA(I,1)*(1.D0/DT-3.D0/(DZ**2.D0))+
     $THETA(I,2)*(1.D0/(DZ**2.D0))
   12 CONTINUE
C
      DO 13 I=NEDGE+1,N,1
      D(I,1)=THETA(I,1)*(1.D0/DT-1.D0/(DZ**2.D0))+THETA(I,2)*
     $(1.D0/(DZ**2.D0))
   13 CONTINUE
C
      DO 14 J=2,L-1,1
      DO 15 I=1,N,1
      D(I,J)=THETA(I,J-1)*(1.D0/(DZ**2.D0))+THETA(I,J)*(1.D0/DT-
     $2.D0/(DZ**2.D0))+THETA(I,J+1)*(1.D0/(DZ**2.D0))
   15 CONTINUE
   14 CONTINUE
C
      DO 16 I=1,N,1
      J=L
      D(I,L)=THETA(I,L-1)*(1.D0/(DZ**2.D0))+THETA(I,L)*(1.D0/DT-1.D0/
```

```
     $(DZ**2.D0))
   16 CONTINUE
C
C     USE TRIDIAGONAL MATRIX SOLVER TO GET
C     THETA VALUES AT THE FIRST TIME STEP
C
      IF=1
      DO 17 J=1,L,1
      BETA(IF,J)=B(1,J)
      GAMMA(IF,J)=D(1,J)/BETA(IF,J)
      IFP1=IF+1
C
      DO 18 I=IFP1,N
      BETA(I,J)=B(I,J)-A(I,J)*C(I-1,J)/BETA(I-1,J)
      GAMMA(I,J)=(D(I,J)-A(I,J)*GAMMA(I-1,J))/BETA(I,J)
C     WRITE(*,67)I,J,GAMMA(I,J),BETA(I,J),D(I,J),A(I,J)
C  67 FORMAT(2(3X,I5),3X,E15.8,2(3X,E8.3),3X,E10.3)
   18 CONTINUE
C
      THETA(N,J)=GAMMA(N,J)
      LAST=N-IF
      DO 19 K=1,LAST
      I=N-K
      THETA(I,J)=GAMMA(I,J)-C(I,J)*THETA(I+1,J)/BETA(I,J)
   19 CONTINUE
   17 CONTINUE
      XTIME=XTIME+DT
C
C     SECOND TIME STEP CALCULATIONS
C     DEFINE H(I,J) VALUES
C
      I=1
      J=1
      H(I,J)=2.D0/(DZ**2.D0)+THETA(1,1)*(1.D0/DT-1.D0/(DH**2.D0)-1.D0/
     $(ETA(I)*(2.D0*DH)))+THETA(2,1)*(1.D0/(DH**2.D0)+1.D0/(ETA(I)*
     $(2.D0*DH)))
C
      DO 20 J=2,L,1
      H(1,J)=THETA(1,J)*(1.D0/DT-1.D0/(DH**2.D0)-1.D0/(ETA(I)*(2.D0*DH
     $)))+THETA(2,J)*(1.D0/(DH**2.D0)+1.D0/(ETA(I)*(2.D0*DH)))
   20 CONTINUE
C
      DO 21 I=2,NEDGE,1
      H(I,1)=2.D0/(DZ**2.D0)+THETA(I-1,1)*(1.D0/(DH**2.D0)-1.D0/(ETA(I)
     $*(2.D0*DH)))+THETA(I,1)*(1.D0/DT-2.D0/(DH**2.D0))+THETA(I+1,1)
     $*(1.D0/(DH**2.D0)+1.D0/(ETA(I)*(2.D0*DH)))
   21 CONTINUE
C
      DO 22 I=NEDGE+1,N-1,1
      H(I,1)=THETA(I-1,1)*(1.D0/(DH**2.D0)-1.D0/(ETA(I)*(2.D0*DH)))
     $+THETA(I,1)*(1.D0/DT-2.D0/(DH**2.D0))+THETA(I+1,1)*(1.D0/(DH**2.D0
     $)+1.D0/(ETA(I)*(2.D0*DH)))
   22 CONTINUE
C
      DO 23 J=2,L,1
```

```
      DO 24 I=2,N-1,1
      H(I,J)=THETA(I-1,J)*(1.D0/(DH**2.D0)-1.D0/(ETA(I)*(2.D0*DH)))
     $+THETA(I,J)*(1.D0/DT-2.D0/(DH**2.D0))+THETA(I+1,J)*(1.D0/(DH**2.D0
     $)+1.D0/(ETA(I)*(2.D0*DH)))
   24 CONTINUE
   23 CONTINUE
C
      DO 25 J=1,L,1
      I=N
      H(N,J)=THETA(N-1,J)*(1.D0/(DH**2.D0)-1.D0/(ETA(I)*(2.D0*DH)))
     $+THETA(N,J)*(1.D0/DT-1.D0/(DH**2.D0)+1.D0/(ETA(I)*(2.D0*DH)))
   25 CONTINUE
C
C     USE TRIDIAGONAL MATRIX SOLVER TO GET
C     THETA VALUES AT SECOND TIME STEP
C
      IF=1
      DO 26 I=1,N,1
      BETA(I,IF)=F(I,1)
      GAMMA(I,IF)=H(I,1)/BETA(I,IF)
      IFP1=IF+1
C
      DO 27 J=IFP1,L,1
      BETA(I,J)=F(I,J)-E(I,J)*G(I,J-1)/BETA(I,J-1)
      GAMMA(I,J)=(H(I,J)-E(I,J)*GAMMA(I,J-1))/BETA(I,J)
   27 CONTINUE
C
      THETA(I,L)=GAMMA(I,L)
      LAST=L-IF
      DO 28 K=1,LAST,1
      J=L-K
      THETA(I,J)=GAMMA(I,J)-G(I,J)*THETA(I,J+1)/BETA(I,J)
C     WRITE(*,65)I,J,GAMMA(I,J),BETA(I,J),H(I,J),E(I,J)
C  65 FORMAT(2(3X,I5),4(3X,E10.3))
   28 CONTINUE
   26 CONTINUE
      XTIME = XTIME +DT
      TIME=XTIME*R**2.D0/ALPHT
   29 CONTINUE
C
C     COMPUTE HEAT FLUX AT INTERFACE OF TISSUE AND PROBE
C
      J=1
      DO 30 I=1,1,1
      Q(I,1)=-((KT*(65.D0-25.D0))/R)*((2.D0*(THETA(I,1)-1.D0))/DZ)
   30 CONTINUE
      WRITE(*,54)TIME,Q(1,1)
   54 FORMAT(2X,F8.4,3X,F15.5)
C  29 CONTINUE
C
      DO 88 J=1,1,1
      WRITE(*,*)'    '
      WRITE(*,87)J
   87 FORMAT(' HEAT TRANSFER DATA FOR ROW:',3X,I2)
      WRITE(*,*)'    '
```

```
      WRITE(*,*)' TIME     COLUMN     TEMP      HEAT FLUX'
      WRITE(*,*)' ----     ------     ----      ---------'
      DO 89 I=1,1,1
      TEMP(I,J)=THETA(I,J)*(65.D0-25.D0)+25.D0
      WRITE(*,99)TIME,I,TEMP(I,J),Q(I,J),THETA(I,J)
   99 FORMAT(1X,F8.4,I5,3X,F9.2,F15.3,E10.3)
   89 CONTINUE
   88 CONTINUE
      STOP
      END
```

VITA

Michael Douglas Michener was born in Baltimore, Maryland on February 2, 1967, and grew up in Rockville, Maryland. After graduating from high school in 1985 he entered into the engineering program at Va Tech. He decided to pursue a masters in mechanical engineering immediately upon graduating in 1989. The author hopes to find a job in engineering design in the heat transfer or biomedical field.

Michael D. Michener